

NASA/TM—2004-213140



Microstructural Evaluation of KM4 and SR3 Samples Subjected to Various Heat Treatments

David Ellis and Timothy Gabb
Glenn Research Center, Cleveland, Ohio

Anita Garg
University of Toledo, Toledo, Ohio

August 2004

The NASA STI Program Office . . . in Profile

Since its founding, NASA has been dedicated to the advancement of aeronautics and space science. The NASA Scientific and Technical Information (STI) Program Office plays a key part in helping NASA maintain this important role.

The NASA STI Program Office is operated by Langley Research Center, the Lead Center for NASA's scientific and technical information. The NASA STI Program Office provides access to the NASA STI Database, the largest collection of aeronautical and space science STI in the world. The Program Office is also NASA's institutional mechanism for disseminating the results of its research and development activities. These results are published by NASA in the NASA STI Report Series, which includes the following report types:

- **TECHNICAL PUBLICATION.** Reports of completed research or a major significant phase of research that present the results of NASA programs and include extensive data or theoretical analysis. Includes compilations of significant scientific and technical data and information deemed to be of continuing reference value. NASA's counterpart of peer-reviewed formal professional papers but has less stringent limitations on manuscript length and extent of graphic presentations.
- **TECHNICAL MEMORANDUM.** Scientific and technical findings that are preliminary or of specialized interest, e.g., quick release reports, working papers, and bibliographies that contain minimal annotation. Does not contain extensive analysis.
- **CONTRACTOR REPORT.** Scientific and technical findings by NASA-sponsored contractors and grantees.

- **CONFERENCE PUBLICATION.** Collected papers from scientific and technical conferences, symposia, seminars, or other meetings sponsored or cosponsored by NASA.
- **SPECIAL PUBLICATION.** Scientific, technical, or historical information from NASA programs, projects, and missions, often concerned with subjects having substantial public interest.
- **TECHNICAL TRANSLATION.** English-language translations of foreign scientific and technical material pertinent to NASA's mission.

Specialized services that complement the STI Program Office's diverse offerings include creating custom thesauri, building customized databases, organizing and publishing research results . . . even providing videos.

For more information about the NASA STI Program Office, see the following:

- Access the NASA STI Program Home Page at <http://www.sti.nasa.gov>
- E-mail your question via the Internet to help@sti.nasa.gov
- Fax your question to the NASA Access Help Desk at 301-621-0134
- Telephone the NASA Access Help Desk at 301-621-0390
- Write to:
NASA Access Help Desk
NASA Center for AeroSpace Information
7121 Standard Drive
Hanover, MD 21076

NASA/TM—2004-213140



Microstructural Evaluation of KM4 and SR3 Samples Subjected to Various Heat Treatments

David Ellis and Timothy Gabb
Glenn Research Center, Cleveland, Ohio

Anita Garg
University of Toledo, Toledo, Ohio

National Aeronautics and
Space Administration

Glenn Research Center

August 2004

Acknowledgments

The authors gratefully acknowledge the extensive work of J. Schirra and E. Huron in processing, testing, and analyzing the materials. Discussions with D. Mourer and P. Reynolds are also acknowledged.

Document History

This research was originally published internally as HSR052 in May 1997.

Trade names or manufacturers' names are used in this report for identification only. This usage does not constitute an official endorsement, either expressed or implied, by the National Aeronautics and Space Administration.

Available from

NASA Center for Aerospace Information
7121 Standard Drive
Hanover, MD 21076

National Technical Information Service
5285 Port Royal Road
Springfield, VA 22100

Available electronically at <http://gltrs.grc.nasa.gov>

Table Of Contents

Table Of Contents	i
Table Of Figures	iii
Table Of Tables	iv
Introduction	1
Experimental Procedure	1
Alloy Compositions And Heat Treatments	1
Transmission Electron Microscopy	2
Image Analysis	2
Size And Shape Measurements	2
Volume Fraction	4
Results and Discussion	5
Microstructural Characterization	5
General Microstructures	5
SR3	5
SR3 Overview	5
SR3 Grain Boundaries	5
KM4	5
KM4 Overview	5
KM4 Grain Boundaries	6
γ' Distributions	6
SR3	6
MS1, MS3, MS7, MS8: Cuboidal Medium γ'	6
MS1, MS3, MS7, MS8: Comparison Of Spherical Fine γ'	7
MS2, MS6, MS4F, MS5F: Dendritic Medium γ'	7
MS2, MS6, MS4F, MS5F: Comparison Of Fine γ'	8
MS4 AND MS5: Irregular Cuboidal Medium γ' , Variable Fine γ'	8

<i>KM4</i>	9
MK1, MK3, MK6, MK8: Cuboidal Medium γ'	9
MK1, MK3, MK6, MK8: Comparison Of Fine γ'	9
MK2, MK4, MK5: Dendritic Medium γ' , Variable Fine γ'	10
MK7: The Most Diverse γ' Microstructure	10
Image Analysis	10
Correlation Of γ' Volume Fractions And Sizes To Mechanical Properties	11
1200°F Tensile Strength	12
1200°F Time To 0.2% Creep	14
1200°F Hold Time Fatigue Crack Growth Rates	15
Comparison To Previous Results	17
<u>Summary and Conclusions</u>	19
<u>References</u>	20

Table Of Figures

Figure 1 - Typical Size Ranges For Different Types Of γ'	47
Figure 2 - Comparison of General Microstructure and Phases Identified in SR3 MS Series MS1 - MS4.....	48
Figure 2 (Cont.) - Comparison of General Microstructure and Phases Identified in SR3 MS Series MS4F - MS6	49
Figure 2 (Cont.) - Comparison of General Microstructure and Phases Identified in SR3 MS Series MS7 - MS8	50
Figure 3 - Comparison of Heavily Loaded Grain Boundaries in SR3 MS Series Samples MS1 - MS4 ..	51
Figure 3 (Cont.) - Comparison of Heavily Loaded Grain Boundaries in SR3 MS Series Samples MS4F - MS6	52
Figure 3 (Cont.) - Comparison of Heavily Loaded Grain Boundaries in SR3 MS Series Samples MS7 - MS8	53
Figure 4 - Comparison of General Microstructure and Phases Identified in KM4 MK Series Samples MK1 - MK4	54
Figure 4 (Cont.) - Comparison of General Microstructure and Phases Identified in KM4 MK Series Samples MK5 - MK8	55
Figure 5 - Comparison of Heavily Loaded Grain Boundaries in KM4 MK Series Samples MK1 - MK4	56
Figure 5 (Cont.) - Comparison of Heavily Loaded Grain Boundaries in KM4 MK Series Samples MK5 - MK8	57
Figure 6 - Comparison of γ' Distributions in SR3 MS Series Samples MS1 - MS4	58
Figure 6 (Cont.) - Comparison of γ' Distributions in SR3 MS Series Samples MS4 - MS8	59
Figure 6 (Cont.) - Comparison of γ' Distributions in SR3 MS Series Samples MS4F and MS5F.....	60
Figure 7a - SR3 MS Series Large γ' Size Distributions	61
Figure 7b - SR3 MS Series Medium γ' Size Distributions.....	62
Figure 7c - SR3 MS Series Fine γ' Size Distributions.....	63
Figure 8 - Comparison of γ' Distributions in KM4 MK Series Samples MK1 - MK4	64
Figure 8 (Cont.) - Comparison of γ' Distributions in KM4 MK Series Samples MK5 - MK8.....	65
Figure 9a - KM4 MK7 Large γ' Size Distribution	66
Figure 9b - KM4 MK Series Medium γ' Size Distributions	67
Figure 9c - KM4 MK Series Fine γ' Size Distributions	68
Figure 10 - 1200°F Yield And Ultimate Tensile Strengths Versus γ' Volume Fractions	69
Figure 11 - 1200°F Yield And Ultimate Tensile Strengths Versus Average γ' Major Axes	70
Figure 12 - Contour Plot Of 1200°F Tensile Strength Two Independent Variable Models.....	71
Figure 13 - Comparison Of Actual And Two Independent Variable Model Predicted 1200°F Tensile Strengths	72
Figure 14 - 1200°F/115 ksi Time To 0.2% Creep Versus γ' Volume Fractions	73
Figure 15 - 1200°F/115 ksi Time To 0.2% Creep Versus Average γ' Major Axes	74
Figure 16 - Contour Plot Of Time to 0.2% Creep Two Independent Variable Model	75
Figure 17 - Comparison Of Actual And Two Independent Variable Model Predicted Times to 0.2% Creep	76
Figure 18 - KM4 MK Series 1200°F Crack Growth Rate Versus γ' Volume Fractions	77
Figure 19 - KM4 MK Series Dependency Of 1200°F Crack Growth Rate On Solutioning Heat Treatment	78
Figure 20 - KM4 MK Series 1200°F Crack Growth Rate Versus Average γ' Feret Diameters	79

Table Of Tables

Table 1 - Nominal Compositions Of SR3 And KM4.....	21
Table 2a - Heat Treatment Matrix For SR3 MS Series	22
Table 2b - Heat Treatment Matrix For KM4 MK Series.....	22
Table 3 - Minor Phases Observed In SR3 MS Series.....	23
Table 4 - Minor Phases Observed In KM4 MK Series	24
Table 5a - Summary Of Image Analysis Results For SR3 MS Series - Large γ'	25
Table 5b - Summary Of Image Analysis Results For SR3 MS Series - Medium γ'	26
Table 5c- Summary Of Image Analysis Results For SR3 MS Series - Fine γ'	27
Table 6a - Summary Of Image Analysis Results For KM4 MK Series - Large γ'	28
Table 6b - Summary Of Image Analysis Results For KM4 MK Series - Medium γ'	29
Table 6c - Summary Of Image Analysis Results For KM4 MK Series - Fine γ'	30
Table 7a - SR3 MS Series γ' Size Distribution Fitted Curves	31
Table 7b - KM4 MK Series γ' Size Distribution Fitted Curves	33
Table 8 - SR3 MS Series γ' Volume Fractions	35
Table 9 - KM4 MK Series γ' Volume Fractions.....	35
Table 10a - SR3 MS Series 1200°F Tensile Strength Versus γ' Volume Fraction Curve Fit	36
Table 10b - KM4 MK Series 1200°F Tensile Strength Versus γ' Volume Fraction Curve Fit	37
Table 11a - SR3 MS Series 1200°F Tensile Strength Versus γ' Size Curve Fit.....	38
Table 11b - KM4 MK Series 1200°F Tensile Strength Versus γ' Size Curve Fit.....	39
Table 12a - SR3 MS Series 1200°F/115 ksi Time To 0.2% Creep Versus γ' Volume Fraction Curve Fit - Common Logarithm Model.....	40
Table 12b - SR3 MS Series 1200°F/115 ksi Time To 0.2% Creep Versus γ' Volume Fraction Curve Fit - Linear Model.....	40
Table 12c - KM4 MK Series 1200°F/115 ksi Time To 0.2% Creep Versus γ' Volume Fraction - Common Logarithm Model	41
Table 12d - KM4 MK Series 1200°F/115 ksi Time To 0.2% Creep Versus γ' Volume Fraction - Linear Model.....	41
Table 13a - SR3 MS Series 1200°F/115 ksi Time To 0.2% Creep Versus γ' Size - Common Logarithm Model	42
Table 13b - SR3 MS Series 1200°F/115 ksi Time To 0.2% Creep Versus γ' Size - Linear Model.....	42
Table 13c - KM4 MK Series 1200°F/115 ksi Time To 0.2% Creep Versus γ' Size - Common Logarithm Model	43
Table 13d - KM4 MK Series 1200°F/115 ksi Time To 0.2% Creep Versus γ' Size - Linear Model	43
Table 14a - KM4 MK Series 1200°F Hold Time Fatigue Crack Growth Rate Versus γ' Volume Fraction - Common Logarithm Model	44
Table 14b - KM4 MK Series 1200°F Hold Time Fatigue Crack Growth Rate Versus γ' Volume Fraction - Linear Model	44
Table 15a - KM4 MK Series 1200°F Hold Time Fatigue Crack Growth Rate Versus γ' Size - Common Logarithm Model	45
Table 15b - KM4 MK Series 1200°F Hold Time Fatigue Crack Growth Rate Versus γ' Size - Linear Model.....	45
Table 16a - Comparison Of Observed Trends For Current And Previous Work (5)	46

Introduction

Advanced supersonic commercial and military aircraft will in some cases require turbine engines capable of sustaining supersonic cruise for extended time periods. This will impose severe challenges for the high pressure compressor and turbine disks, which will operate at near maximum stress and temperature during the entire supersonic flight. Such applications could be limited by the tensile, creep, and dwell fatigue crack growth properties of disk alloys. These mechanical properties have been shown to vary with both the microstructure and composition in disk alloys (1). However, no current powder metallurgy disk alloy appears capable of simultaneously achieving sufficient tensile, creep, and dwell fatigue crack growth properties through variations of microstructure alone (2). Therefore, disk alloys having new compositions and careful microstructural control will be necessary to give sufficient properties for such applications.

KM4 and SR3 are two advanced powder metallurgy disk alloys offering improved strength, creep resistance, and fatigue crack growth properties over current production alloys (3, 4). Their improvements were achieved using different alloy design approaches. KM4 and SR3 have significantly different compositions, which affect γ and γ' phase contents and chemistries. KM4 was designed to have a higher “cooling” γ' phase content of near 55% to improve strength and creep resistance in comparison with many current disk alloys. The γ' composition in KM4 has only moderate levels of the γ' solid solution strengtheners Ti and Nb and has no other refractory additions intended for this purpose. SR3 was designed to have a γ' composition with higher Ti and lower Al, and contains Hf along with Nb. This could increase the solid solution strengthening of γ' in SR3 for improved strength. The γ' content of SR3 is near 47% which is more typical among current disk alloys and lower than KM4.

The improved strength and creep resistance of KM4 can be attributed in large part to its higher γ' content. The improved strength and creep resistance of SR3 can be attributed to the higher solution strengthening of its γ' precipitates. The microstructure-property relationships in such advanced alloys could differ substantially from those of current alloys due to these different alloy design approaches. Therefore, it is essential to understand the microstructure-property relationships in these advanced alloys in order to attain sufficient mechanical properties for supersonic cruise applications.

A series of heat treatments was designed and applied to SR3 and KM4 in order to vary each alloy's microstructure (5). Tensile, creep, and fatigue crack growth tests have been performed for each alloy-heat treatment combination to assess the governing microstructure-mechanical property relationships. The objective of this study was to quantitatively characterize the γ' size-frequency distributions of SR3 and KM4 specimens given these different heat treatments. The γ' sizes and volume fractions of each specimen were related to the heat treatments, and correlated with the mechanical properties.

Experimental Procedure

Alloy Compositions And Heat Treatments

The actual compositions of SR3 and KM4 argon-atomized powder from Homogeneous Metals Inc. are listed in Table 1 (6). Table 1 also contains the solvus temperatures for each alloy. The SR3 and KM4 powder was screened, hot compacted, and extruded into three inch diameter billets. The billets were forged to yield one inch thick by seven inch diameter pancakes.

Heat treatments were chosen using a Taguchi L8 matrix varying grain size, γ' size, γ' volume fraction, and stabilization heat treatment cycle (5). The heat treatment matrices for SR3 MS series and KM4 MK series are listed in Table 2. Table 2 also includes the ASTM grain size numbers previously reported by Pratt & Whitney (6). The various steps in the heat treatment are listed in the format of temperature in degrees Fahrenheit/time in hours. Hence, 2140/1 means 2140°F for 1 hour. Specimen blanks were first subjected to a grain size coarsening heat treatment of 2130°F (1166°C) to 2180°F (1193°C) for 2 to 3 hours. Grain size increased with higher temperature and duration in the grain coarsening treatment. Cooling γ' content was controlled by solution heat treatments between 2045°F (1118°C) and 2140°F (1171°C) for 1 hour in SR3, and 2060°F (1127°C) to 2150°F (1177°C) for 1 hour in KM4. Increasing amounts of γ' were dissolved with increasing temperature in this step. The dissolved elements were then available for precipitation as cooling γ' during the quench from the solutioning temperature. The size of this cooling γ' was controlled by the cooling rate from the solution temperature. Cooling rates were varied from 70°F (39°C)/min to greater than 300°F (167°C)/min using, in order of increasing cooling rates, insulated air cooling, air cooling, fan air cooling, and oil quenching. Cooling γ' size increased with decreasing cooling rate.

Selected specimens were subjected to carbide stabilization heat treatments following the solution heat treatment quench. The stabilization heat treatments were intended to encourage $M_{23}C_6$ carbides to nucleate and grow at the grain boundaries. Such heat treatments also would be useful in production disks to allow relief of residual stresses generated during the quench from solution heat treatments. The SR3 experimental matrix was used to assess the effects of including a 1550°F (843°C)/4 h stabilization heat treatment on microstructures and mechanical properties. The KM4 experimental matrix was employed to compare the microstructures and mechanical properties of alternative stabilization heat treatments, 1550°F/4 h and 1600°F (871°C)/2 h. All specimens were given a final aging heat treatment of 1400°F (760°C)/8 h.

Transmission Electron Microscopy

Specimens for transmission electron microscopy (TEM) were prepared normal to the loading axis of grip sections of tensile specimens and from coupons. TEM foils were thinned in a twin-jet Tenupol-3 electropolisher using a solution of 10% perchloric acid and 90% methanol cooled to 32°F (0°C). An applied potential of 20 to 25V with a corresponding current of 10 to 15 mA produced electron transparent foils. The foils were lightly ion milled to remove electropolishing contamination and examined in a Phillips 400T TEM operating at 120 keV. Energy dispersive spectroscopy was performed with an integrated EG&G detector. A minimum of three foils was examined from each alloy specimen. Typical representative areas were selected for detailed evaluations. Microbeam electron diffraction (MBED) patterns, selective area diffraction (SAD) patterns, and energy dispersive X-ray (EDX) analyses were employed to determine the chemistry and crystal structure of different particles and phases. At least five particles of each type observed were identified and measured to obtain particle size ranges.

Image Analysis

Size And Shape Measurements

TEM dark field negatives showing γ' precipitates in a $\langle 100 \rangle$ orientation were digitized using a Relisys 9612 flatbed scanner equipped with a transparency adapter. A minimum resolution of 300 dots per inch (dpi) was used for all scans. Most scans were conducted at 400 or 600 dpi. The resolutions were sufficient to give an average number of pixels per precipitate greater than 50 pixels for the aging γ' .

SigmaScan¹ image analysis software was used to determine the sizes of the γ' precipitates. Due to differences in the supersolvus and subsolvus heat treatments, the size of each type of γ' (secondary, cooling or aging) varied, but for all samples the precipitates could be classified in three classes based on size. The first class contained large (greater than 600 nm), irregularly shaped precipitates. These were secondary γ' precipitates, and this class will be referred to as coarse. This class of γ' appeared only in the samples receiving a supersolvus heat treatment. The second class consisted of intermediate size (100 nm to 600 nm) γ' precipitates. These could be either cuboidal or an irregular, dendritic shape. These precipitates were cooling γ' in samples given a supersolvus solutioning heat treatment or secondary γ' in samples given a subsolvus solutioning heat treatment. This class will be referred to as medium γ' . The third and final class of γ' precipitates were the very fine (less than 100 nm), spherical precipitates. These were generally aging γ' precipitates, but subsolvus solutioned samples also had cooling γ' precipitates included in this size range. This class will be referred to as fine γ' . Figure 1 shows the generally observed ranges for the three different types of γ' present in the alloys and the overlap between the various types.

To determine the edge of each precipitate, the typical grayscale intensity of the interior of the precipitate and the immediate surrounding matrix were determined. The intensity threshold for the precipitate edge was set at the average of these two values. The image analysis program automatically selected all pixels within the precipitate that were below the threshold value.

Once each precipitate was filled, the compactness, feret diameter, major axis, minor axis, and shape factor were calculated by the program. The major axis was the maximum length chord connecting pixels on the perimeter of the precipitate. The minor axis was the maximum length chord perpendicular to the major axis connecting pixels on the perimeter of the precipitate. The feret diameter is the diameter of a circle with an area equal to the measured area of the precipitate. The software examined all pixels on the perimeter rather than examining the image at preset angular intervals. These chords generally fell within the precipitate image, but in the case of some irregular precipitates go outside the boundary of the precipitate perimeter.

The compactness is defined as

$$Compactness = \frac{Perimeter^2}{Area} \quad [1]$$

Compactness is a measure of how close the precipitate image is to a perfect circle. The minimum value is 4π (12.5664) for a perfect circle. As the value increases, the measured object tends away from a circle.

The shape factor is defined as

$$Shape\ Factor = \frac{4\pi\ Area}{Perimeter^2} \quad [2]$$

The shape factor is a measure of how close the object is to a perfect circle or other regular polygons. A perfect circle has a shape factor of 1, and a line a shape factor of 0. While the theoretical maximum value of the shape factor is 1, very small objects, typically consisting of 25 or less pixels, can break this

¹ SigmaScan Version 3.0 is produced by Jandel Scientific Software, P.O. Box 7005, San Rafael, CA 94912-7005

rule and have a shape factor greater than 1. For reference, the shape factor of a pentagon is 0.86, a square is 0.79 and an equilateral triangle is 0.61.

After measurements were completed, the aspect ratio of each precipitate was calculated. The aspect ratio is defined as

$$\text{Aspect Ratio} = \frac{\text{Minor Axis}}{\text{Major Axis}} \quad [3]$$

Values of the aspect ratio range from 0 for a line to 1 for a circle, square or other shape with equal “length” and “width”.

The average, standard deviation, minimum and maximum value for each measured and calculated quantity were computed. In the case of feret diameter, histograms of the various γ' classes were generated. The feret diameter was chosen since it is shape independent. As such, γ' from the three classes and the different samples could be compared even though they did not have the same morphology.

Volume Fraction

The volume fraction of the coarse and medium γ' classes were determined using the point count method (7). In this method, a grid is overlaid on the image, and the number of intersections falling on the γ' type of interest is counted. This number is divided by the total number of grid intersections to get the area fraction. Since the coarse and medium γ' extend through the foil thickness, the area fraction is equal to the volume fraction. The process was repeated for at least five views from each sample.

The volume fraction of the fine γ' could not be directly measured because more than one aging γ' precipitate could be stacked through the thickness of the foil. Instead, the MS and MK series samples were examined via the TEM to see if any of the samples had no fine γ' . In both alloys there existed heat treatment conditions where most if not all the γ' was present as medium γ' . After measuring the volume fractions for these samples, the total amount of γ' in all samples of a given alloy was assumed to be the average amount of medium γ' measured. The fine γ' for the other samples was calculated by subtracting the measured amount of medium and coarse γ' from the total amount present.

For samples MK7 and MK8, very large primary γ' was present in the samples. While these large precipitates do not contribute to strengthening the samples, they do account for a fraction of the γ' that cannot be used in coarse, medium or fine γ' which could strengthen the samples. It also affects the calculations of the volume fraction of fine γ' precipitates. Additional 1000X optical micrographs were taken of etched pieces of MK7 and MK8. The etching clearly revealed the primary γ' . These micrographs were digitized, and the volume fraction determined by the point count method as with the coarse and medium γ' classes. The volume fractions of the fine γ' precipitates was calculated by subtracting the primary, coarse and medium γ' fractions from the total γ' in these samples.

Results and Discussion

Microstructural Characterization

General Microstructures

SR3

SR3 Overview

The general microstructures and phases identified in the SR3 specimens are compared in Figure 2. The grain sizes (6) are listed in Table 2. MS1 through MS8 had average grain sizes ranging from 34 to 170 μm (ASTM 2.1 to 6.7). The microstructures consisted of assorted coarse γ' , medium γ' and fine γ' precipitates in a γ matrix. Primary γ' precipitates were not observed in any of the SR3 specimens. Minor phases observed within the grains and at grain boundaries are listed in Table 3. SAD patterns and corresponding EDS spectra of each minor phase were the same as those observed previously for the baseline SR3 sample (8). All specimens contained a comparable number of equiaxed (Ti,Nb)C carbides 200 to 800 nm in diameter within the grains, as identified in Figure 2. A similar number of finer (Hf,Zr)O₂ oxide particles were also present. Each SR3 TEM foil also contained several (Ti,Mo)₆C carbide needles, about 300 to 500 nm wide and 1000 to 2000 nm long. In general, the minor phases observed in these SR3 specimens compared closely with the morphology to those found in the evaluation of the baseline SR3 sample (8).

SR3 Grain Boundaries

Grain boundaries were characterized for each specimen, and those having the highest densities of minor phases are compared in Figure 3 and Table 3. The grain boundaries had a high number density (90%) of fine (Cr,Mo)₂₃C₆ carbides. Small numbers of larger equiaxed (Ti,Nb)C carbides (5%) and elongated (Mo,Cr)₃B₂ borides (5%) were also present at grain boundaries. The frequency of carbides at the grain boundaries was variable and generally low for specimens not subjected to the carbide stabilization heat treatment (MS1, MS4, MS4F, MS6, and MS7). The grain boundaries of specimens subjected to the stabilization heat treatment (MS2, MS3, MS5, MS5F, and MS8) had a more consistent carbide density, which was significantly higher than unstabilized specimens. The grain boundaries of all specimens were serrated to an amplitude varying between 0 and 1 μm by the localized coarsening of some γ' precipitates along the grain boundaries. This was most pronounced in MS4F and MS5F, apparently due to enhanced coarsening along the grain boundaries of remnant cooling γ' during the solution heat treatment.

In summary, SR3 grain boundaries predominantly contained (Cr,Mo)₂₃C₆ carbides. The frequency and consistency of these carbides increased in specimens subjected to a stabilization heat treatment.

KM4

KM4 Overview

The general microstructures and minor phases identified in the KM4 specimens are compared in Figure 4. The grain sizes are listed in Table 2. MK1 through MK8 had average grain sizes of 32 to 78 μm (ASTM 4.4 to 7.0). The microstructures again predominantly consisted of assorted coarse, medium

and fine γ' precipitates in a γ phase matrix. Primary γ' precipitates (1000 to 5000 nm diameter) which were not dissolved during the heat treatment of MK7 and MK8 were also present. Minor phases observed within the grains and at grain boundaries are listed in Table 4. SAD patterns and corresponding EDS spectra of each minor phase were the same as those reported previously for the baseline KM4 sample (8). All KM4 specimens contained a comparable number density (60%) of (Ti,Nb)C equiaxed carbides 200 to 800 nm in diameter as identified in Figure 4. The KM4 specimens contained a smaller number (30%) of finer Al_2O_3 and ZrO_2 oxides. A small number (5%) of $(\text{Mo,Cr})_3\text{B}_2$ borides 500 to 1,500 nm in diameter were also present in the grains. Each KM4 TEM foil contained several $(\text{Ti,Mo})_6\text{C}$ carbide needles which were 300 to 500 nm wide and 1,000 to 2,500 nm long. Overall, the minor phases identified in these KM4 specimens were quite comparable in composition and morphology to those found in previous evaluations of KM4 (3,8). KM4 and SR3 had similar minor phase morphologies and compositions, although $(\text{Hf,Zr})\text{O}_2$ oxides formed in SR3 rather than the Al_2O_3 and ZrO_2 oxides of KM4.

KM4 Grain Boundaries

Grain boundaries having the highest densities of minor phases are compared in Figure 5 and Table 4. The KM4 grain boundaries had a high number density (90%) of fine $(\text{Cr,Mo})_{23}\text{C}_6$ carbides. Smaller numbers of larger (Ti,Nb)C carbides (5%) and elongated $(\text{Mo,Cr})_3\text{B}_2$ borides (5%) were also present. All KM4 specimens were subjected to carbide stabilization heat treatments of either 1550°F/4 h or 1600°F/2 h. These stabilization heat treatments gave comparable $(\text{Cr,Mo})_{23}\text{C}_6$ carbide frequencies and sizes in MK1 through MK7. The KM4 carbide frequencies were similar to those of stabilized SR3 specimens, but were higher and less variable than the unstabilized SR3 specimens. Continuous carbides films or layers were not observed in any specimens. MK8 had a significantly lower frequency of carbides at the grain boundaries. This was probably caused by the finer grain size of MK8 compared to other specimens which increased the total grain boundary surface area available for carbide precipitation (9).

In summary, MK1 through MK7 had comparable frequencies and size distributions of $(\text{Cr,Mo})_{23}\text{C}_6$ carbides at the grain boundaries, due to the stabilization heat treatments. MK8 had a lower frequency of these carbides, probably due to its finer grain size.

γ' Distributions

SR3

A wide variety of γ' distributions were produced by the heat treatments on SR3. Typical micrographs of the γ' distributions of SR3 specimens are compared in Figure 6. The γ' size distributions are described by the histograms in Figure 7. γ' sizes and shapes are compared in Table 5. Primary γ' was not observed in any of the SR3 specimens, indicating the grain coarsening and solution heat treatment temperatures applied were high enough to dissolve all primary γ' . Most of the SR3 specimens had only medium γ' and fine γ' precipitates of varying morphologies and volume fractions. However, MS4F and MS5F also had coarse γ' precipitates. Similarities and variations in the γ' distributions of the specimens were apparent which could be related to the heat treatments applied to each specimen. The specimens will be grouped according to morphology of the medium γ' for description purposes.

MS1, MS3, MS7, MS8: Cuboidal Medium γ'

MS1, MS3, MS7, and MS8 had similar cuboidal medium γ' morphologies. These specimens were subjected to two subsolvus temperature solution heat treatments with varying solution cooling rates, so the cuboidal shape and size of this medium γ' are apparently associated with the subsolvus solution heat treatment temperatures and time rather than the solution quench cooling rate. This cuboidal medium

γ' was apparently remnant “cooling” γ' formed during the grain coarsening heat treatments. Such cooling γ' would not all dissolve during the subsequent subsolvus solution heat treatments. Rather, some would be expected to remain and coarsen as previously observed in René 95 (9). This gave similar sizes of medium γ' in MS1 and MS3 which were subjected to the same subsolvus solution heat treatment temperature but different cooling rates. MS7 and MS8 were solution heat treated at a higher subsolvus temperature where more coarsening of remnant γ' would be expected. This evidently accounted for the larger size of cuboidal medium γ' in MS7 and MS8. The size of the cuboidal medium γ' did not seem to be a strong function of the different solution quench cooling rates in these specimens.

In summary, MS1, MS3, MS7, and MS8 had similar cuboidal medium γ' , apparently grown during the subsolvus solution heat treatments.

MS1, MS3, MS7, MS8: Comparison Of Spherical Fine γ'

The fine γ' in MS1, MS3, MS7, and MS8 could form during the subsolvus solution heat treatment quench, the stabilization heat treatment, and the aging heat treatment. It can be postulated that nucleation of the fine γ' preferentially occurred during the quench, and growth occurred during the stabilization and aging heat treatment. However, microstructural evaluations after each heat treatment step would be required to substantiate this sequence. The lower subsolvus solution temperatures of MS1 and MS3 would be expected to give lower nucleation and growth rates of fine γ' during the solution quench than in MS7 and MS8. This produced smaller fine γ' sizes after stabilization and aging heat treatments in MS1 and MS3. MS1 had the smallest fine γ' size, partly due to its fast solution heat treatment quench and the lack of a stabilization heat treatment. MS3 had a larger average fine γ' size than MS1, due to a slower solution quench cooling rate and the stabilization heat treatment cycle before aging. MS7 was quenched from a higher subsolvus solution temperature at an intermediate cooling rate with respect to MS1 and MS3 and was not subjected to the 1550°F/4h stabilization heat treatment before aging at 1400°F/8h. This produced a larger size and wider size range of fine γ' in MS7 than in MS1 and MS3. MS8 was quenched from the same higher subsolvus solution temperature at a faster cooling rate than MS7 and did receive the stabilization heat treatment before aging. This produced in MS8 the largest size and widest size range of fine γ' among this group of SR3.

In summary, the fine γ' in MS1, MS3, MS7, and MS8 apparently nucleated and grew during the solution quench, stabilization, and aging heat treatments.

MS2, MS6, MS4F, MS5F: Dendritic Medium γ'

Branched, dendritic medium γ' was observed in MS2, MS6, MS4F, and MS5F. This apparently formed during quenches from solution heat treatment temperatures near the solvus at cooling rates less than 300°F (167°C)/min. MS2 and MS6 were quenched from the same near-solvus solution temperature (2140°F) at comparable cooling rates of 120 and 164°F/min (67 and 91°C/min) and have similar dendritic medium γ' sizes. The volume fraction of medium γ' was higher in MS6 than in MS2, for unclear reasons. MS2 and MS6 had no evidence of remnant cooling γ' from the grain coarsening heat treatments, indicating that all γ' precipitates had been dissolved during their solution heat treatments. However, MS4F and MS5F subjected to the same solution heat treatment temperature and higher quench cooling rates had a small volume fraction of cuboidal coarse γ' precipitates along with the branched, dendritic medium γ' . The cuboidal coarse γ' appeared to be coarsened remnant cooling γ' from the grain coarsening heat treatments which survived the 2140°F solution heat treatment of these specimens. This suggests the solvus temperature of SR3 is very close to 2140°F and was within the temperature tolerance of the furnace. Based on this, the full solutioning of the γ' precipitates at the nominal temperature of 2140°F could not be assured.

In summary, MS2, MS6, MS4F, and MS5F had similar dendritic medium γ' formed during the quench from the supersolvus solution heat treatments.

MS2, MS6, MS4F, MS5F: Comparison Of Fine γ'

The fine γ' in MS2, MS6, MS4F, and MS5F could form during the solution quench, stabilization, and aging heat treatments. Although MS2 and MS6 had comparable solution temperatures and quench cooling rates, MS6 was not subjected to the stabilization heat treatment of MS2 before aging. This gave MS6 the smallest size of fine γ' among this group of specimens, while MS2 had larger fine γ' . This confirmed that the stabilization heat treatment could strongly influence the fine γ' size in SR3 by encouraging nucleation and growth of fine γ' during the higher temperature stabilization heat treatment. The fine γ' in MS4F and MS5F was relatively large with wider size distributions than for MS2 and MS6. This wider size distribution of fine γ' could not be attributed to the effects of a stabilization heat treatment since one was not applied to MS4F. In these specimens, it is likely that some of the larger fine γ' formed during the solution quench. As in MS7 and MS8 which also contained cuboidal remnant γ' from the grain coarsening heat treatment, quenches of these microstructures from high subsolvus solution temperatures can encourage the precipitation of fine γ' . Additional precipitation and growth of fine γ' could occur during subsequent heat treatment steps, to produce the wide size range of fine γ' size in MS4F and MS5F.

MS4 AND MS5: Irregular Cuboidal Medium γ' , Variable Fine γ'

MS4 and MS5 had irregular cuboidal medium γ' which was intermediate between the cuboidal and dendritic morphologies previously described. This morphology was apparently due to oil quenching at cooling rates greater than 300°F/min applied to these specimens from near solvus solution heat treatments. This fast quench apparently did not allow the favored dendritic morphology observed in other specimens sufficient time to occur. No evidence of remnant cooling γ' from the grain coarsening cycle was observed in these specimens, indicating full solutioning of all γ' precipitates did occur during the solution heat treatments.

The insertion of the stabilization heat treatment between the solution and aging heat treatments affected the size distributions and volume fractions of both medium and fine γ' precipitates in these oil quenched specimens. The stabilization heat treatment applied to MS5 gave a significantly larger size and volume fraction of medium γ' as compared to MS4. This suggests the medium γ' precipitates produced during the solution heat treatment quench coarsened during the stabilization. The stabilization also gave a larger average size of fine γ' while reducing its volume fraction to about 1% in MS5. The increase in fine γ' size could be attributed to earlier nucleation and growth of fine γ' in MS5 during the stabilization heat treatment. The higher volume fraction of medium γ' in MS5 could be related to the interactions of the rapid solution quench cooling rate and the stabilization heat treatment.

It can be postulated that the fast solution heat treatment cooling rates of MS4 and MS5 did not allow the equilibrium content of medium “cooling” γ' to nucleate and grow to uniform size. This could have left the γ matrix in a supersaturated state. The subsequent aging heat treatment of MS4 at 1400°F promoted the nucleation and growth of ample fine γ' . However, the intervening stabilization heat treatment of MS5 could have promoted enhanced nucleation and more rapid growth of additional γ' at the higher temperature of 1550°F. The size of these precipitates could approach the medium γ' size. Only a small population of fine γ' appeared to remain in such conditions after the stabilization and aging heat treatments.

In summary, the irregular cuboidal medium γ' of MS4 and MS5 was attributable to the fast oil quench from the solution heat treatment of these specimens. Subsequent insertion of the stabilization heat treatment after this quench apparently promoted enhanced nucleation and growth of additional γ' , with only a very small population of fine γ' remaining after the aging heat treatment in MS5.

KM4

Typical micrographs of the γ' distributions in KM4 specimens are compared in Figure 8. The γ' size distributions are described by the histograms in Figure 9. γ' sizes and shapes are compared in Table 6. Primary γ' was only observed in MK7 and MK8. This was due to their subsolvus grain coarsening and solution heat treatments, neither of which dissolved these large γ' particles formed during the powder solidification. MK1 through MK6 had only medium and fine γ' of varying morphologies and volume fractions. Variations and similarities were apparent in the γ' distributions of KM4 specimens and were related to the individual heat treatments as in SR3. The specimens will again be grouped according to medium γ' morphology for description purposes.

MK1, MK3, MK6, MK8: Cuboidal Medium γ'

MK1, MK3, MK6, and MK8 had generally similar cuboidal medium γ' morphologies that generally corresponded to the heat treatments as in SR3 specimens. The cuboidal medium γ' appeared to be remnant “cooling” γ' formed during the supersolvus grain coarsening heat treatments of these specimens as observed in SR3 specimens MS1, MS3, MS7, and MS8. This accounted for the comparable sizes of medium γ' in MK1 and MK3 even though they were subjected to the same solution heat treatment temperature but differing solution cooling rates. The medium γ' size in these specimens again was related to the subsolvus solution heat treatment temperature and time rather than the differing solution cooling rates. This is also consistent with the smaller volume fraction and larger size of the medium γ' in MK6 and MK8 which were solutioned at a higher subsolvus temperature. This higher subsolvus temperature would allow a smaller volume fraction of cooling γ' to survive, but would also promote more coarsening of these remaining precipitates.

In summary, MK1, MK3, MK6, and MK8 had similar cuboidal medium γ' , again formed during subsolvus solution heat treatments as in SR3.

MK1, MK3, MK6, MK8: Comparison Of Fine γ'

The fine γ' in these specimens formed during the solution heat treatment quench, stabilization, and aging heat treatments. As suggested in SR3, nucleation may predominate during the quench, and growth may largely occur during stabilization and aging heat treatments. Unlike SR3, the stabilization heat treatments did not seem to invariably produce large average sizes of fine γ' in KM4. This may be due to slower γ' nucleation and growth rates in KM4 related to differences in the γ' compositions of KM4 and SR3. MK1 and MK3 had small average sizes of fine γ' , despite their stabilization heat treatments. The lower solution heat treatment temperatures in MK1 and MK3 would be expected to allow less nucleation and growth of the fine γ' during the solution quench than in MK6 and MK8. Therefore, a large portion of the fine γ' in MK1 and MK3 may have been formed during the stabilization and aging heat treatments. This gave smaller sizes of fine γ' in these specimens. Conversely, a larger portion of the fine γ' in MK6 and MK8 may have been formed during the quench from their higher subsolvus solution heat treatments. This gave a larger average fine γ' size and produced skewed or multi-modal fine γ' size distributions. The fine γ' size distribution in MK6 was shifted to larger sizes, while that of MK8 possessed two identifiable peaks.

In summary, the fine γ' in MK1, MK3, MK6, and MK8 apparently nucleated and grew during the solution quench, stabilization, and aging heat treatments as in SR3. However, the fine γ' sizes after stabilization heat treatments were generally smaller in KM4 than in SR3.

MK2, MK4, MK5: Dendritic Medium γ' , Variable Fine γ'

MK2, MK4, and MK5 had dendritic medium γ' , which varied in morphology as a function of heat treatment in a manner similar to SR3 specimens. The supersolvus solution heat treatments in MK2, MK4, and MK5 apparently dissolved all γ' . The dendritic medium γ' shape is preferred (10) in nucleation and growth during the solution quench. MK2 had a lower volume fraction of dendritic medium γ' , but it was larger in size than MK4 and MK5. The slower solution heat treatment cooling rate of MK2 would be expected to produce a larger average dendritic medium γ' size than MK4 and MK5 during these solution quenches. MK4 and MK5 both had high volume fractions of smaller dendritic medium γ' and very low volume fractions of fine γ' precipitates. As in the SR3 specimen MS5, the fast cooling rates produced by oil quenching may have not allowed the equilibrium content of medium “cooling” γ' to nucleate and grow to uniform size. This could have left the γ matrix in a supersaturated state. The subsequent stabilization heat treatments would have promoted enhanced nucleation and growth of additional γ' with many of the new precipitates approaching the medium γ' in size. Only a small population of fine γ' appeared to remain under these conditions after the heat treatments for MK4 and MK5.

In summary, MK2, MK4, and MK5 had similar dendritic medium γ' , apparently formed during the quenches from their solution heat treatments. MK4 and MK5 had very low volume fractions of fine γ' , apparently due to the combination of a supersolvus solution treatment, oil quench, and stabilization heat treatment as in the SR3 specimen MS5.

MK7: The Most Diverse γ' Microstructure

MK7 had the most diverse γ' microstructure of all SR3 and KM4 specimens, containing primary γ' , coarse γ' , dendritic medium γ' , and very small fine γ' . The primary γ' was not solutioned during the subsolvus grain coarsening and solution heat treatments. The small amount of coarse γ' appeared to be remnant “cooling” γ' left from grain coarsening heat treatment. It grew considerably during the high subsolvus solution heat treatment of MK7, as described for MK1, MK3, MK6, and MK8. The dendritic medium γ' apparently formed during the quench from the solution heat treatment, as discussed for MK2, MK4, and MK5. The fine γ' appeared to form during the subsequent stabilization and aging heat treatments.

Image Analysis

The results of the size and shape measurements for the SR3 MS series are summarized in Table 5. Table 6 summarizes the results for the KM4 MK series. In both tables the average, standard deviation, minimum and maximum values for the six measured and calculated quantities are listed. For comparison, the corresponding results for both baseline alloys were also included.

Figure 7 shows the size distributions for the various observed classes of γ' in the SR3 MS series. Figure 9 shows the distributions for the KM4 MK series. The histograms show the size distributions of the γ' as measured by the feret diameter. The feret diameter was chosen for these size distributions since it is shape independent. As such, the size of the dendritic γ' can be directly compared to the square and

circular γ' . To better characterize the SR3 MS and KM4 MK γ' size distributions, the data was analyzed using PeakFit² peak analysis software to deconvolute the observed peaks. One of two types of peaks were fitted to the data. Most of the peaks were fitted with a Gaussian amplitude peak which is described by the mathematical formula

$$y = a_0 \exp \left[-\frac{1}{2} \left(\frac{x - a_1}{a_2} \right)^2 \right] \quad [4]$$

where

- a_0 = maximum peak amplitude (%)
- a_1 = center of the peak (nm)
- a_2 = half height peak width (which is also equal to the standard deviation) (nm)
- y = amplitude of the peak at a given x (feret diameter) (%)
- x = feret diameter (nm)

For several of the peaks, there was a distinct tail at higher values of the feret diameter. This is most likely caused by coarsening of the γ' precipitates. To describe these size distributions, a log normal function which allows for accurate fitting of curves to the tailed distributions was used. The mathematical formula for the log normal function is

$$y = a_0 \exp \left[-\frac{1}{2} \left(\frac{\ln \frac{x}{a_1}}{a_2} \right)^2 \right] \quad [5]$$

where

- a_0 = maximum peak amplitude (%)
- a_1 = peak center (nm)
- a_2 = half height peak width (nm)
- y = amplitude of the peak at a given x (feret diameter) (%)
- x = feret diameter (nm)

The results of the analysis are presented in Table 7.

In general, an attempt was made to fit the size distributions with a single peak based on the expectation that the size classes were from γ' that formed at about the same time. In some cases the peak fitting revealed the strong probability of a second peak. In Table 7 additional information is given if the peak fitting indicated that alternative fits were possible.

The volume fraction for each of the three classes of γ' are listed in Table 8 for the MS series and Table 9 for the MK series. The values for total and fine γ' assume that the total amount present in all samples of a given alloy was constant. In the case of the SR3 MS series this value was the average of samples MS5 and MS6 or 60.4%. For the KM4 MK series the total amount was the average of the medium γ' in samples MK4 and MK5 or 64.3%.

² PeakFit Version 4.0 is produced by Jandel Scientific Software, P.O. Box 7005, San Rafael, CA 94912-7005

Correlation Of γ' Volume Fractions And Sizes To Mechanical Properties

The detailed microstructural quantification of the γ' precipitates and the corresponding mechanical test matrices of the materials allow for a chance to correlate and compare the effects of microstructure on mechanical properties. In particular, the detailed quantification of the aging γ' reported in this work is unique in the authors' knowledge.

Examination of the microstructures and the heat treatment histories lead to the exclusion of certain samples. Specimens containing only medium and fine γ' were selected for correlations. From the KM4 MK series, samples with the MK7 and MK8 heat treatments were excluded since the subsolvus solutioning heat treatments lead to the presence of significant amounts of primary γ' . From the SR3 MS series, samples MS4F and MS5f were excluded due to the presence of very coarse cuboidal γ' . The grain coarsening heat treatment of certain samples produced either finer or coarser grained materials. It was decided for this correlation that grain size effects such as Hall-Petch strengthening would not be considered. The size range was therefore limited to a range in ASTM grain size number of 1.5 or less. This gives a change in the average diameter of less than a factor of 2. Based on this criteria, samples MS1, MS2, MK7 and MK8 were excluded from the correlations.

To determine if a correlation was significant, the values for R^2 and adjusted R^2 were examined. Correlations were not considered significant if the value of R^2 was less than 0.3. A correlation was considered of increasing significance for R^2 greater than 0.3 and less than 0.5. In these cases the adjusted R^2 values were also examined, where R^2 is adjusted for the number of variables (11). If the adjusted R^2 values were below 0.3 the correlation is probably not significant. For R^2 values greater than 0.7, the correlation was considered very significant. In correlations of a response with a single variable using 12 data points, $R^2 = .30$ implies a correlation is statistically significant at a probability of 51% (11). The t values of the coefficients and constants are also reported, and were greater than 1.5 unless otherwise noted. In most cases the t values for the coefficients were greater than 2.5 for cases where the R^2 values indicated a significant correlation. The major exceptions were for the correlations where R^2 was less than 0.3 and in the two variable cases. In correlations of a response with a single variable using 12 data points, $t = 2.5$ implies a correlation is statistically significant at a probability of 98.5%.

The cross-correlation factors for the two variable cases are not reported, but all two variable models reported passed tests to determine that the independent variables were truly independent and the models could be improved through the addition of a second variable. Examination of the t values for certain cases does indicate that additional independent variable has a marginal value and additional testing should be conducted.

1200°F Tensile Strength

The first attempted correlation was between the volume fraction of the medium and fine γ' and the 1200°F (649°C) tensile strengths of the alloys. Since the total volume fraction of each sample was equal to the sum of only the medium and fine γ' classes and the total amount in each sample was fixed at a single value, the variables for the two volume fractions are not independent. As a result, the slopes are identical in magnitude but opposite in sign. However, for completeness and a check on the statistical analysis, the analysis was extended to include both classes instead of just one. For the statistical analysis, SigmaStat³ statistical analysis software was used for linear and multiple linear regression as well as best subset regression.

³ SigmaStat Version 2.0 is produced by Jandel Scientific Software, P.O. Box 7005, San Rafael, CA 94912-7005

Figure 10 shows the dependency of the 1200°F yield and ultimate tensile strengths on the volume fraction of each class of γ' for both the SR3 MS series and the KM4 MK series. Table 10 gives the statistical analysis of the fit of the data.

In both cases, there was a good correlation between the volume fractions of the γ' and the strength of the alloys. The analysis corroborates the previously observed trend of larger volume fractions of medium γ' giving higher strengths. The interdependency of the medium and fine γ' volume fractions leads to the opposite trend of lower volume fractions of fine γ' giving higher strengths. However, the direct correlation of strength with volume fraction of medium γ' is more physically realistic.

Figure 11 shows the dependency of the 1200°F yield and ultimate tensile strengths on the average size of each γ' class for both the SR3 MS series and the KM4 MK series. In this case, the major axis was used for both plots since it gave a better fit for the regression. The average sizes of the various classes of γ' are independent of each other, so the size variables are fully independent.

The results of the statistical analysis of linear regression of the data are presented in Table 11. Strength increased with decreasing size of medium γ' and increasing size of fine γ' . The results for both feret diameters and major axes are presented. The trend for each was the same, but for the tensile strengths the major axis gave higher values for R^2 . The independence of the variables also allowed for multiple linear regression of the data using both the fine and medium γ' sizes as the independent variables versus either the yield or ultimate tensile strength as the dependent variable. The results showed that both the R^2 and adjusted R^2 values increased above the values for either size class alone. This indicates that using both values in the correlation gives a better fitting model. Analysis also indicated that the two variable cases were marginal improvements over the one variable cases. The t value for the fine γ' coefficients in the SR3 models were lower than desirable, but the KM4 t values are sufficiently large to warrant further examination of the two variable models.

Figure 12 shows the results for plotting the model generated using both the fine and medium γ' sizes as the independent variables. A contour plot was used to present the three dimensional space. The lines indicate combinations of medium and fine γ' sizes that give the strength indicated by the value associated with each line.

The two variable model uses the limited number of points in the test matrix to generate a large space. However, the trends do appear to be consistent with previous and expected results. Decreasing the medium γ' sizes increases the strength of the samples as would be expected from strengthening models such as the Ashby-Orowan (12) or similar models. Increasing the fine γ' sizes increases the strength. The effects of the fine γ' has not been reported previously to the authors' knowledge. Examination of the model indicates that there may be an optimum size of between 60 and 200 nm for all of the γ' to give maximum strengthening.

Figure 13 gives a comparison between the actual values of the tested samples and the predicted values. In the best case where the values predicted by the two variable model exactly matches the experimental data, the points will fall on a line with a slope of 1, and the R^2 value for a linear regression through the data points will be 1. Deviations from the ideal plot indicates how well the two variable model describes the strength of the alloys.

Examination of results in Figure 13 for the SR3 MS series shows that the slope of the line is very close to 1, but the R^2 values are low ($R^2 \leq 0.4326$). Looking at the data points, the strength of the MS3 samples was the lowest of the MS samples, but the γ' sizes were in the middle of the MS series size range. The MS3 data points may be outliers, but the small number of data points precludes the exclusion of the two results. Nonetheless, examinations of the plots and the goodness of fit of the data when the

MS3 data points are excluded leads to the conclusion that the two variable model accurately predicts the strengths of SR3.

In the case of the KM4 MK series, the yield data gives excellent results with a very high R^2 value and a slope very close to 1. The slope and the R^2 values for the UTS are not as good, but are close enough to the ideal values that, given the small number of data points, the two variable model can be considered valid and capable of predicting the KM4 UTS.

Further analysis was done trying to fit the results to a simple models combining size and volume fraction. The results did not show any good correlation between the models and the results for either alloy and are therefore not presented here. Additional attempts were made to correlate the strength with subsolvus and supersolvus heat treatments. The strong correlation between γ' size and heat treatment appear to fully confound the statistical analysis. Therefore no results are presented here. An analysis was also done to correlate the strength with stabilization for the SR3 samples. The results showed no correlation between the strength and stabilization.

1200°F Time To 0.2% Creep

In the regression of the data for the time to 0.2% creep and crack growth rates, analysis was done using both the measured values and the common (base 10) logarithm of the measured values. These two models will be referred to as the linear and logarithmic models respectively. The determination of which gave a better fit was again based on the R^2 values. When a difference was observed it tended to be distinct.

The time to 0.2% creep was plotted against the γ' volume fractions in Figure 14. Time to 0.2% creep increased with increasing volume fraction of medium γ' in SR3. Both the actual creep rate and the common logarithm of the creep rate were used in analyzing the best fit of the data. Table 12 shows the results of the statistical analysis of the fits. In the case of the SR3 MS series, the linear model using the actual creep rate gives a significantly better fit ($R^2 = 0.675$ vs. $R^2 = 0.345$). A similar increase was observed in the adjusted R^2 values. For the KM4 MK series, both models gave only a marginal fit. The R^2 values for the logarithmic model were slightly higher than the linear model, but both were only just above 0.3. Based on this result, either model could be used, but neither indicates a strong correlation between the γ' volume fraction and the KM4 creep rate. The low correlations in KM4 appear related in part to the small range of times to 0.2% creep observed (300 to 850 hours).

The dependency of the time to 0.2% creep was plotted against the major axis sizes for the MS and MK series in Figure 15. Time to 0.2% creep linearly increased with increasing size of medium γ' and decreasing size of fine γ' in SR3. The statistical analysis presented in Table 13 indicated that the major axis values gave a better fit than the feret diameters for the data based on the R^2 values. Table 13 also shows that, in the case of the SR3 MS series, the best results in fitting the data are obtained using the unmodified time as the dependent variable instead of the common logarithm of the time. The increase in the fit as measured by the R^2 values is very large. Since the test conditions were held constant at 1200°F and 115 ksi, the testing actually measures the variation in the creep life at a given condition caused by changes in the microstructure. As such, it does not have to follow a logarithmic relationship such as those observed for Hall-Petch, power law creep and other logarithmic models. It is therefore probably most appropriate to use the best fitting model, in this case the linear models, for the SR3 correlations.

The SR3 results were also analyzed to determine if the stabilization and solution heat treatments were contributing factors to the observed trends. Statistical analysis showed that there was no statistically significant correlation between the observed times to 0.2% creep and stabilization. However, inspection of Figures 14 and 15 suggests this lack of correlation is due to confounding of stabilization and solution heat treatments in this limited data set. Stabilized specimens consistently had lower creep resistance than

unstabilized specimens after either supersolvus or subsolvus heat treatments. This was consistent with previous observations (5). The other factor examined was the role of the solutioning heat treatment on the time to 0.2% creep. The results appear to be confounded by the strong correlation of the γ' size with the solution heat treatment. As such, no correlation is reported for the solutioning heat treatment. However, inspection of the Figures 14 and 15 indicated supersolvus solution treated specimens have longer creep lives.

For the SR3 samples, the statistical analysis shows that the inclusion of a second variable in the model increases the R^2 and adjusted R^2 values. For the logarithmic value, the correlation remains marginal ($R^2 \leq 0.387$), and the t values for some of the coefficients are lower than desirable. In the linear case, the two variable models have t values for the coefficients greater than 2.40. This is a very strong indication that the two variable linear model is a significant improvement over the single variable model. The linear two variable model for the major axis was used to generate the contour plot shown in Figure 16. The model for the feret diameter shows the same trends and has the same R^2 value. The trend observed is somewhat contradictory in that the model shows increased times to 0.2% creep when the medium γ' size increases but the fine γ' size decreases. The reason for this is unclear, but could involve deformation mechanisms involving movement of dislocations through regions of fine γ' by particle shearing combined with the effective pinning of dislocations by the medium γ' to produce Orowan looping. It also points to a minimum γ' size being required to get improvements in the creep life of SR3. The detailed analysis of the dislocation/ γ' precipitate interactions is beyond the scope of the present study. However, the operative deformation mechanisms do govern these correlations.

Figure 17 compares the actual and predicted values for the creep lives of the SR3 samples. As with the two variable tensile models, the plots should generate a line with a slope of 1 and an R^2 value of 1 if the model accurately describes the actual data. The results do show that the criteria are met. However, the plot also shows that while the statistics of the model are very favorable, the predicted times to 0.2% creep for some of the samples are actually negative. Reviewing the groupings of the data in Figure 17, the values tend to be either very high or very low. Under these conditions the regression would automatically tend to R^2 values near 1. The slope of the line is essentially 1, though, indicating the trend is correct in direction and magnitude. The small number of data points in the data set and the manner in which they are grouped at two extremes are probably causing the coefficients to be slightly incorrect, resulting in the negative values. If additional data points are generated, the model may be improved to eliminate the negative values. Until that time, the best way to view the model is there is a strong probability that both the fine and medium γ' sizes affect the creep lives of SR3 according to the indicated trends, though the magnitude of each coefficient in the model could change with additional data.

In the case of the KM4 specimens, neither the linear nor logarithmic models showed significant correlation ($R^2 \leq 0.238$) using either the feret diameters or the major axes. From this the conclusion is that there is no correlation between γ' size and the time to 0.2% creep in these KM4 specimens.

Limited attempts were made to correlate the time to 0.2% creep with some combination of volume fraction and size. The results did not indicate any strong correlations for simple models such as the summation of each volume fraction times the average size. It was felt that further work and analysis of theoretical models was required, so no correlations of this type are presented.

1200°F Hold Time Fatigue Crack Growth Rates

Both 1200°F and 1300°F (704°C) hold time fatigue crack growth tests were conducted on the SR3 MS series. Of those samples tested at 1200°F with data available, only four were from samples that met the other criteria for inclusion in the analysis. The previous analysis (5) employed a multiplication factor of 0.05 on 1300°F dwell fatigue crack growth rates to approximate 1200°F dwell fatigue crack growth rates. To minimize complications to the analysis of the data, the decision was made not to

convert the 1300°F data. Without those additional data points, it was felt that an insufficient number of tests were run on the SR3 MS series to give meaningful results. As a result, the 1200°F hold time fatigue crack growth rate analysis is limited to the KM4 MK series.

The crack growth rate was plotted against the γ' volume fraction in Figure 18. As with the creep data, the crack growth rate was analyzed as both the common logarithm of the crack growth rate and the crack growth rate itself. Table 14 presents the statistical results of the analysis for both the linear and logarithmic models. The logarithmic model did not give a significant correlation ($R^2 = 0.210$), but the linear model did give a marginal correlation ($R^2 = 0.424$). The linear case should be treated with caution, though, as the adjusted R^2 value was only 0.180.

Examination of the plots of the data show that the results are strongly influenced by the highest medium γ' data point. Without that point there would be no significant correlation observed for the data. Based on this analysis of the data and the statistical analysis leads to the conclusion that there is probably no strong dependence of the 1200°F hold time fatigue crack growth rate on the volume fractions of the medium and fine γ' for the KM4 specimens.

There was a strong correlation observed between the heat treatment and the crack growth rate. Figure 19 shows plots of the crack growth rate dependency on the heat treatment. The strongest correlation ($R^2 = 0.9972$) was determined to be the natural logarithm of the crack growth rate versus the type of heat treatment, subsolvus or supersolvus. A weaker but still very statistically significant correlation ($R^2 = 0.8787$) was observed between the natural logarithm of the crack growth rate and the solutioning heat treatment temperature. The observation that the crack growth rate for the intermediate solution temperature specimens did not differ significantly from the lower temperature solution heat treatment tends to reinforce the importance of the solutioning heat treatment temperature relative to the actual solvus temperature of the alloy as opposed to simply the absolute temperature.

The correlation observed between the crack growth rate and the type of solutioning heat treatment is consistent with the failure mode of the samples previously observed (6). Inspection of Table 2b indicated the grain sizes varied among the regressed samples by only 1 ASTM grain size number (ASTM 4.4-5.4). However, for the six heat treatments used in this correlation, subsolvus heat treated samples failed by intergranular crack propagation while supersolvus heat treated samples failed by either mixed mode or transgranular crack propagation. This suggests the crack propagation mode was sensitive to microstructural parameters other than grain size, which varied with solution heat treatment temperature. Insufficient information was available on the crack growth modes to meaningfully correlate the crack growth rate and the degree of transgranular cracking or similar characteristics of the cracks.

Table 15 presents the statistical results of the analysis for both the linear and logarithmic models of crack growth dependency on γ' size. Crack growth rate decreased with decreasing size of medium γ' . In the case of the crack growth rate data, the statistical analysis indicated that the feret diameter gave a better fit for the data. The logarithmic model gives a very good fit to the feret diameter data ($R^2 \geq 0.815$) and the major axis data ($R^2 \geq 0.691$). However, the linear model using the feret diameter increases R^2 to 0.932, a value improved even beyond the logarithmic case. The same trends are true for the adjusted R^2 values. Given the high values of R^2 in both cases, the final choice of which model to use should be determined based on metallurgical principles rather than statistics.

Figure 20 shows the crack growth rate plotted against the average feret diameters for the medium and fine γ' classes. Both the logarithmic and linear models are presented. The observation must be made that the results tended to be grouped into two extremes that were dependent on the type of solutioning heat treatment used. These groupings will significantly improve the fit of the models to the data. The grouping were most likely related to the change in crack growth mode from intergranular in inferior specimens to mixed or transgranular modes in specimens having slow crack growth rates (6). The groupings and overlap of the data lead to questions regarding the form of the function. It may be

that the results indicate a step function or some other discontinuous function instead of the presented linear functions. Without intermediate data the question cannot be fully resolved.

Table 15 also includes an analysis of the two variable case using both the fine and medium γ' sizes. The value of R^2 is high for both the feret diameter and major axis cases. Analysis of the adjusted R^2 and t values indicates the inclusion of a second term in the model has marginal benefits at best. In particular, the low t values for the fine γ' coefficients indicates a one variable model would probably be preferable for the crack growth. Based on this no contour plots were generated for the crack growth models.

Comparison To Previous Results

The previous analysis (5, 6) of the microstructure-property relationships in these SR3 and KM4 specimens also included data from a broad range of alloys including IN100, 456, René 88DT, and CH98, with varied compositions and microstructures. This was necessary to provide guidance for the design of compositions and microstructures which could improve mechanical properties for supersonic cruise applications. It also did not always include all measurements of fine γ' distributions, since these data were not available for all the alloys and conditions examined. The major factors affecting strength, creep life and crack growth were determined to generally be related to the chemistry and the medium γ' size. By focusing the present analyses on constant SR3 and KM4 compositions and limiting the microstructural variables to only the γ' sizes and volume fractions, a more focused evaluation of the effects of the γ' distribution on mechanical properties was possible. The single variable microstructural trends determined here for the SR3 and KM4 specimens are presented in Table 16. For comparison, the microstructural results from the previous study are also presented (5). Microstructure-property relationships reported significant in both analyses tended to be consistent. In two cases there is no reported correlation for the present analysis, where a correlation was observed in the previous analysis. In these cases, the values of R^2 were below the threshold of 0.3 deemed to be significant in the present study. For example, in the case of the hold time fatigue crack growth rate, a correlation was previously reported for the fine γ' , but the correlation was only at a value of $R^2 = 0.23$. This falls below the level chosen for significance in the current study. The advantages of eliminating compositional and grain size variables allow for the determination of γ' size and volume fraction effects that could have been previously masked by other effects. Therefore, the present observations act to supplement the previous analysis and give information on desirable microstructural changes that could be useful for current and future alloys.

As part of this supplementary analysis, γ' volume fraction and size correlations were assessed separately, rather than simultaneously. This allowed unfettered evaluations of which types of γ' had potential relationships with mechanical properties, using either volume fraction or size as indicators. Statistical forward or reverse selection processes among all of these variables have been used to select the best linear correlation of mechanical properties with these variables (5,6). However, constitutive models usually do not relate mechanical properties to linear combinations of volume fractions and sizes of different strengthening precipitates. Such constitutive models usually employ functional relationships using precipitate volume fraction and size to relate mechanical properties to deformation mechanisms, e.g. interparticle spaces available for unimpeded dislocation motion, total particle area which must be sheared by dislocations, and the critical radius a dislocation must bend to loop around a particle (1). In future work, the KM4 and SR3 microstructure and mechanical property data will be evaluated using these constitutive models to relate both volume fraction and size of different types of γ' to mechanical properties.

The microstructure-property relationships observed here agreed with some empirical trends previously reported for other disk alloys. The increase of strength with γ' content, and inverse dependence of strength with medium γ' size is well-documented (1). The correlations of fine γ' size and

content with strength and creep resistance have not been widely reported to the authors' knowledge. Relationships of dwell crack growth rates with grain boundary serration amplitude and carbide density have been suggested throughout the general literature, due to the predominantly intergranular crack growth mode often observed in these conditions. However, dwell crack growth rates were correlated in the present study only for stabilized KM4 specimens, which had comparable carbide densities and similar serrations at the grain boundaries. Therefore, such relationships could not be assessed here.

The correlations of KM4 γ' microstructures with properties may be considered representative of disk alloys in this general composition class having near 55% medium γ' content, which are subjected to current stabilization heat treatments. These trends indicate tensile strength and dwell fatigue crack growth resistance can be strongly affected by changing γ' distributions. This should be of use in optimizing heat treatments, and should also be considered when heat treating large disks. For example, slower cooling rates or lower solution temperatures in the interiors of thick disks could induce significantly different microstructures from surface locations. This could produce lower strengths and faster crack growth rates at these interiors than at surface locations. However, 0.2% creep resistance is relatively low for all KM4 microstructural variations tested, with no strong γ' microstructure-creep correlations observed. This was apparently due to the stabilization heat treatments applied to all KM4 specimens. Judging from the trends observed in SR3, this appears related in part to the effects of the stabilization heat treatment on fine γ' size. It appears that alternative stabilization heat treatments and altered compositions (5, 6) will be necessary for improved creep resistance.

Summary and Conclusions

The γ - γ' microstructures of two advanced powder metallurgy disk alloys, KM4 and SR3, were quantified after a series of heat treatments using transmission electron microscopy and image analysis. Generally three size classes of γ' were observed in the samples. Large (600 nm or greater), irregularly shaped γ' were classified as the coarse γ' precipitates. Cuboidal or irregularly shaped γ' precipitates between 100 nm and 600 nm were classified as medium γ' precipitates. Spherical γ' precipitates less than 100 nm were classified as fine γ' precipitates. Relationships between the heat treatments and the resulting γ' distributions were evaluated. Statistical correlations between the sizes and volume fractions of γ' and the reported tensile strengths, creep resistances, and dwell crack growth resistances were separately assessed for each alloy.

- Subsolvus solution heat treatments produced varying quantities of cuboidal medium γ' which were apparently remnant “cooling” γ' medium from the previous grain coarsening heat treatment. Supersolvus solution heat treatments produced dendritic medium γ' which apparently formed during the quench from the solution treatment. Faster cooling rates produced finer dendritic medium γ' . This is consistent with the supposition.
- Spherical fine γ' formed during the solution quench, stabilization, and aging heat treatments. The insertion of stabilization heat treatments before aging heat treatments consistently gave larger fine γ' sizes in SR3, but stabilization produced varying fine γ' sizes in KM4.
- In both alloys, yield and tensile strength increased with increasing volume fraction of medium γ' . Strengths also increased as the size of the medium γ' decreased and the size of the fine γ' increased.
- Time to 0.2% creep in SR3 increased with increasing volume fraction and size of medium γ' , and decreasing size of fine γ' . However, 0.2% creep time was not clearly correlated with the γ' microstructures of KM4 specimens. It appears the effects of the stabilization heat treatments on KM4 were a greater influence than the other variables assessed in this study.
- Dwell fatigue crack growth rate decreased with increasing volume fraction of medium γ' , indicating more medium γ' is beneficial. The crack growth rate also decreased with decreasing γ' size, indicating finer γ' is better. A correlation also was observed between the crack growth rate and the type of solutioning heat treatment, and it is probably interrelated with the γ' size.
- In alloys similar to KM4 subjected to the present stabilization heat treatments, tensile strength and dwell crack growth resistance can be affected by γ' microstructural modifications. However, the 0.2% creep resistance does not strongly respond to γ' variations, and may vary more with composition.

References

1. R. F. Decker, "Strengthening Mechanisms in Nickel-Base Superalloys", Steel Strengthening Mechanisms Symposium May 5-6, 1969, Zurich, Switzerland, Climax Molybdenum Co., 1969.
2. Enabling Propulsion Materials Program Annual Technical Progress Report, Vol. 5: Task K-Long-Life Compressor/Turbine Disks, FR-22596-3, NASA Contract NAS3-26385, Nov. 30, 1996.
3. D. P. Mourer, E. Raymond, S. Ganesh, and J. M. Hyzak, "Dual Alloy Disk Development", *Proceedings of the Eighth International Symposium on Superalloys*, September 22-26, 1996, Champion, PA, ed. R. D. Kissinger, D. J. Deye, D. L. Anton, A. D. Cetel, M. V. Nathal, T. M. Pollock, and D. A. Woodford, The Minerals, Metals, and Materials Society, Warrendale, PA, 1996.
4. Enabling Propulsion Materials Program Annual Technical Progress Report, Vol. 2-Task K-Long-Life Compressor/Turbine Disks, NASA Contract NAS3-26385, June 25, 1995.
5. J. J. Schirra, HSR/EPM Coordination Memorandum 05-P96062809, June 28, 1996.
6. R. Montero, M. L. Henne, HSR/EPM Coordination Memorandum 05-P96112714, Nov. 27, 1996.
7. "Applications of Quantitative Metallography," E.E. Underwood, *Metals Handbook, Vol. 8*, 8th Ed., ASM International, Materials Park, OH (1973), pp. 37-47.
8. T. P. Gabb, A. Garg, D. L. Ellis, "Microstructural Evaluations of Baseline HSR/EPM Disk Alloys", NASA HSR034, National Aeronautics and Space Administration, Lewis Research Center, Cleveland, OH, 1996.
9. R. L. Dreshfield, "Effects of Heat Treating PM René 95 Slightly Below The γ' Solvus", NASA TM X-73663, National Aeronautics and Space Administration, Washington, D.C., 1977.
10. R. A. Ricks, A. J. Porter, R. C. Ecob, "The Growth of γ' Precipitates in Nickel-Base Superalloys", *Acta Metall.*, V. 31, 1983, pp. 43-53.
11. J. Neter, W. Wasserman, M. H. Kutner, *Applied Linear Statistical Models*, Richard D. Irwin, Inc., Homewood, Illinois, 1985, pp. 67-503.
12. M.F. Ashby, *Oxide Dispersion Strengthening, AIME Conference Proc.*, New York, NY, 1966, p. 143.

Table 1 -
Nominal Compositions Of SR3 And KM4

Element	SR3	KM4
Al	2.6	4.0
B	0.015	0.030
C	0.030	0.030
Co	11.9	18.0
Cr	12.8	12.0
Hf	0.20	
Mo	5.1	4.0
Nb	1.6	2.0
Ni	Bal.	Bal.
Ti	4.9	4.0
Zr	0.030	0.030
Solvus	2140°F (1171°C)	2140°F (1171°C)

All values are in weight percent

Table 2a -
Heat Treatment Matrix For SR3 MS Series

MS	Grain Coarsening	Solution	Cooling Rate	Stabilization	Aging	ASTM Grain Size	Average Grain Diameter (mm)
1	2070/1 + 2180/3 + AC	1975/1 + AC	190°F/min		1400/8 + AC	3.2	0.119
2	2070/1 + 2180/3 + AC	2140/1 + IAC	120°F/min	1550/4 + AC	1400/8 + AC	2.3	0.162
3	2075/1 + 2160/2 + AC	1975/1 + IAC	70°F/min	1550/4 + AC	1400/8 + AC	6.0	0.045
4	2075/1 + 2160/2 + AC	2140/1 + OQ	>300°F/min		1400/8 + AC	6.5	0.038
4F	2075/1 + 2160/2 + AC	2140/1 + FAC	250°F/min		1400/8 + AC	5.9	0.047
5	2075/1 + 2160/2 + AC	2140/1 + OQ	>300°F/min	1550/4 + AC	1400/8 + AC	6.7	0.035
5F	2075/1 + 2160/2 + AC	2140/1 + FAC	280°F/min	1550/4 + AC	1400/8 + AC	5.8	0.048
6*	2140/2 + AC	2140/1 + IAC	130°F/min		1400/8 + AC	6.0	0.045
7*	2075/1 + 2160/2 + AC	2045/1 + IAC	164°F/min		1400/8 + AC	5.8	0.048
8	2140/2 + AC	2045/2 + FAC	250°F/min	1550/4 + AC	1400/8 + AC	6.6	0.037

*MS6 and MS7 reflect the actual heat treatments of the samples (see text)

AC - Air cooled (medium cooling rate)

IAC - Insulated air cooled (slow cooling rate)

FAC - Fast air cooled (fast cooling rate)

OQ - Oil quench (very fast cooling rate)

All temperatures in degrees Fahrenheit and times in hours

Table 2b -
Heat Treatment Matrix For KM4 MK Series

MK	Grain Coarsening	Solution	Cool Rate (1600°F)	Cool Rate (1000°F)	Stabilization	Aging	ASTM Grain Size	Average Grain Diameter (mm)
1	2070/1 + 2180/3 + AC	1990/1 + FAC	780°F/min	350°F/min	1600/2 + AC	1400/8 + AC	4.4	0.078
2	2070/1 + 2180/3 + AC	2150/1 + IAC	110°F/min	85°F/min	1550/4 + AC	1400/8 + AC	4.6	0.073
3	2075/2 + 2160/2 + AC	1990/1 + IAC	68°F/min	68°F/min	1550/4 + AC	1400/8 + AC	5.3	0.057
4	2075/2 + 2160/2 + AC	2150/1 + FAC	611°F/min	338°F/min	1600/2 + AC	1400/8 + AC	5.4	0.055
5	2075/2 + 2160/2 + AC	2150/1 + FAC	367°F/min	288°F/min	1550/4 + AC	1400/8 + AC	5.2	0.059
6	2075/2 + 2160/2 + AC	2060/1 + IAC	85°F/min	68°F/min	1600/2 + AC	1400/8 + AC	5.1	0.061
7	2075/2 + 2130/2 + AC	2130/1 + IAC	113°F/min	84°F/min	1600/2 + AC	1400/8 + AC	5.9	0.047
8	2075/2 + 2130/2 + AC	2060/1 + FAC	3067°F/min	815°F/min	1550/4 + AC	1400/8 + AC	7.0	0.032

AC - Air cooled (medium cooling rate)

IAC - Insulated air cooled (slow cooling rate)

FAC - Fast air cooled (fast cooling rate)

All temperatures in degrees Fahrenheit and times in hours

Table 3 -
Minor Phases Observed In SR3 MS Series

Phase	Baseline		MS1-1		MS2-1		MS3-1		MS4-1		MS5-1		MS5F-1		MS6-1		MS7-1		MS8-2	
	No. Dens.	Size Range																		
Matrix	50%	200-600	48%	300-1,200	48%	150-400	48%	200-900	48%	140-600	48%	170-700	48%	500-1000	48%	170-1000	48%	200-800	48%	200-800
(Ti,Nb)C	50%	50-400	48%	100-450	48%	50-250	48%	50-250	48%	50-250	48%	50-270	48%	100-550	48%	50-650	48%	50-290	48%	50-290
(Hf,Zr)O ₂	ND																			
(Mo,Cr) ₃ B ₂	ND																			
(Ti,Mo) ₆ C	ND																			
Present occasionally (4%), Size Range = 500 - 3600 nm																				
Grain Bound.	95%	10-100	92%	300-600	92%	150-500	92%	20-200	92%	20-700	92%	100-300	92%	30-400	92%	50-150	92%	50-150	92%	50-250
(Ti,Nb)C	5%	300-600	5%	700-1000	5%	300-600	5%	300-1500	5%	300-1500	5%	400-900	5%	600-700	5%	400-900	5%	600-700	5%	600-800
(Hf,Zr)O ₂	ND		ND		ND		Very Few	300-400	ND											
(Mo,Cr) ₃ B ₂	ND		ND		ND		Very Few	800-2200	ND											
(Ti,Mo) ₆ C	ND		ND		ND		Very Few		ND											
Present occasionally (3%), Size Range = 500 - 3600 nm																				

All dimensions in nm
ND-Not Detected

Table 4 -
Minor Phases Observed In KM4 MK Series

Phase	Baseline			MK1-1			MK2-1			MK3-2			MK4-1			MK5-1			MK6-1			MK7-1			MK8-2		
	No. Dens.	Size Range	No. Dens.	Size Range	No. Dens.	Size Range	No. Dens.	Size Range	No. Dens.	Size Range	No. Dens.	Size Range	No. Dens.	Size Range	No. Dens.	Size Range	No. Dens.	Size Range	No. Dens.	Size Range	No. Dens.	Size Range	No. Dens.	Size Range			
Matrix	60%	150-600	60%	200-900	60%	300-1,200	60%	200-600	60%	200-700	60%	200-700	60%	200-700	60%	300-700	60%	300-700	60%	300-700	60%	200-700	60%	200-700	60%	300-800	
Al_2O_3/ZrO_2	30%	200-800	30%	50-200	30%	50-200	30%	50-200	30%	50-450	30%	50-450	30%	50-450	30%	50-500	30%	50-500	30%	50-500	30%	50-250	30%	50-250	30%	50-250	
$(Mo,Cr)_3B_2$	5%	500-1,000	5%	500-1,000	5%	500-1,000	Present occasionally (5%), Size Range = 500 - 1500 nm																				
$(Ti,Mo)_6C$	5%	1000-2,500	5%	1000-2,500	Present occasionally (5%), Size Range = 1000 - 2500 nm																						
Grain Bound.	90%	20-100	90%	100-700	90%	100-450	90%	350-700	90%	100-350	90%	100-350	90%	100-300	90%	100-300	90%	100-300	90%	100-300	90%	100-300	90%	100-300	90%	100-150	
$(Ti,Nb)C$	5%	150-600	5%	500-700	5%	500-700	5%	500-800	5%	350-750	5%	350-750	5%	350-750	5%	350-750	5%	350-750	5%	350-750	5%	350-750	5%	350-750	5%	350-700	
Al_2O_3/ZrO_2	ND		ND		Generally not present along the grain boundaries																						
$(Mo,Cr)_3B_2$	2.5%	500-1,000	2.5%	500-1,000	Present occasionally (2.5%), Size Range = 500 - 2600 nm																						
$(Ti,Mo)_6C$	2.5%	1500-2500	2.5%	1500-2500	Present occasionally (2.5%), Size Range = 1500-4500 nm																						

All dimensions in nm
ND-Not Detected

Table 5a -
Summary Of Image Analysis Results For SR3 MS Series - Coarse γ'

		MS4F	MS5F
Precipitates Measured		142	118
Major Axis (nm)	Average	1231.47	1564.46
	σ	200.86	290.51
	Minimum	294.47	968.12
	Maximum	1714.17	2407.48
Minor Axis (nm)	Average	1043.22	1135.96
	σ	232.62	370.92
	Minimum	275.93	396.27
	Maximum	1507.71	2256.56
Ferret Diameter (nm)	Average	925.66	1108.81
	σ	140.34	200.86
	Minimum	276.93	631.00
	Maximum	1280.59	1721.36
Aspect Ratio	Average	0.84	0.71
	σ	0.10	0.14
	Minimum	0.56	0.39
	Maximum	1.00	0.98
Compactness	Average	26.57	31.94
	σ	11.16	19.43
	Minimum	14.00	18.77
	Maximum	88.92	170.49
Shape Factor	Average	0.52	0.46
	σ	0.13	0.13
	Minimum	0.14	0.07
	Maximum	0.90	0.67

Table 5b -
Summary Of Image Analysis Results For SR3 MS Series - Medium γ'

		As-Rcvd	MS1*	MS2	MS3*	MS4	MS4F	MS5	MS5F	MS6*	MS7	MS8*
Precipitates Measured		144	130	500	231	153	439	163	284	134	71	301
Major Axis (nm)	Average	312.39	397.42	441.23	347.41	141.58	335.59	186.60	525.93	340.44	557.51	539.60
	σ	146.12	82.51	179.88	204.06	24.51	143.38	32.99	184.22	89.45	92.36	111.68
	Minimum	80.33	216.17	119.58	32.86	64.98	76.30	111.61	124.93	151.38	362.50	257.19
	Maximum	634.09	640.71	968.58	721.38	217.91	796.97	288.63	1129.22	525.29	829.41	1013.47
Minor Axis (nm)	Average	233.44	325.05	326.36	233.55	115.48	258.88	145.35	381.81	254.22	461.86	447.48
	σ	126.12	82.24	157.93	158.40	24.47	116.71	31.57	148.80	82.86	104.91	131.95
	Minimum	37.87	153.52	83.09	12.98	52.80	52.90	74.93	107.05	98.76	204.01	114.02
	Maximum	498.28	516.25	912.86	562.65	165.25	607.33	236.12	804.64	424.30	670.21	905.57
Ferret Diameter (nm)	Average	243.77	345.99	344.22	272.41	121.22	270.81	157.35	398.81	271.30	470.26	450.18
	σ	107.28	73.56	132.13	167.09	20.73	105.02	26.08	121.64	69.52	49.26	100.04
	Minimum	56.94	193.08	105.51	25.97	60.05	70.63	90.03	122.64	126.54	297.67	192.10
	Maximum	471.59	499.51	738.71	551.73	179.26	597.69	225.93	732.12	398.33	652.25	873.03
Aspect Ratio	Average	0.73	0.82	0.74	0.67	0.81	0.78	0.78	0.73	0.75	0.83	0.82
	σ	0.13	0.12	0.15	0.18	0.10	0.13	0.11	0.14	0.14	0.12	0.14
	Minimum	0.41	0.32	0.30	0.20	0.55	0.36	0.49	0.38	0.40	0.49	0.35
	Maximum	0.98	0.99	0.99	0.98	0.99	1.00	0.97	0.99	0.98	0.98	0.99
Compactness	Average	21.35	19.82	25.35	25.61	25.21	20.88	20.35	28.90	22.78	19.21	22.75
	σ	8.08	7.94	20.37	14.80	14.01	7.15	6.30	14.14	9.17	7.82	9.40
	Minimum	13.66	14.20	13.59	14.55	13.98	12.98	13.93	14.14	14.09	14.44	14.51
	Maximum	67.59	60.96	238.62	117.21	99.46	68.58	47.36	102.15	75.01	67.03	76.95
Shape Factor	Average	0.65	0.70	0.61	0.58	0.60	0.65	0.66	0.51	0.61	0.71	0.62
	σ	0.18	0.17	0.20	0.18	0.22	0.16	0.15	0.18	0.17	0.15	0.17
	Minimum	0.19	0.21	0.05	0.11	0.13	0.18	0.28	0.12	0.17	0.19	0.16
	Maximum	0.92	0.89	0.92	0.86	0.90	0.97	0.90	0.89	0.89	0.87	0.87

*These samples were given a subsolvus solutioning and may contain secondary and cooling γ'

Table 5c-
Summary Of Image Analysis Results For SR3 MS Series - Fine γ'

		As-Rcvd	MS1*	MS2	MS3*	MS4	MS4 F	MS5	MS5 F	MS6*	MS7	MS8*
Precipitates Measured		283	345	568	366	137	778	91	241	233	323	653
Major Axis (nm)	Average	26.00	30.51	48.19	47.83	18.48	50.49	42.00	73.84	19.45	57.15	65.30
	σ	12.39	11.36	17.44	16.30	6.12	27.72	15.12	38.02	8.58	27.38	34.90
	Minimum	2.5	6.00	5.75	14.52	8.17	11.60	13.07	21.70	6.33	14.62	9.28
	Maximum	85.15	72.08	188.93	144.05	41.78	177.70	84.21	234.64	50.48	139.33	247.56
Minor Axis (nm)	Average	18.12	24.74	37.98	37.02	13.98	38.59	33.55	57.33	12.90	47.45	51.80
	σ	9.59	9.21	13.50	0.00	4.44	22.55	12.40	27.87	4.56	22.61	28.00
	Minimum	0.00	3.00	0.00	90.12	5.05	0.00	10.54	14.46	3.92	8.23	0.00
	Maximum	52.43	57.37	144.92	12.45	33.66	141.02	65.67	191.08	28.36	120.73	174.88
Feret Diameter (nm)	Average	23.58	27.30	44.45	40.64	16.92	45.22	37.36	64.99	15.29	51.04	57.12
	σ	9.64	9.75	14.27	12.82	5.02	23.12	13.02	30.21	5.00	23.97	29.07
	Minimum	3.99	5.87	9.17	13.78	7.74	11.80	13.19	22.35	5.77	13.13	9.46
	Maximum	63.21	62.62	143.22	85.24	37.98	147.11	70.06	205.16	30.31	126.63	204.84
Aspect Ratio	Average	0.72	0.82	0.80	0.78	0.77	0.76	0.80	0.79	0.70	0.84	0.80
	σ	0.22	0.10	0.13	0.13	0.13	0.14	0.50	0.13	0.16	0.09	0.12
	Minimum	0	0.44	0.00	0.00	0.33	.00	1.00	0.39	0.29	0.42	0.00
	Maximum	1.00	0.99	1.00	1.00	1.00	1.00	0.10	1.00	1.00	1.00	1.00
Compactness	Average	15.26	15.99	16.01	24.07	14.01	16.11	17.16	16.56	24.39	19.69	19.06
	σ	4.25	4.89	4.40	12.35	1.37	4.04	5.07	5.40	14.50	6.26	7.22
	Minimum	8.00	12.43	8.00	95.58	11.14	9.77	12.49	11.39	12.64	12.37	10.36
	Maximum	39.46	55.42	41.47	11.12	21.08	58.83	40.77	53.48	87.16	73.15	80.18
Shape Factor	Average	0.87	0.83	0.83	0.59	0.90	0.82	0.78	0.81	0.64	0.68	0.72
	σ	0.19	0.14	0.17	0.18	0.08	0.16	0.16	0.16	0.24	0.14	0.17
	Minimum	0.32	0.23	0.30	0.13	0.60	0.21	0.31	0.23	0.14	0.17	0.16
	Maximum	1.57	1.01	1.57	1.02	1.13	1.29	1.01	1.10	0.99	1.02	1.21

*These samples were given a subsolvus solutioning and may contain aging and cooling γ'

Table 6a -
Summary Of Image Analysis Results For KM4 MK Series - Coarse γ'

		MK7
Precipitates Measured		77
Major Axis (nm)	Average	756.75
	σ	127.65
	Minimum	477.73
	Maximum	1003.68
Minor Axis (nm)	Average	627.17
	σ	170.28
	Minimum	243.60
	Maximum	977.98
Feret Diameter (nm)	Average	584.28
	σ	98.47
	Minimum	362.47
	Maximum	763.95
Aspect Ratio	Average	0.82
	σ	0.14
	Minimum	0.45
	Maximum	1.00
Compactness	Average	26.61
	σ	13.94
	Minimum	17.94
	Maximum	116.76
Shape Factor	Average	0.53
	σ	0.13
	Minimum	0.11
	Maximum	0.70

Table 6b -
Summary Of Image Analysis Results For KM4 MK Series - Medium γ'

		As-Rcvd	MK1*	MK2	MK3*	MK4	MK5	MK6*	MK7*	MK8*
Precipitates Measured		38	256	471	229	176	352	321	268	269
Major Axis (nm)	Average	393.80	408.80	346.65	381.37	273.10	240.58	514.89	283.10	493.64
	σ	127.24	84.48	144.08	92.77	70.41	54.19	98.38	72.29	96.00
	Minimum	130.58	122.10	86.98	141.56	87.70	96.36	282.12	121.28	244.70
	Maximum	758.90	608.91	725.38	623.03	450.56	435.87	790.99	495.81	726.99
Minor Axis (nm)	Average	318.59	351.59	223.92	324.11	201.79	163.14	441.75	217.67	429.45
	σ	114.28	87.36	119.16	100.44	64.32	53.64	115.46	66.19	107.48
	Minimum	95.48	102.36	36.30	96.52	57.86	57.22	129.17	77.58	151.23
	Maximum	597.86	542.22	590.77	598.48	345.67	323.57	737.16	405.04	687.91
Feret Diameter (nm)	Average	317.36	355.73	258.61	328.18	219.12	186.88	433.33	230.88	424.24
	σ	90.48	73.99	108.88	82.74	54.75	43.90	84.36	54.94	83.58
	Minimum	111.40	113.25	60.22	123.15	67.37	85.73	213.99	112.98	201.23
	Maximum	535.94	524.53	542.91	544.86	359.35	325.55	648.86	382.94	630.76
Aspect Ratio	Average	0.81	0.86	0.63	0.84	0.74	0.68	0.85	0.77	0.86
	σ	0.12	0.11	0.15	0.12	0.14	0.15	0.12	0.13	0.10
	Minimum	0.45	0.46	0.27	0.48	0.36	0.28	0.43	0.35	0.53
	Maximum	0.98	1.00	0.97	1.00	0.97	0.99	1.00	1.00	0.99
Compactness	Average	19.29	16.53	22.35	18.55	19.95	20.97	17.35	20.52	17.38
	σ	4.98	3.36	8.14	3.96	6.32	5.79	3.09	6.82	3.40
	Minimum	14.39	13.54	14.07	14.33	13.95	14.16	14.20	14.25	14.26
	Maximum	32.75	38.95	95.05	45.44	58.23	50.12	41.13	71.08	35.13
Shape Factor	Average	0.69	0.78	0.61	0.70	0.67	0.64	0.74	0.65	0.74
	σ	0.14	0.10	0.15	0.10	0.15	0.14	0.09	0.13	0.11
	Minimum	0.38	0.32	0.13	0.28	0.22	0.25	0.31	0.18	0.36
	Maximum	0.87	0.93	0.89	0.88	0.90	0.89	0.88	0.88	0.88

*These samples were given a subsolvus solutioning and may contain secondary and cooling γ'

Table 6c -
Summary Of Image Analysis Results For KM4 MK Series - Fine γ'

		As-Rcvd	MK1*	MK2	MK3*	MK4	MK5	MK6*	MK7*	MK8*
Precipitates Measured		77	313	626	261	153	352	590	438	618
Major Axis (nm)	Average	41.52	50.43	33.62	25.65	43.14	30.76	69.06	42.73	71.76
	σ	17.42	15.27	9.56	8.63	17.23	8.85	31.30	17.47	37.08
	Minimum	9.81	13.44	9.43	5.62	9.53	9.93	15.90	17.85	12.93
	Maximum	83.75	103.78	90.30	50.26	117.62	65.99	189.05	126.08	162.59
Minor Axis (nm)	Average	33.76	41.56	22.42	21.75	32.18	30.76	56.26	35.29	55.23
	σ	15.39	13.82	6.73	7.58	12.41	8.85	26.10	15.01	29.35
	Minimum	8.34	7.29	0.00	5.03	7.01	9.93	9.47	9.41	7.01
	Maximum	69.91	93.46	50.98	43.24	73.31	65.99	174.15	112.90	133.77
Feret Diameter (nm)	Average	42.73	45.95	29.58	24.48	37.75	35.04	64.28	40.10	63.02
	σ	15.73	13.70	7.01	7.74	13.56	9.26	27.10	15.30	31.12
	Minimum	9.81	13.26	10.65	7.50	11.78	13.78	15.86	16.69	11.19
	Maximum	73.12	97.43	63.16	47.71	82.02	70.20	177.30	109.09	140.73
Aspect Ratio	Average	.77	0.82	0.67	0.85	0.76	0.80	0.82	0.83	0.78
	σ	.12	0.10	0.13	0.09	0.15	0.11	0.11	0.10	0.12
	Minimum	.43	0.51	0.00	0.50	0.25	0.46	0.36	0.45	0.28
	Maximum	.96	1.00	1.00	1.00	1.00	1.00	1.00	1.00	1.00
Compactness	Average	14.71	16.29	14.46	14.24	16.45	14.64	14.77	14.85	16.62
	σ	1.13	4.06	2.34	2.46	5.90	2.34	2.70	2.62	3.29
	Minimum	12.90	12.53	10.99	10.29	12.22	12.35	10.29	11.49	11.08
	Maximum	19.41	45.73	45.77	35.17	49.79	32.28	30.87	32.85	33.85
Shape Factor	Average	0.85	0.80	0.88	0.90	0.82	0.87	0.87	0.87	0.78
	σ	0.07	0.13	0.10	0.11	0.17	0.10	0.13	0.12	0.14
	Minimum	0.65	0.27	0.27	0.36	0.25	0.39	0.41	0.38	0.37
	Maximum	0.97	1.00	1.14	1.22	1.03	1.02	1.22	1.09	1.13

*These samples were given a subsolvus solutioning and may contain aging and cooling γ'

Table 7a -
SR3 MS Series γ' Size Distribution Fitted Curves

Sample	γ' Class	Peak	Type Of Curve	a_0	a_1	a_2	R^2	
MS1	Medium	1	Gaussian	12.4683	354.9554	82.9117	0.8854	
	Fine	1	Gaussian	22.5243	27.4277	8.7820	0.9390	
MS2	Medium	1	Log Normal	7.4828	281.7680	0.4541	0.9072	
		1	Gaussian	7.6924	248.6565	64.2772		
		2	Gaussian	5.6105	445.5340	86.9776		
	Fine	1	Log Normal	16.8854	41.9960	0.2697	0.9920	
MS3	Medium	1	Gaussian	12.4259	417.8938	73.1812	0.6649	
		1	Gaussian (FFT Filter)	10.1600	419.2817	102.1043	0.9959	
	Fine	1	Gaussian	15.5556	41.7731	12.8575	0.9689	
MS4	Medium	1	Gaussian	42.7195	135.6756	20.7148	0.9751	
	Fine	1	Gaussian	48.6128	18.4137	3.9019	0.9943	
MS4F	Large	1	Gaussian	8.9761	894.8847	77.4302	0.7597	
		2	Gaussian	4.9042	1098.5884	49.7574		
	Medium	1	Gaussian	7.5889	185.5089	47.2897	0.9330	
		2	Gaussian	7.7315	331.3429	79.9952		
		1	Log Normal	9.1757	220.2185	0.4710		0.8818
			1	Gaussian	9.3007	262.5617	107.7951	0.8561
	Fine	1	Log Normal	13.7377	33.8766	0.3579	0.9594	
MS5	Medium	1	Gaussian	38.2255	165.8659	25.6576	0.9906	
	Fine	1	Log Normal	16.6022	34.6953	0.3242	0.9588	

Table 7a (Continued) -
SR3 MS Series γ' Size Distribution Fitted Curves

Sample	γ' Class	Peak	Type Of Curve	a_0	a_1	a_2	R^2
MS5F	Large	1	Gaussian	9.4848	1124.4956	214.1227	0.7919
	Medium	1	Gaussian	6.4765	279.0555	44.1569	0.8748
		2	Log Normal	7.1939	444.7944	0.2246	
		1	Gaussian	7.3699	408.9530	141.7007	0.7846
	Fine	1	Log Normal	10.2401	52.0079	0.3319	0.9475
MS6	Medium	1	Gaussian	6.2463	179.4832	34.4922	0.9402
		2	Gaussian	16.6235	308.4372	46.1234	
	Fine	1	Log Normal	44.7756	15.3503	0.2739	0.9821
MS7	Medium	1	Gaussian (FFT Filter)	11.4780	490.1741	86.1590	0.9772
		1	Gaussian	6.0354	385.4232	41.7101	0.6906
		2	Gaussian	19.0387	505.7411	32.9604	
		1	Gaussian	13.6293	488.6875	74.2807	0.6246
	Fine	1	Log Normal	9.6071	38.9594	0.4836	0.9224
MS8	Medium	1	Gaussian	9.6779	463.5395	106.2913	0.9242
	Fine	1	Log Normal	9.5069	42.6679	0.4427	0.9530

Table 7b -
KM4 MK Series γ' Size Distribution Fitted Curves

Sample	γ' Class	Peak	Type Of Curve	a_0	a_1	a_2	R^2
MK1	Medium	1	Gaussian	14.2531	376.0416	68.5616	0.9767
	Fine	1	Gaussian	15.5659	46.3639	12.3375	0.9142
MK2	Medium	1	Gaussian	7.4460	154.0401	42.067	0.9383
		2	Gaussian	7.2801	324.6491	97.0168	
	1	Log Normal	8.5060	199.0795	0.5559	0.8247	
	Fine	1	Gaussian	28.9954	31.3807	6.8733	0.9956
MK3	Medium	1	Gaussian	4.8974	247.5705	52.6088	0.8986
		2	Gaussian	14.6362	370.8001	44.2572	
		1	Gaussian	14.4123	359.4994	60.5255	0.8426
	Fine	1	Gaussian	24.5968	27.0859	8.1926	0.9954
MK4	Medium	1	Gaussian	17.3124	230.6250	58.3039	0.9857
	Fine	1	Gaussian	14.5618	39.5704	13.8887	0.9134
MK5	Medium	1	Log Normal	21.1829	187.6796	0.2493	0.9562
	Fine	1	Gaussian	22.8513	35.9400	8.2377	0.9750
MK6	Medium	1	Gaussian	11.6900	448.9910	85.4157	0.9309
	Fine	1	Log Normal	9.9855	51.4845	0.3430	0.9226

Table 7b (Continued) -
 KM4 MK Series γ' Size Distribution Fitted Curves

Sample	γ' Class	Peak	Type Of Curve	a_0	a_1	a_2	R^2
MK7	Large	1	Gaussian	18.9633	623.8193	108.1253	0.9692
	Medium	1	Gaussian	17.4178	243.5435	58.0967	0.9794
	Fine	1	Log Normal	18.8359	36.1016	0.2686	0.9832
MK8	Medium	1	Gaussian	5.0462	326.4586	35.4643	0.9133
		2	Gaussian	12.8780	460.4450	61.6735	
		1	Gaussian	12.3886	454.7014	74.2010	0.8568
	Fine	1	Log Normal	9.1231	29.2851	0.2951	0.9233
		2	Log Normal	6.1448	81.3356	0.2011	

Table 8 -
SR3 MS Series γ' Volume Fractions

	Sample									
	MS1	MS2	MS3	MS4	MS4F	MS5	MS5F	MS6	MS7	MS8
Total Area Fraction*	60.4%	60.4%	60.4%	60.4%	60.4%	60.8%	60.4%	60.0%	60.4%	60.4%
Coarse (>600 nm) Volume Fraction					28.0%		25.0%			
Medium (100-600 nm) Volume Fraction	37.0%	56.0%	45.4%	49.0%	18.0%	59.2%	20.0%	60.0%	40.9%	42.8%
Fine (<100 nm) Volume Fraction	23.4%	4.4%	15.0%	11.4%	14.4%	1.6%	15.4%	<1 %	19.5%	17.6%

* Assumed based on average of MS5 and MS6
MS5 and MS6 are direct measurements

Table 9 -
KM4 MK Series γ' Volume Fractions

	Sample							
	MK1	MK2	MK3	MK4	MK5	MK6	MK7	MK8
Total Area Fraction*	64.3%	64.3%	64.3%	67.6%	61.0%	64.3%	64.3%	64.3%
Primary (>1 μ m) Volume Fraction							3.8%	5.9%
Coarse (>600 nm) Volume Fraction							22.6%	
Medium (100-600 nm) Volume Fraction	57.1%	52.1%	54.3%	~67.5%	59.3%	53.2%	29.5%	31.3%
Fine (<100 nm) Volume Fraction	7.2%	12.2%	10.0%	«1%	1.6%	11.1%	8.4%	27.0%

* Assumed based on average of MK 4-1 and MK 5-1
MK4 and MK5 are direct measurements

Table 10a -
 SR3 MS Series 1200°F Tensile Strength Versus γ' Volume Fraction Curve Fit

$$\sigma = b_0 + b_1 f_{Medium} + b_2 f_{Fine}$$

1200°F Yield Strength					
Independent Variables	Medium	Fine	Constant	R ²	Adj. R ²
1	0.861 (1.536)		105.0 (3.729)	0.208	0.12
1		-0.861 (-1.536)	157.1 (20.589)	0.208	0.12

1200°F Ultimate Tensile Strength					
Independent Variables	Medium	Fine	Constant	R ²	Adj. R ²
1	0.705 (2.517)		179.2 (12.739)	0.413	0.348
1		-0.705 (-2.517)	221.9 (58.009)	0.413	0.348

Models represent the best fit for a given number of independent variables
 Best fit is defined as the highest R² value

Values in parentheses are the t values for the constants

Table 10b -
 KM4 MK Series 1200°F Tensile Strength Versus γ' Volume Fraction Curve Fit

$$\sigma = b_0 + b_1 f_{Medium} + b_2 f_{Fine}$$

1200°F Yield Strength					
Independent Variables	Medium	Fine	Constant	R ²	Adj. R ²
1	0.802 (3.854)		93.6 (7.827)	0.598	0.557
1		-0.802 (-3.854)	147.8 (61.388)	0.598	0.557

1200°F Ultimate Tensile Strength					
Independent Variables	Medium	Fine	Constant	R ²	Adj. R ²
1	-1.160 (4.084)		210.8 (8.107)	0.625	0.588
1		1.160 (-4.084)	132.4 (64.124)	0.625	0.588

Models represent the best fit for a given number of independent variables
 Best fit is defined as the highest R² value

Values in parentheses are the t values for the constants

Table 11a -
 SR3 MS Series 1200°F Tensile Strength Versus γ' Size Curve Fit

$$\sigma = b_0 + b_1 d_{Medium} + b_2 d_{Fine}$$

1200°F Yield Strength										
Independent Variables	Ferret Diameter					Major Axis				
	Medium	Fine	Constant	R ²	Adj. R ²	Medium	Fine	Constant	R ²	Adj. R ²
1	-0.0655 (-2.038)		167.7 (15.746)	0.316	0.240	-0.0602 (-2.314)		170.0 (16.312)	0.373	0.303
2	-0.0964 (-2.084)	0.361 (0.934)	163.4 (13.983)	0.383	0.229	-0.0847 (-2.62)	0.306 (0.918)	165.7 (0.918)	0.433	0.291

1200°F Ultimate Tensile Strength										
Independent Variables	Ferret Diameter					Major Axis				
	Medium	Fine	Constant	R ²	Adj. R ²	Medium	Fine	Constant	R ²	Adj. R ²
1	-0.0368 (-1.943)		225.5 (35.920)	0.296	0.217	-0.0336 (-2.175)		226.7 (36.624)	0.344	0.272
2	-0.0479 (-1.698)	0.129 (0.549)	223.9 (31.453)	0.321	0.151	-0.0423 (-1.840)	0.108 (0.530)	225.2 (31.847)	0.367	0.208

Models represent the best fit for a given number of independent variables
 Best fit is defined as the highest R² value

Values in parentheses are the t values for the constants

Table 11b -
 KM4 MK Series 1200°F Tensile Strength Versus γ' Size Curve Fit

$$\sigma = b_0 + b_1 d_{Medium} + b_2 d_{Fine}$$

1200°F Yield Strength										
Independent Variables	Ferret Diameter					Major Axis				
	Medium	Fine	Constant	R ²	Adj. R ²	Medium	Fine	Constant	R ²	Adj. R ²
1	-0.0519 (-4.443)		154.9 (42.961)	0.664	0.630	-0.0508 (-5.161)		157.8 (43.122)	0.727	0.700
2	-0.0705 (-5.277)	0.184 (2.116)	153.2 (47.614)	0.775	0.726	-0.0689 (-7.507)	0.189 (3.161)	156.2 (57.596)	0.870	0.841

1200°F Ultimate Tensile Strength										
Independent Variables	Ferret Diameter					Major Axis				
	Medium	Fine	Constant	R ²	Adj. R ²	Medium	Fine	Constant	R ²	Adj. R ²
1	-0.0603 (-2.845)		216.7 (33.136)	0.447	0.392	-0.0613 (-3.359)		220.9 (32.523)	0.530	0.483
2	-0.084 (-3.104)	0.236 (1.335)	214.4 (32.882)	0.539	0.436	-0.0847 (-3.964)	0.243 (1.743)	218.8 (1.743)	0.649	0.571

Models represent the best fit for a given number of independent variables
 Best fit is defined as the highest R² value

Values in parentheses are the t values for the constants

Table 12a -
 SR3 MS Series 1200°F/115 ksi Time To 0.2% Creep Versus γ' Volume Fraction Curve Fit -
 Common Logarithm Model

$$\log(\text{Time to 0.2\% Creep}) = b_0 + b_1 f_{\text{Medium}} + b_2 f_{\text{Fine}}$$

Independent Variables	Medium	Fine	Constant	R ²	Adj. R ²
1	0.0647 (1.921)		-0.406 (-0.245)	0.345	0.252
1		-0.0647 (-1.921)	3.255 (4.617)	0.345	0.252

Models represent the best fit for a given number of independent variables
 Best fit is defined as the highest R² value

Values in parentheses are the t values for the constants

Table 12b -
 SR3 MS Series 1200°F/115 ksi Time To 0.2% Creep Versus γ' Volume Fraction Curve Fit -
 Linear Model

$$\text{Time to 0.2\% Creep} = b_0 + b_1 f_{\text{Medium}} + b_2 f_{\text{Fine}}$$

Independent Variables	Medium	Fine	Constant	R ²	Adj. R ²
1	267.3 (3.813)		-10994.3 (-3.184)	0.675	0.629
1		-267.3 (-3.813)	3569.9 (1.721)	0.675	0.629

Models represent the best fit for a given number of independent variables
 Best fit is defined as the highest R² value

Values in parentheses are the t values for the constants

Table 12c -
 KM4 MK Series 1200°F/115 ksi Time To 0.2% Creep Versus γ' Volume Fraction -
 Common Logarithm Model

$$\log(\text{Time to } 0.2\% \text{ Creep}) = b_0 + b_1 f_{\text{Medium}} + b_2 f_{\text{Fine}}$$

Independent Variables	Cooling	Aging	Constant	R ²	Adj. R ²
1	0.0183 (2.406)		1.669 (3.815)	0.367	0.303
1		-0.0183 (-2.406)	2.907 (33.005)	0.367	0.303

Models represent the best fit for a given number of independent variables
 Best fit is defined as the highest R² value

Values in parentheses are the t values for the constants

Table 12d -
 KM4 MK Series 1200°F/115 ksi Time To 0.2% Creep Versus γ' Volume Fraction -
 Linear Model

$$\text{Time to } 0.2\% \text{ Creep} = b_0 + b_1 f_{\text{Medium}} + b_2 f_{\text{Fine}}$$

Independent Variables	Cooling	Aging	Constant	R ²	Adj. R ²
1	21.036 (2.241)		-648.5 (-1.202)	0.334	0.268
1		-21.036 (-2.241)	773.5 (-2.241)	0.334	0.268

Models represent the best fit for a given number of independent variables
 Best fit is defined as the highest R² value

Values in parentheses are the t values for the constants

Table 13a -
 SR3 MS Series 1200°F/115 ksi Time To 0.2% Creep Versus γ' Size -
 Common Logarithm Model

$$\log(\text{Time to } 0.2\% \text{ Creep}) = b_0 + b_1 d_{\text{Medium}} + b_2 d_{\text{Fine}}$$

Independent Variables	Feret Diameter					Major Axis				
	Medium	Fine	Constant	R ²	Adj. R ²	Medium	Fine	Constant	R ²	Adj. R ²
1		-0.0265 (-1.348)	3.819 (4.476)	0.206	0.093		-0.026 (-1.456)	3.957 (4.470)	0.232	0.123
2	0.0047 (1.329)	-0.0504 (-1.945)	3.174 (3.362)	0.387	0.182	0.0037 (1.205)	-0.045 (-1.922)	3.322 (3.298)	0.382	0.176

Models represent the best fit for a given number of independent variables
 Best fit is defined as the highest R² value

Values in parentheses are the t values for the constants

Table 13b -
 SR3 MS Series 1200°F/115 ksi Time To 0.2% Creep Versus γ' Size -
 Linear Model

$$\text{Time to } 0.2\% \text{ Creep} = b_0 + b_1 d_{\text{Medium}} + b_2 d_{\text{Fine}}$$

Independent Variables	Feret Diameter					Major Axis				
	Medium	Fine	Constant	R ²	Adj. R ²	Medium	Fine	Constant	R ²	Adj. R ²
1		-153.4 (-5.126)	8227.6 (6.345)	0.790	0.760		-142.2 (-5.266)	8654.4 (6.461)	0.798	0.770
2	10.76 (2.520)	-208.0 (-6.656)	6754.6 (5.936)	0.898	0.864	8.79 (2.409)	-187.9 (-6.672)	7127.1 (5.886)	0.898	0.863

Models represent the best fit for a given number of independent variables
 Best fit is defined as the highest R² value

Values in parentheses are the t values for the constants

Table 13c -
 KM4 MK Series 1200°F/115 ksi Time To 0.2% Creep Versus γ' Size -
 Common Logarithm Model

$$\log(\text{Time to 0.2\% Creep}) = b_0 + b_1 d_{\text{Medium}} + b_2 d_{\text{Fine}}$$

Independent Variables	Feret Diameter					Major Axis				
	Medium	Fine	Constant	R ²	Adj. R ²	Medium	Fine	Constant	R ²	Adj. R ²
1	-0.000856 (-1.642)		2.972 (18.468)	0.212	0.134	-0.000962 (-2.105)		2.801 (18.023)	0.307	0.238
2	-0.0011 (-1.525)	0.00239 (0.509)	2.949 (17.030)	0.234	0.064	-0.00128 (-2.159)	0.00335 (0.862)	3.036 (17.285)	0.360	0.218

Models represent the best fit for a given number of independent variables
 Best fit is defined as the highest R² value

Values in parentheses are the t values for the constants

Table 13d -
 KM4 MK Series 1200°F/115 ksi Time To 0.2% Creep Versus γ' Size -
 Linear Model

$$\text{Time to 0.2\% Creep} = b_0 + b_1 d_{\text{Medium}} + b_2 d_{\text{Fine}}$$

Independent Variables	Feret Diameter					Major Axis				
	Medium	Fine	Constant	R ²	Adj. R ²	Medium	Fine	Constant	R ²	Adj. R ²
1	-0.955 (-1.496)		839.5 (4.258)	0.183	0.101	-1.086 (-1.924)		947.7 (4.514)	0.270	0.197
2	-1.315 (-1.503)	3.563 (0.625)	805.3 (3.822)	0.217	0.043	-1.530 (-2.106)	4.626 (0.975)	907.2 (4.229)	0.340	0.193

Models represent the best fit for a given number of independent variables
 Best fit is defined as the highest R² value

Values in parentheses are the t values for the constants

Table 14a -
 KM4 MK Series 1200°F Hold Time Fatigue Crack Growth Rate Versus γ' Volume Fraction -
 Common Logarithm Model

$$\log(\text{Crack Growth Rate}) = b_0 + b_1 f_{\text{Medium}} + b_2 f_{\text{Fine}}$$

Variables	Cooling	Aging	Constant	R ²	Adj. R ²
1	-0.139 (1.631)		1.299 (-8.207)	0.210	0.131
1		0.139 (1.631)	-8.073 (0.266)	0.210	0.131

Models represent the best fit for a given number of independent v
 Best fit is defined as the highest R² value

Values in parentheses are the t values for the constants

Table 14b -
 KM4 MK Series 1200°F Hold Time Fatigue Crack Growth Rate Versus γ' Volume Fraction -
 Linear Model

$$\text{Crack Growth Rate} = b_0 + b_1 f_{\text{Medium}} + b_2 f_{\text{Fine}}$$

Variables	Medium	Fine	Constant	R ²	Adj. R ²
1	-3.71 E-7 (-1.479)		2.56 E-5 (1.774)	0.424	0.180
1		3.71 E-7 (1.479)	5.00 E-7 (0.172)	0.424	0.180

Models represent the best fit for a given number of independent variables
 Best fit is defined as the highest R² value

Values in parentheses are the t values for the constants

Table 15a -
 KM4 MK Series 1200°F Hold Time Fatigue Crack Growth Rate Versus γ' Size -
 Common Logarithm Model

$$\log(\text{Crack Growth Rate}) = b_0 + b_1 d_{\text{Medium}} + b_2 d_{\text{Fine}}$$

Independent Variables	Feret Diameter					Major Axis				
	Medium	Fine	Constant	R ²	Adj. R ²	Medium	Fine	Constant	R ²	Adj. R ²
1	0.0168 (6.638)		-11.617 (-14.898)	0.815	0.797	0.0144 (4.725)		-11.845 (-10.427)	0.691	0.660
2	0.0198 (6.189)	-0.0296 (-1.425)	-11.333 (-14.740)	0.849	0.816	0.0166 (4.182)	-0.0226 (-0.872)	-11.647 (-9.937)	0.715	0.651

Models represent the best fit for a given number of independent variables

Values in parentheses are the t values for the constants

Table 15b -
 KM4 MK Series 1200°F Hold Time Fatigue Crack Growth Rate Versus γ' Size -
 Linear Model

$$\text{Crack Growth Rate} = b_0 + b_1 d_{\text{Medium}} + b_2 d_{\text{Fine}}$$

Independent Variables	Feret Diameter					Major Axis				
	Medium	Fine	Constant	R ²	Adj. R ²	Medium	Fine	Constant	R ²	Adj. R ²
1	5.01 E-8 (8.137)		-1.05 E-5 (-5.545)	0.932	0.869	4.38 E-8 (5.655)		-1.15 E-5 (-3.983)	0.873	0.762
2	4.89 E-8 (5.694)	1.16 E-8 (0.206)	-1.06 E-5 (-5.146)	0.932	0.840	4.17 E-8 (3.999)	2.21 E-8 (0.324)	-1.17 E-5 (-3.791)	0.765	0.712

Models represent the best fit for a given number of independent variables

Best fit is defined as the highest R² value

Values in parentheses are the t values for the constants

Table 16 -
Comparison Of Observed Trends For Current And Previous Work (5)

Independent Variable	Dependent Variable											
	1200°F YS			1200°F UTS			1200° Creep			1200°F HTFCGR		
	MS	MK	All Data	MS	MK	All Data	MS	MK	All Data	MS	MK	All Data
γ'_{Medium} Fraction	+	+	+	+	+		+	+			NC	
γ'_{Medium} Size	-	-	-	-	-	-	NC	-			-	
γ'_{Fine} Fraction	-	-		-	-		-	-			NC	
γ'_{Fine} Size	NC	+		-	+		-	NC	-		-	NC

NC = No good correlation ($R^2 < 0.3$)

Increasing magnitude produces:

- + Beneficial effect (higher strength, longer life, slower crack growth)
- Detrimental effect (lower strength, shorter life, faster crack growth)

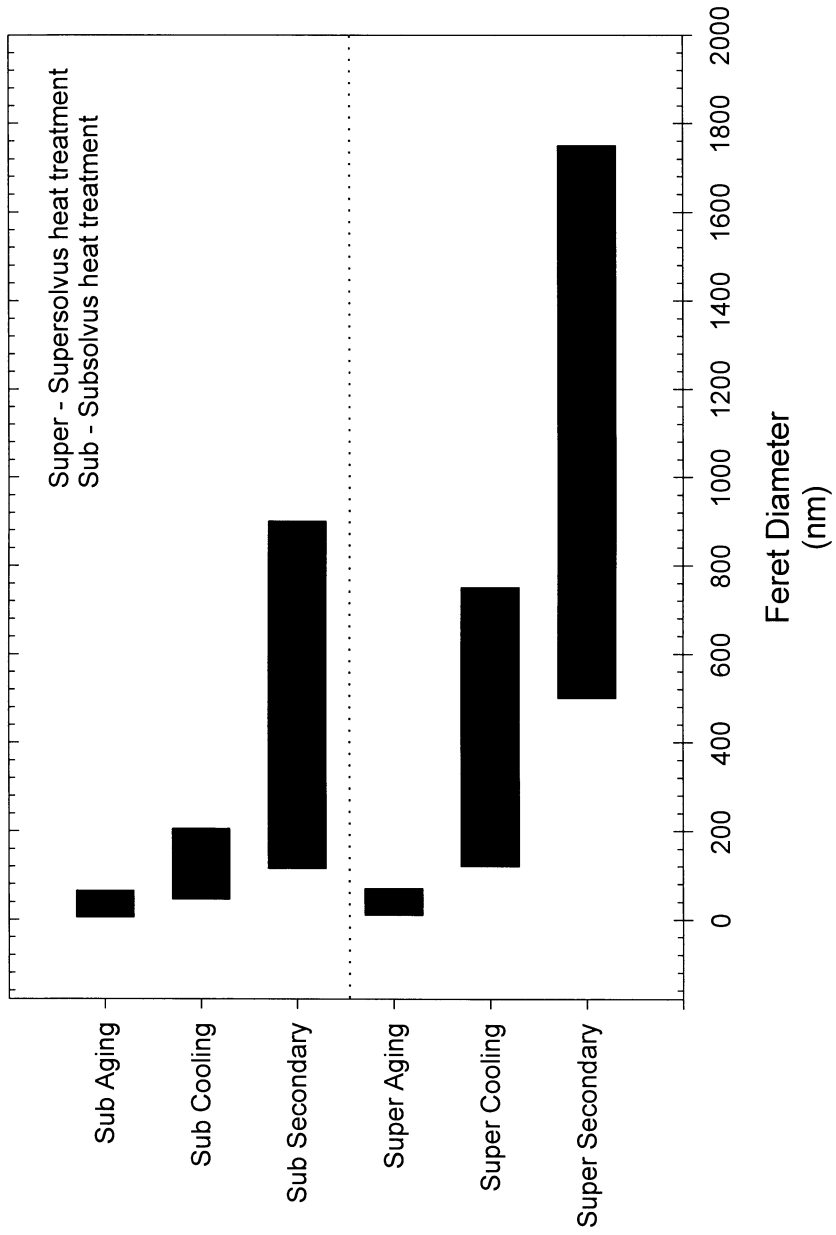
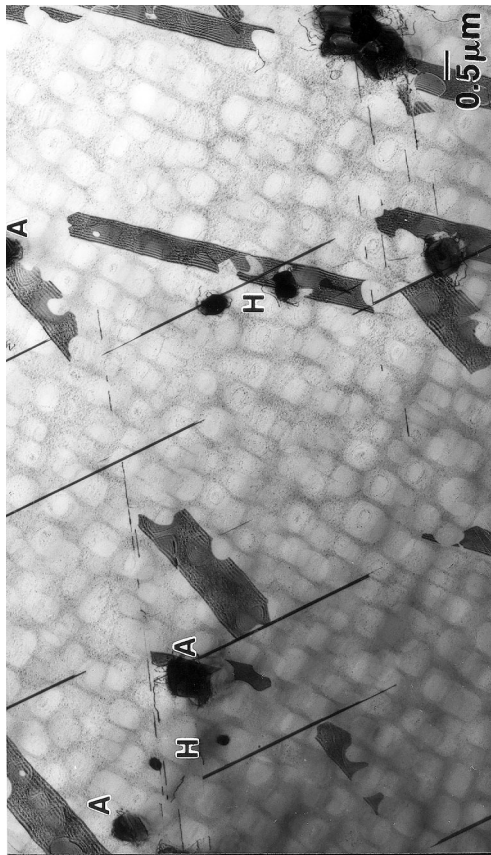
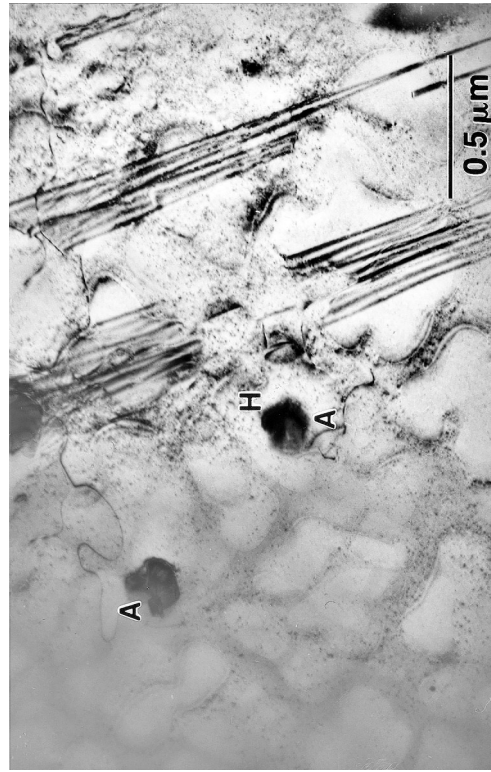


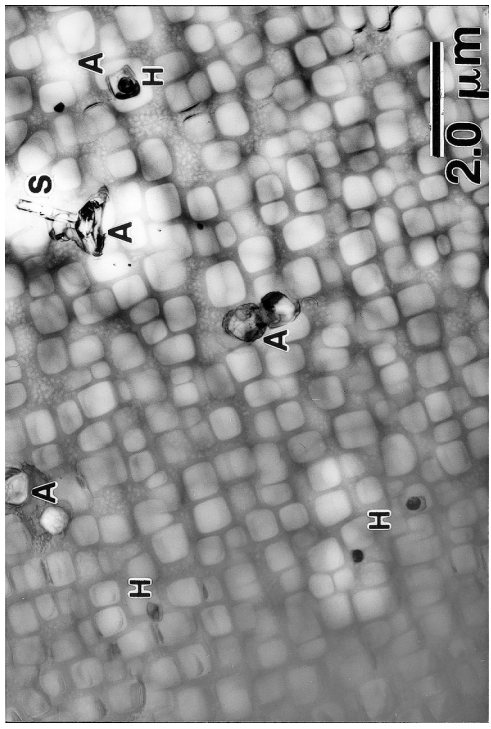
Figure 1 -
Typical Size Ranges For Different Types Of γ



(a) MS1.



(b) MS2.

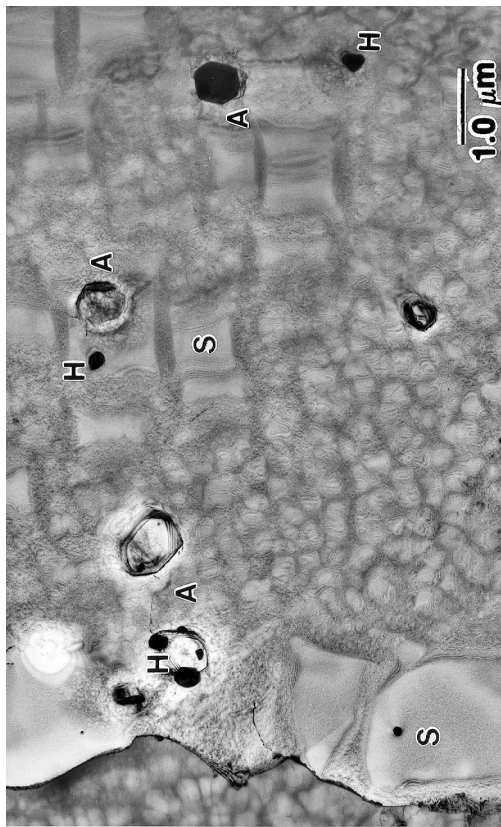


(c) MS3.

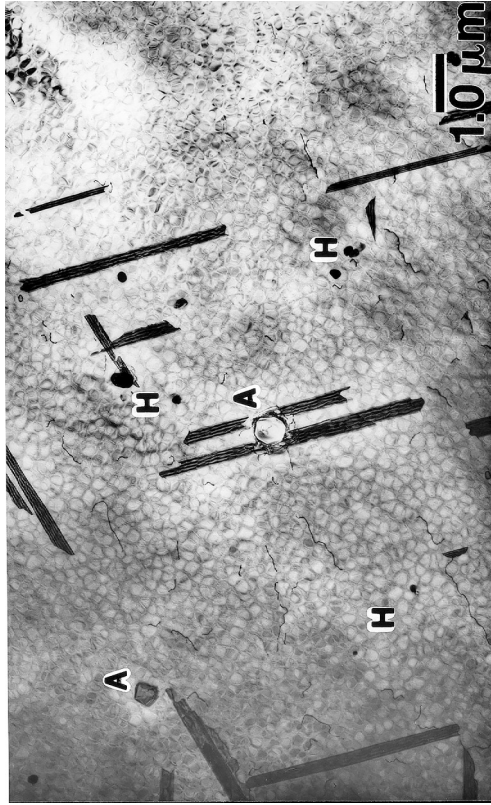


(d) MS4.

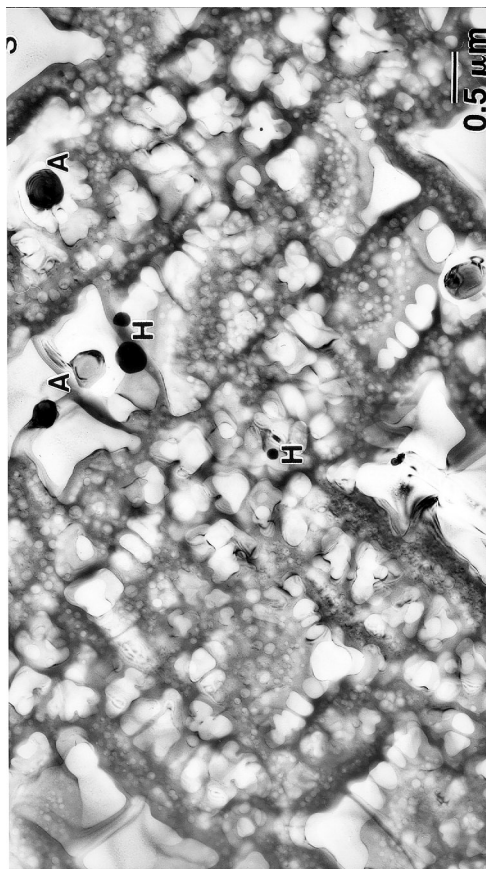
Figure 2.—Comparison of general microstructure and phases identified in SR3 MS series samples MS1–MS4. A = (Ti,Nb)C. H = (Hf,Zr)O₂. S = Secondary γ .



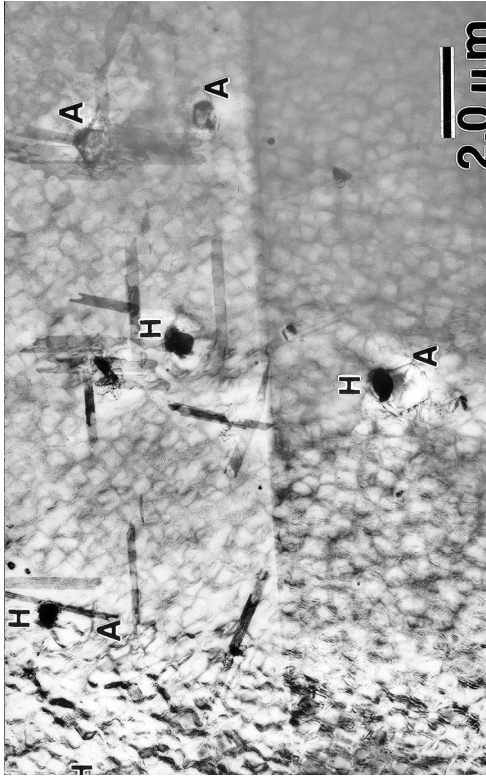
(e) MS4F.



(f) MS5.

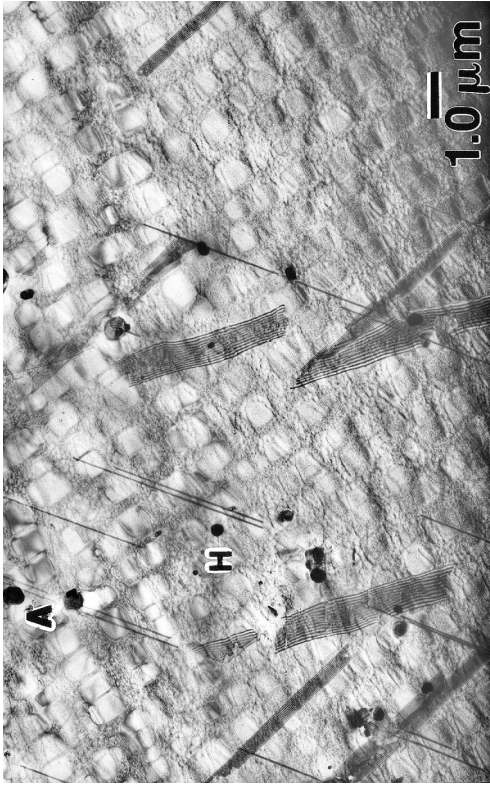


(g) MS5F.

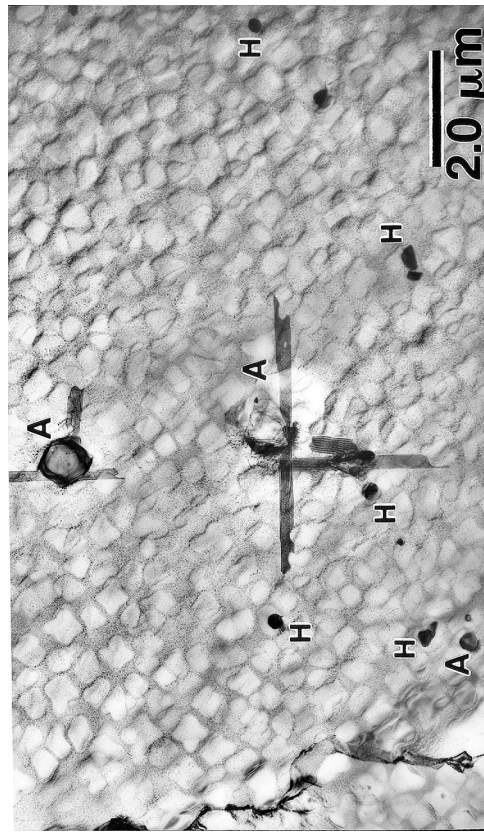


(h) MS6.

Figure 2.—Continued. Comparison of general microstructure and phases identified in SR3 MS series samples MS4F–MS6. A = (Ti,Nb)C. H = (Hf,Zr)O₂. S = Secondary γ '.

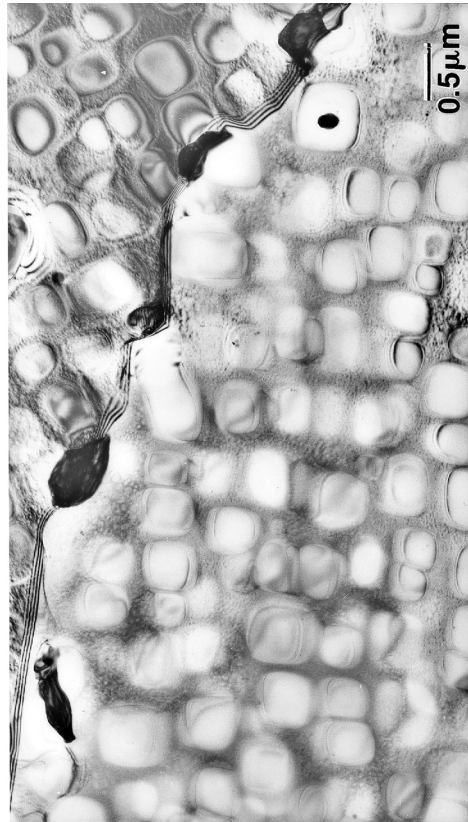


(j) MS8.

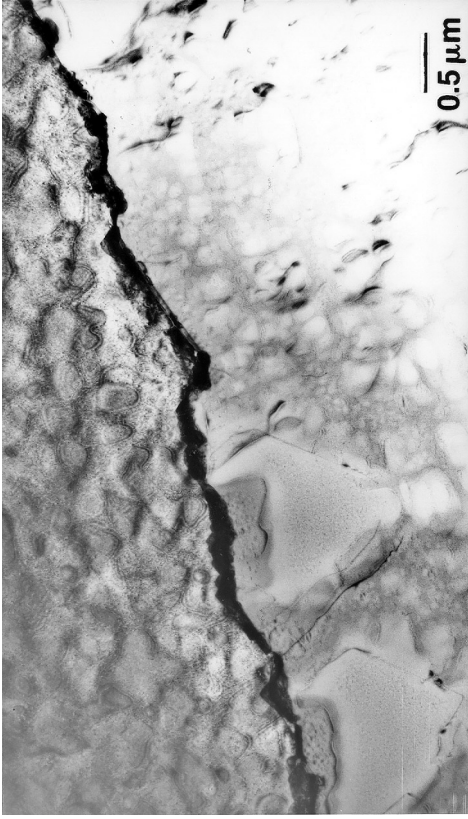


(i) MS7.

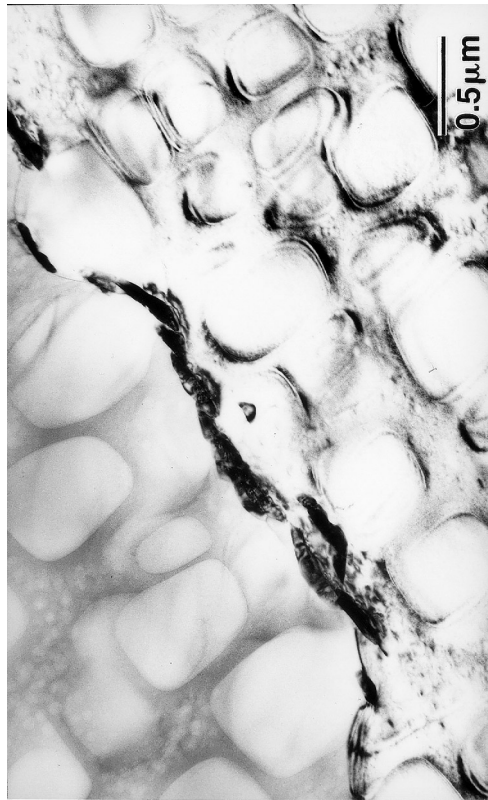
Figure 2.—Concluded. Comparison of general microstructure and phases identified in SR3 MS series samples MS7–MS8. A = (Ti,Nb)C. H = (Hf,Zr)O₂. S = Secondary γ' .



(a) MS1.



(b) MS2.

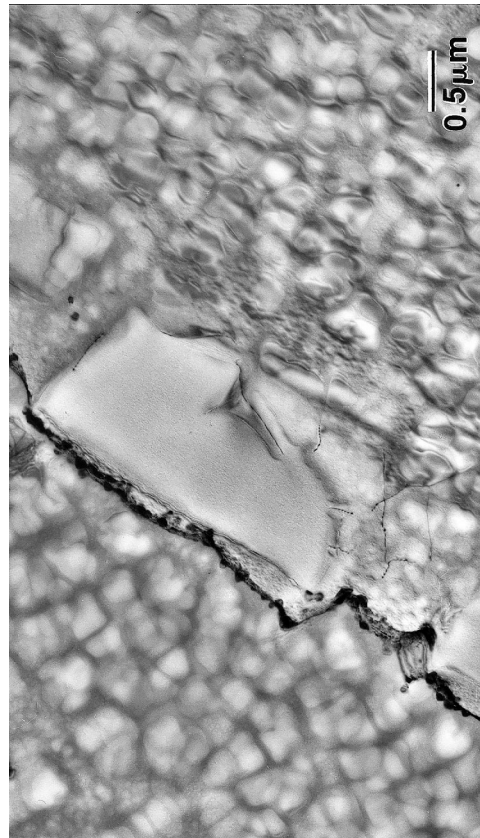


(c) MS3.

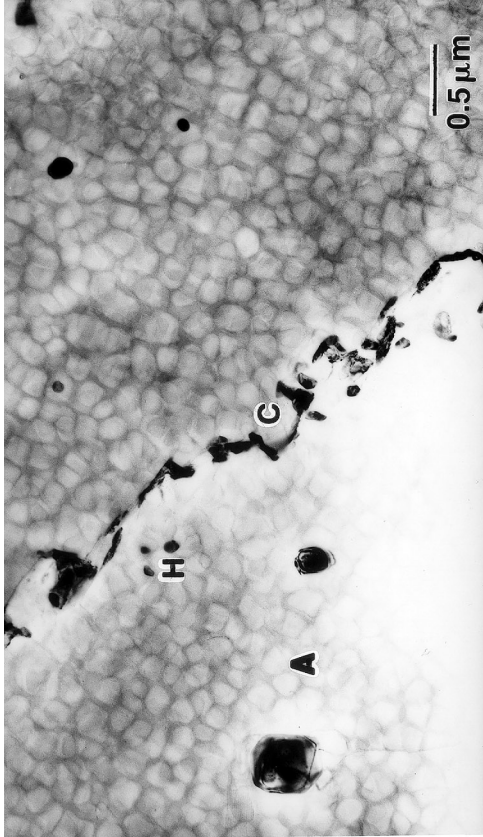


(d) MS4.

Figure 3.—Comparison of heavily loaded grain boundaries in SR3 MS series samples MS1–MS4. A = (Ti,Nb)C. B = (Hf,Zr)O₂. C = (Cr,Mo)₂₃C₆.



(e) MS4F.



(f) MS5.

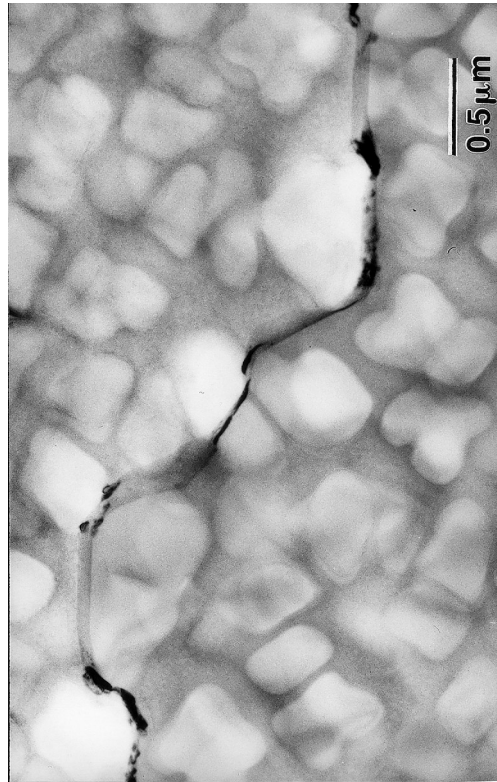


(g) MS5F.

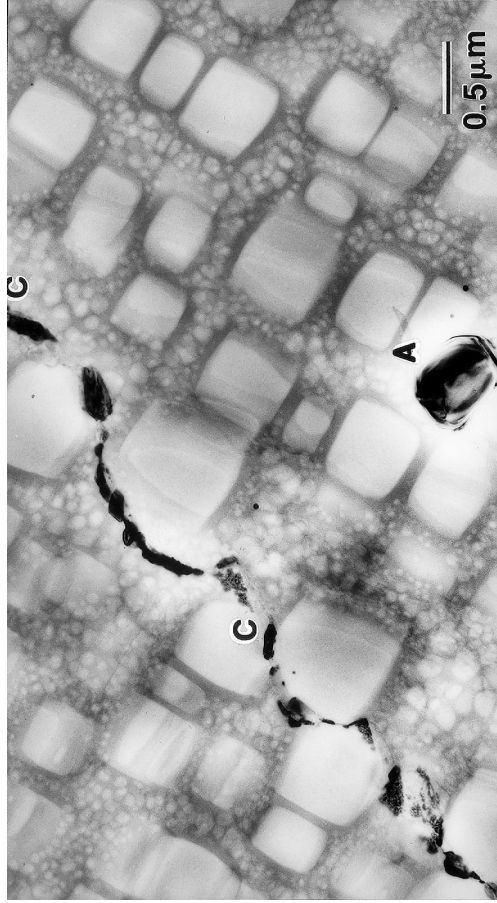


(h) MS6.

Figure 3.— Continued. Comparison of heavily loaded grain boundaries in SR3 MS series samples MS4F–MS6. A = (Ti,Nb)C. H = (Hf,Zr)O₂. S = Secondary γ' . C = (Cr,Mo)₂₃C₆.



(i) MS7.

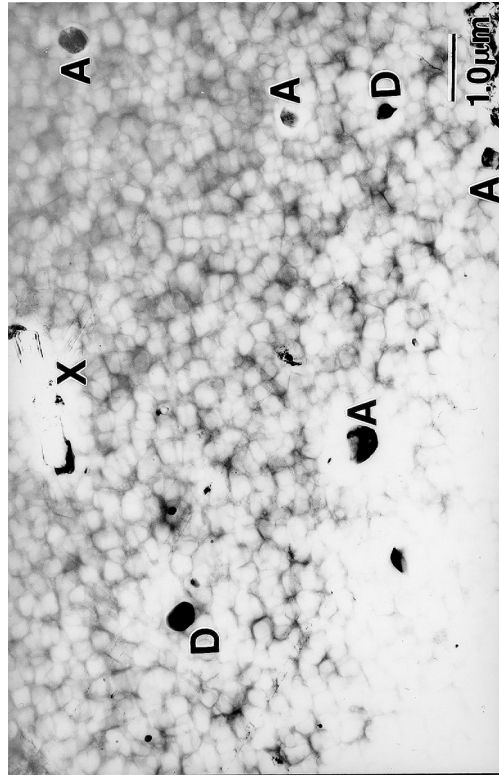


(j) MS8.

Figure 3.— Concluded. Comparison of heavily loaded grain boundaries in SR3 MS series samples MS7-MS8. A = (Ti,Nb)C. H = (Hf,Zr)O₂. S = Secondary γ .
C = (Cr,Mo)₂₃C₆.



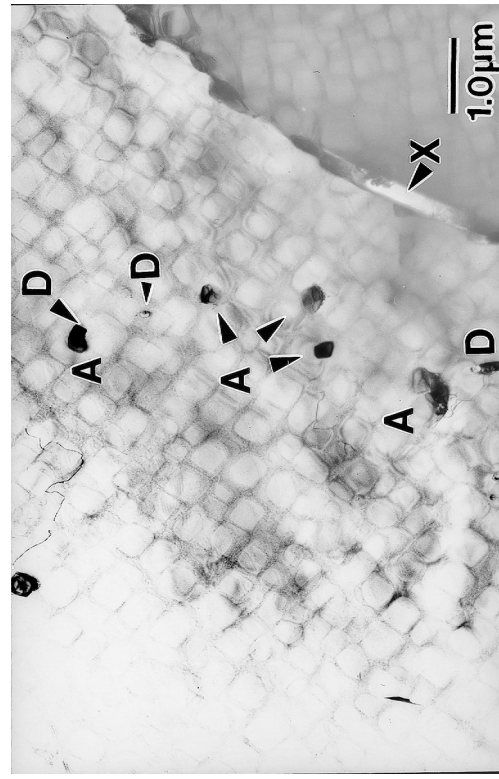
(b) MK2.



(d) MK4.

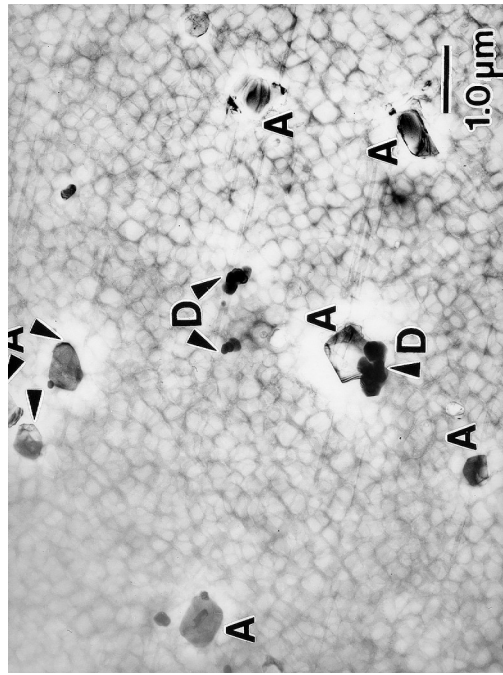


(a) MK1.

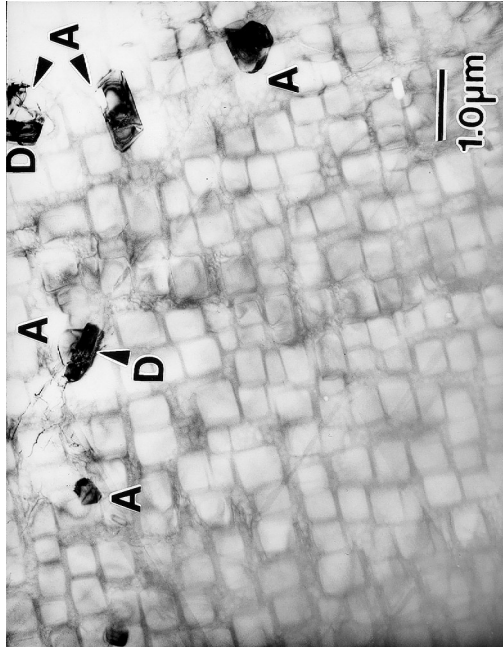


(c) MK3.

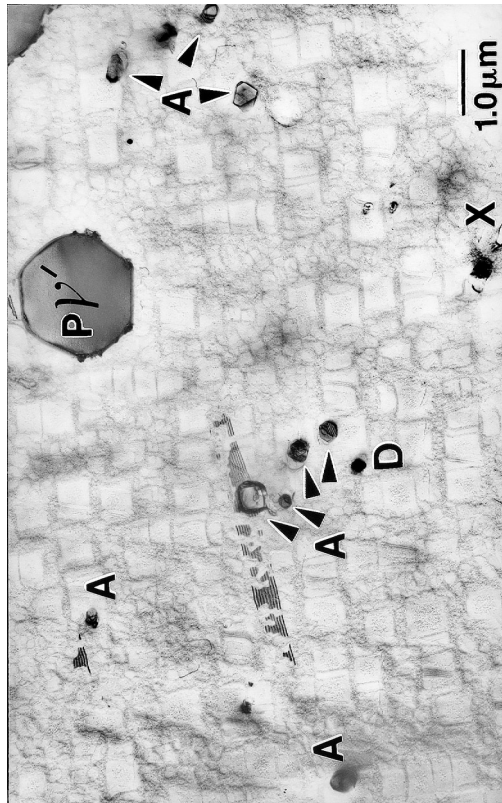
Figure 4.—Comparison of general microstructure and phases identified in KM4 MK series samples MK1–MK4. A = $(Ti,Nb)C$. D = Al_2O_3 . S = Secondary γ' . X = $(Ti,Mo)_6C$. C = $(Cr,Mo)_{23}C_6$.



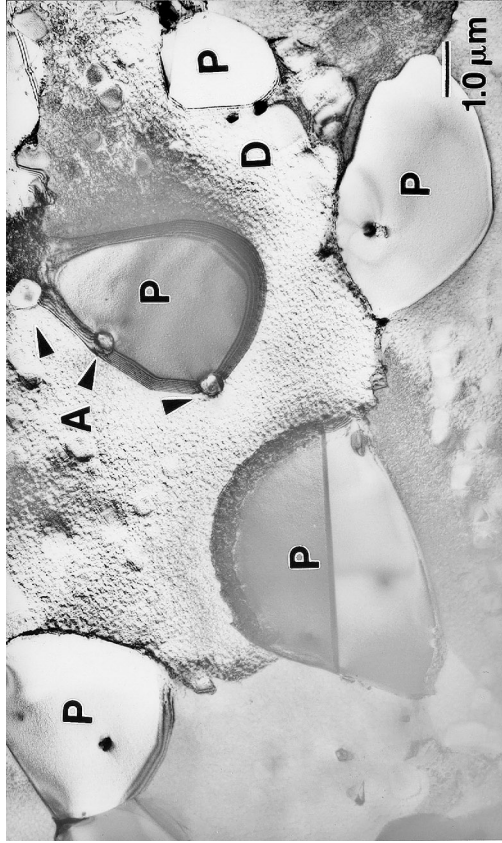
(e) MK5.



(f) MK6.

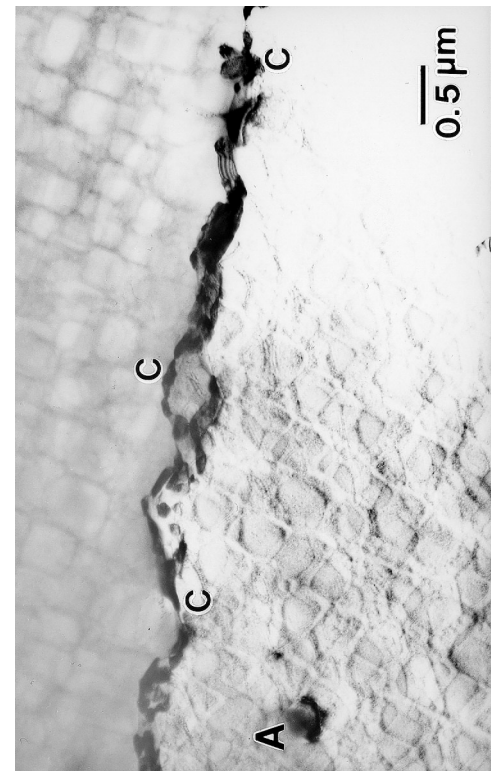


(g) MK7.

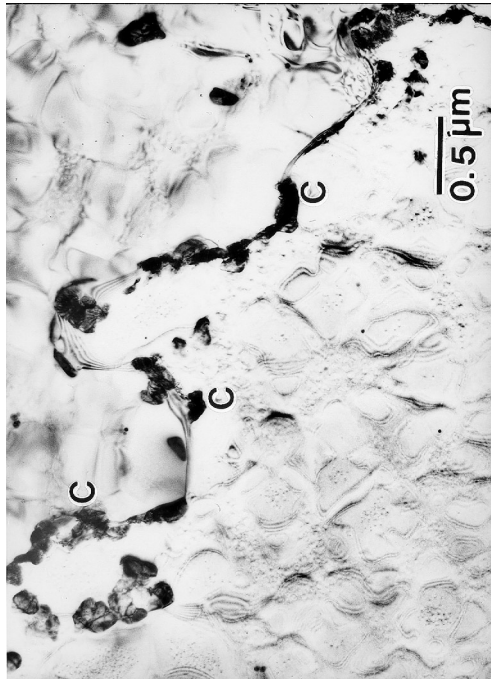


(h) MK8.

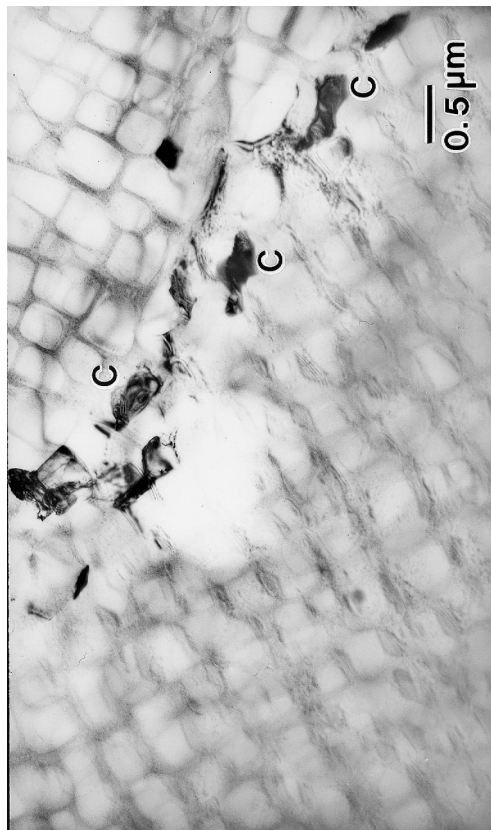
Figure 4.—Concluded. Comparison of general microstructure and phases identified in KM4 MK series samples MK5–MK8. A = $(Ti,Nb)C$. D = Al_2O_3 . S = Secondary γ' . X = $(Ti,Mo)_6C$. C = $(Cr,Mo)_{23}C_6$.



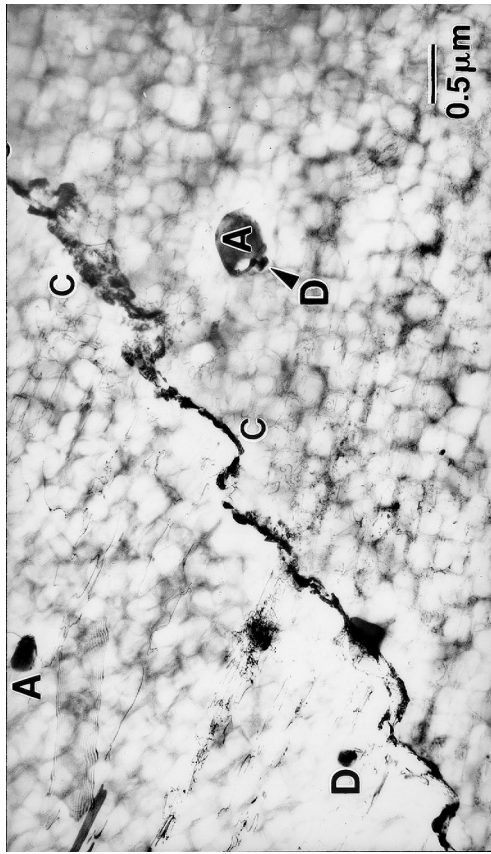
(a) MK1.



(b) MK2.

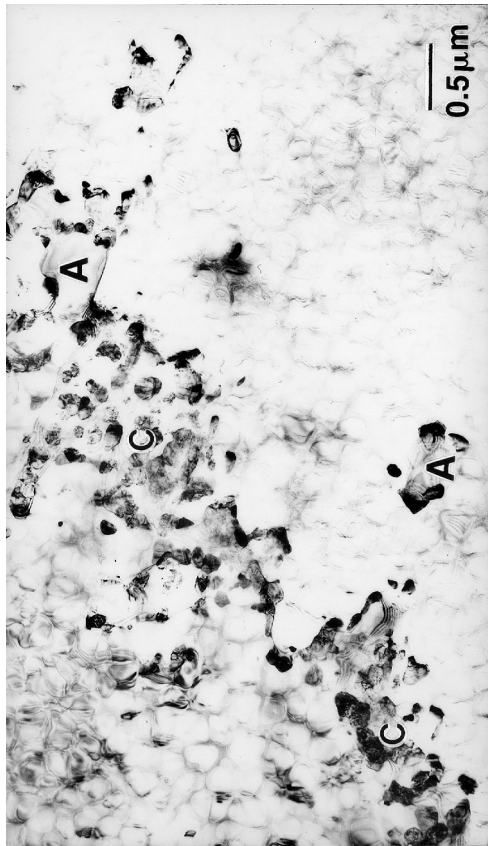


(c) MK3.

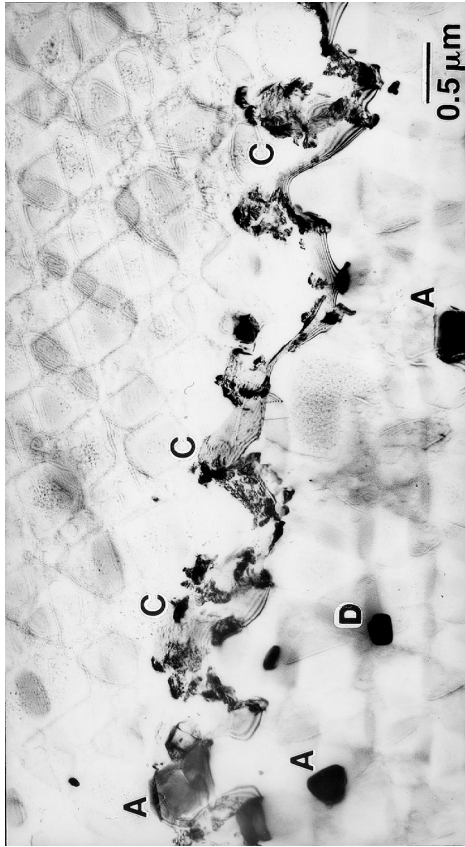


(d) MK4.

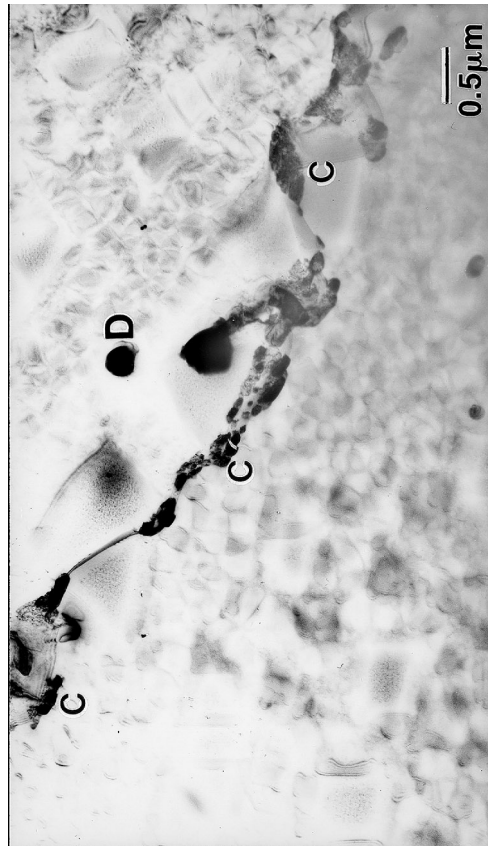
Figure 5.—Comparison of heavily loaded grain boundaries in KM4 MK series samples MK1–MK4. A = (Ti,Nb)C. D = Al₂O₃. S = Secondary γ'. X = (Ti,Mo)₆C. C = (Cr,Mo)₂₃C₆.



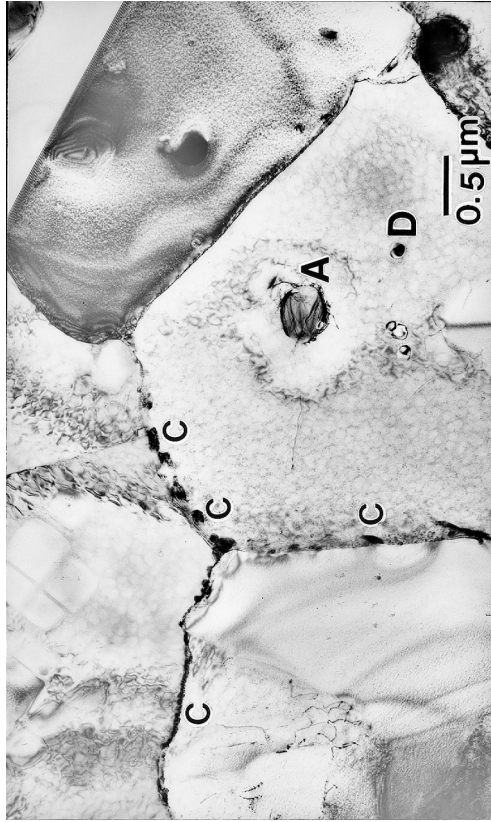
(e) MK5.



(f) MK6.



(g) MK7.



(h) MK8.

Figure 5.—Concluded. Comparison of heavily loaded grain boundaries in KM4 MK series samples MK5–MK8. A = $(Ti,Nb)C$. D = Al_2O_3 . S = Secondary γ . X = $(Ti,Mo)_6C$. C = $(Cr,Mo)_{23}C_6$.

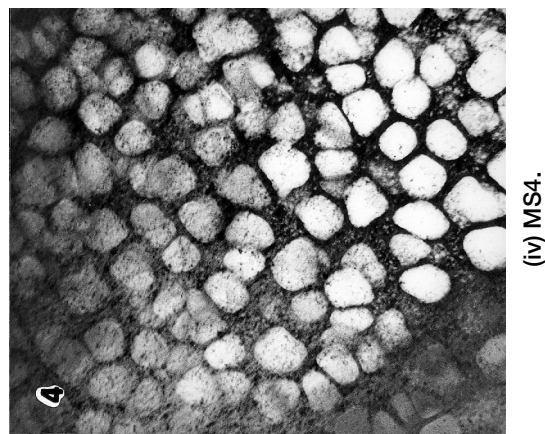
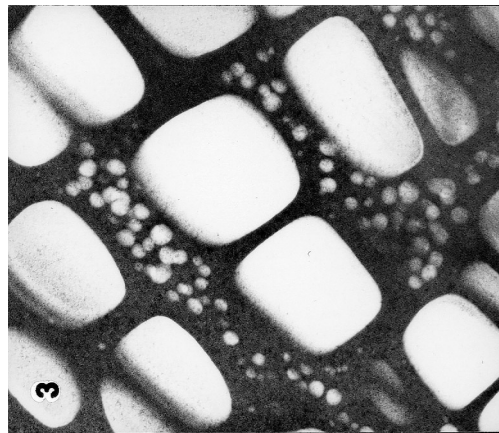
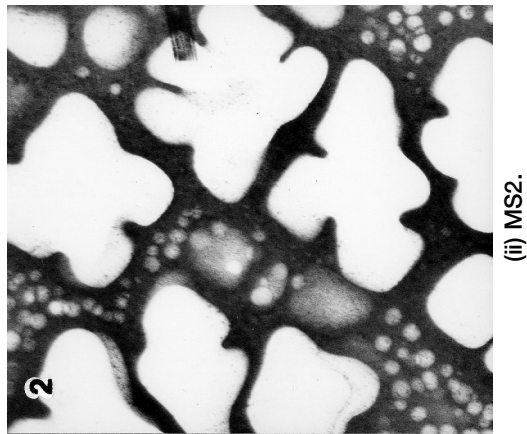
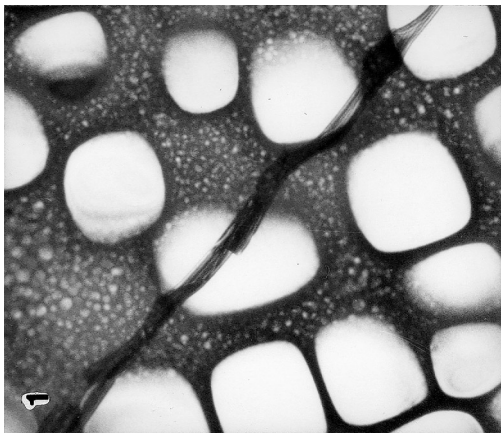
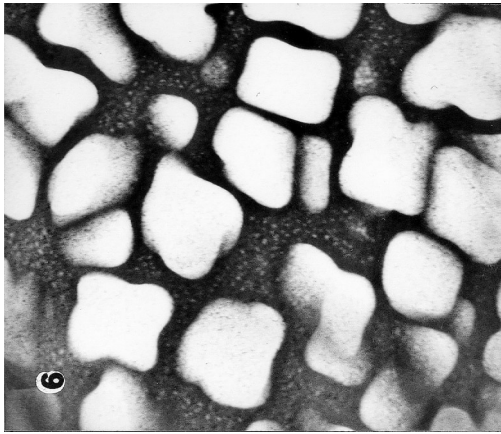
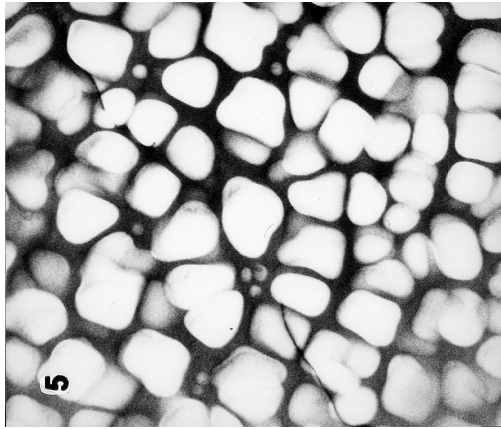


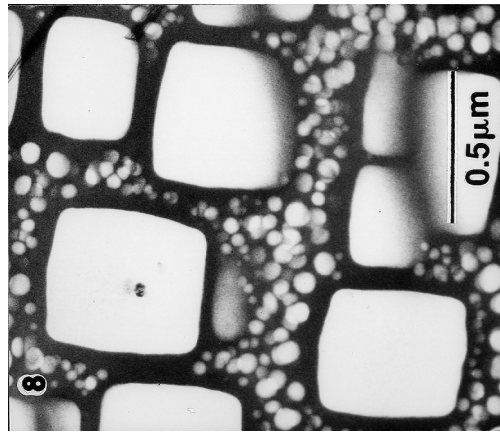
Figure 6.—Comparison of γ' distributions in SR3 MS series samples MS1–MS4.



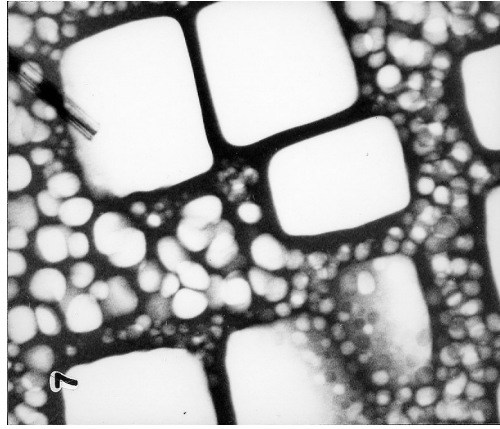
(vi) MS6.



(v) MS5.

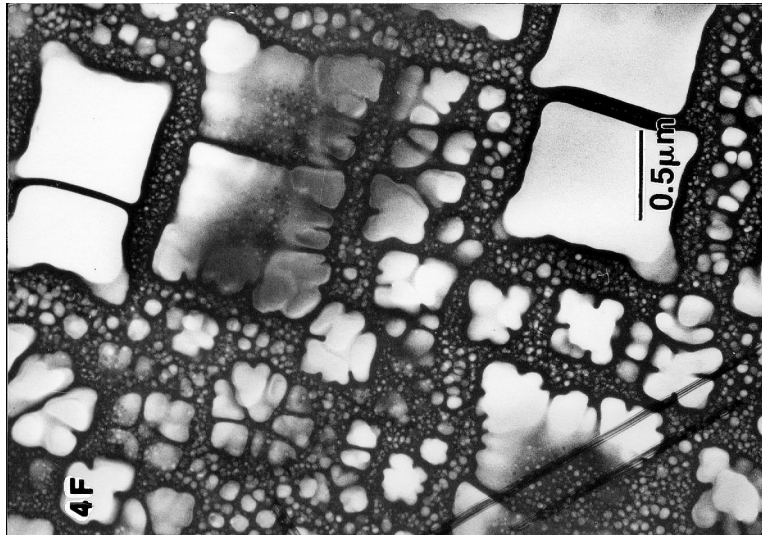


(viii) MS8.

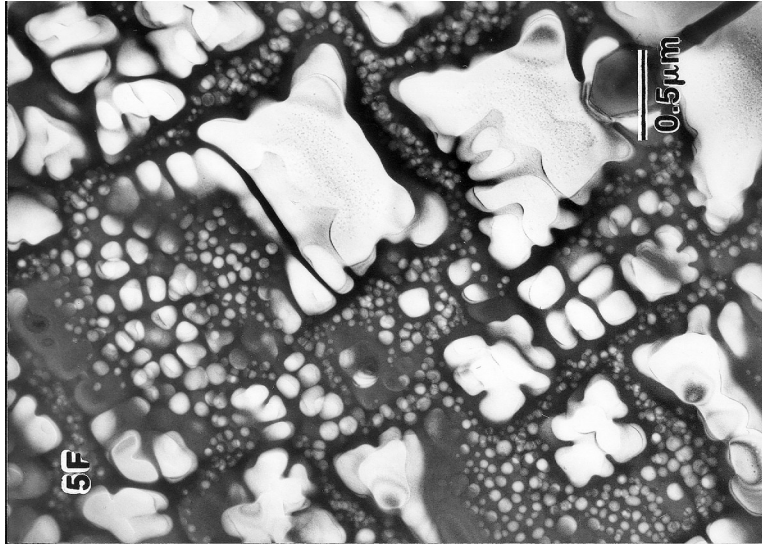


(vii) MS7.

Figure 6.—Continued. Comparison of γ distributions in SR3 MS series samples MS5–MS8.

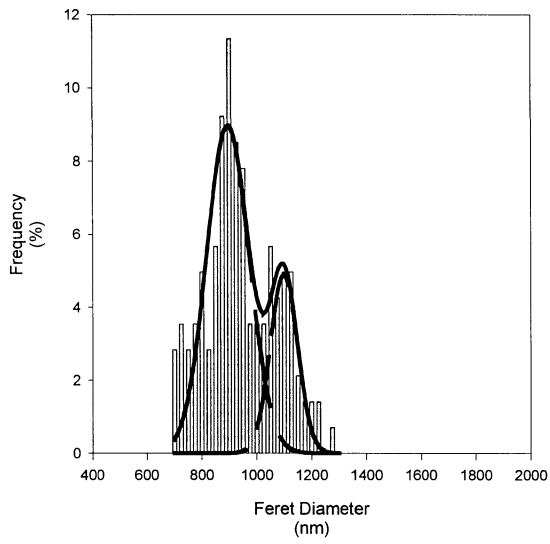


(i) MS4F.

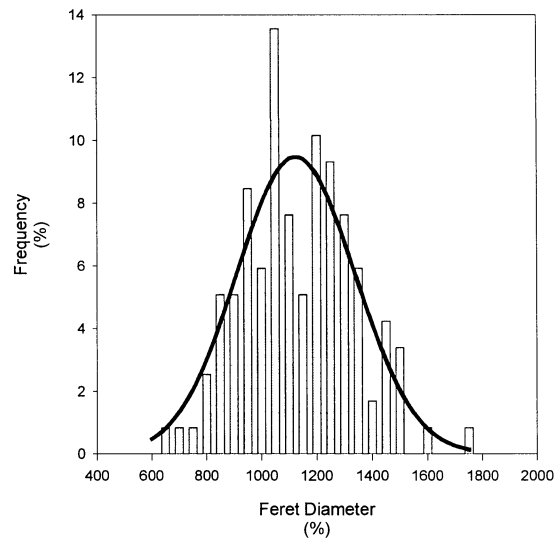


(ii) MS5F.

Figure 6.—Concluded. Comparison of γ distributions in SR3 MS series samples MS4F–MS5F.



i) MS4F



ii) MS5F

Figure 7a -
SR3 MS Series Large γ' Size Distributions

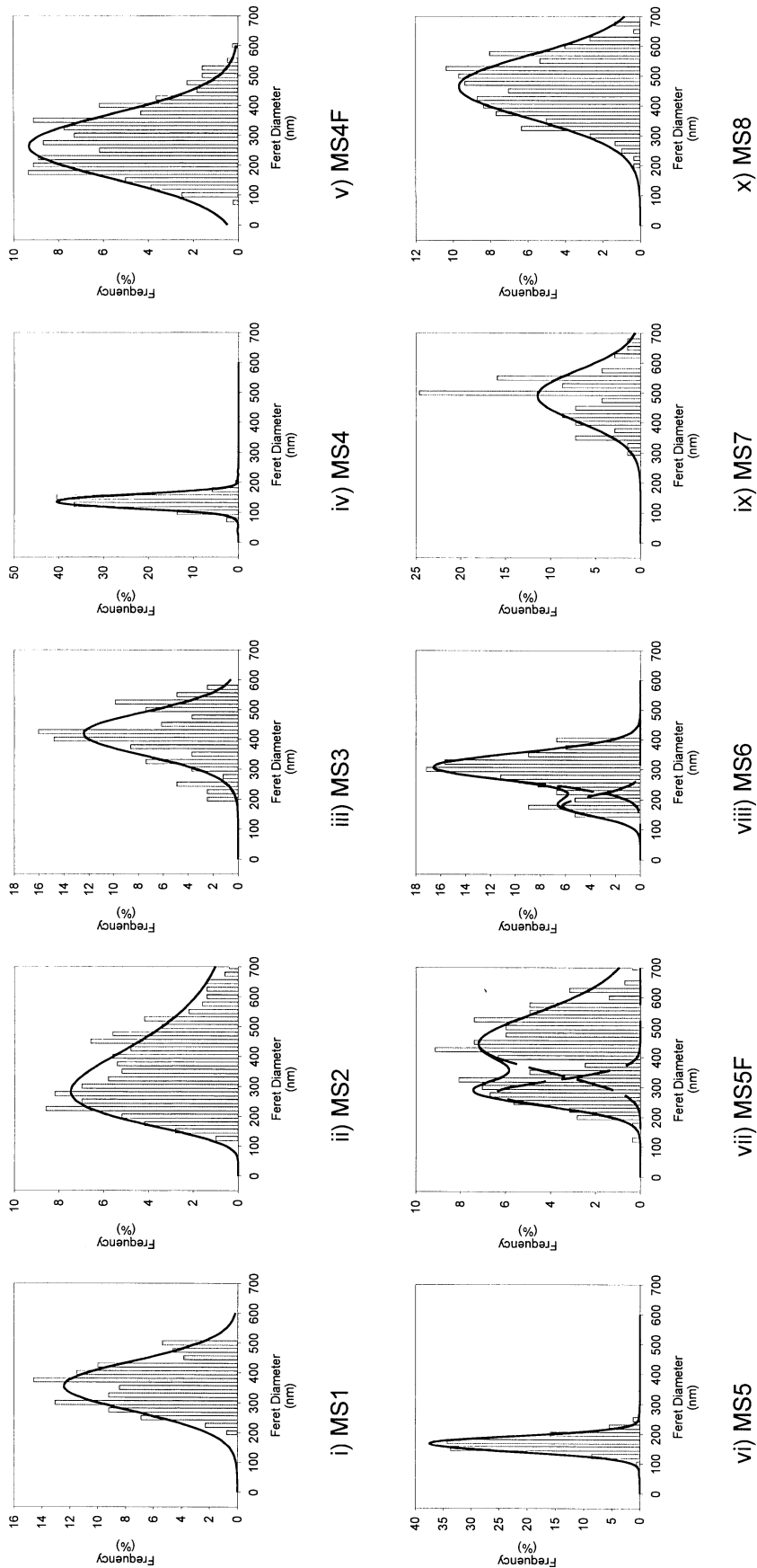


Figure 7b -
SR3 MS Series Medium γ' Size Distributions

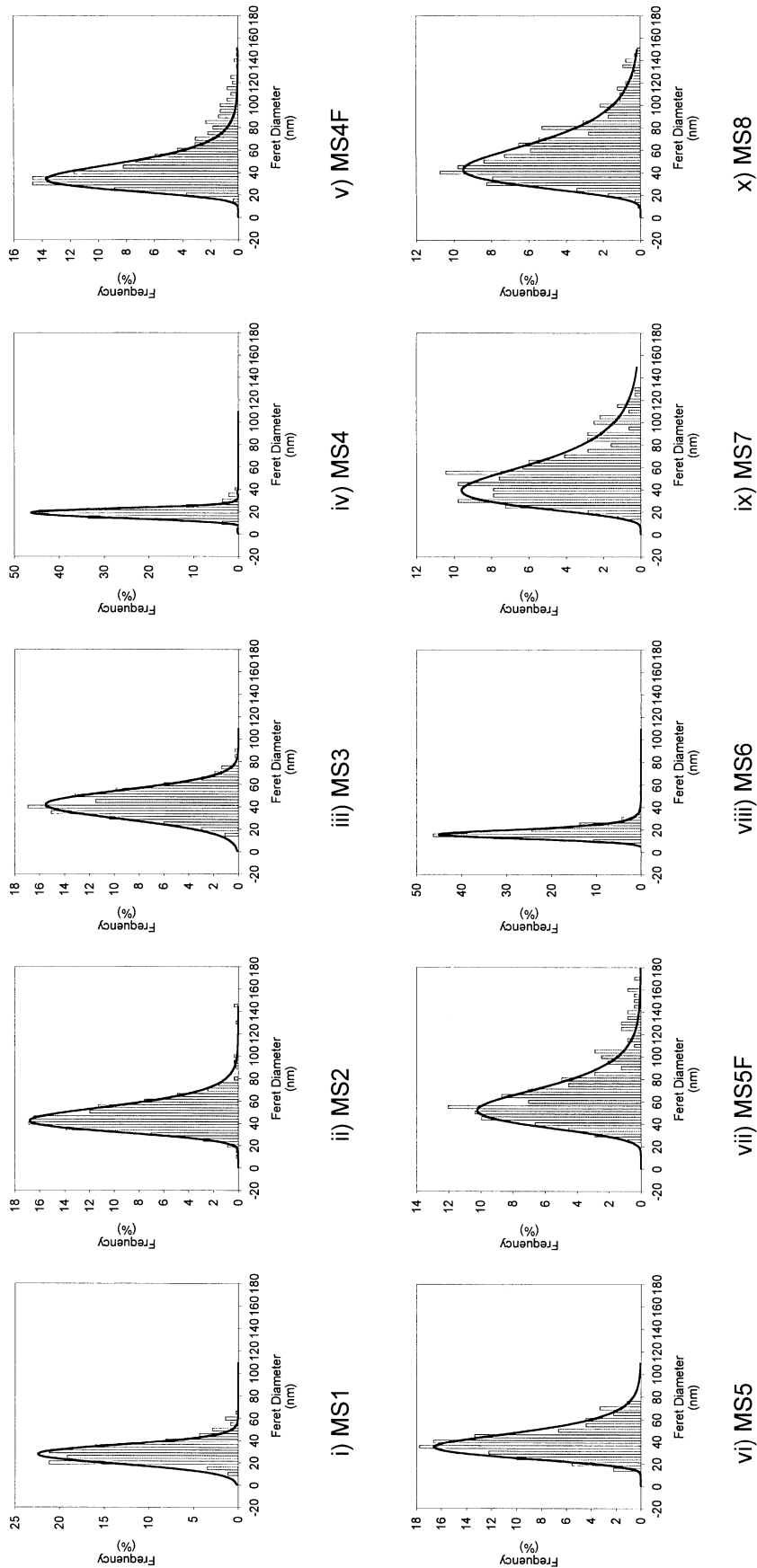
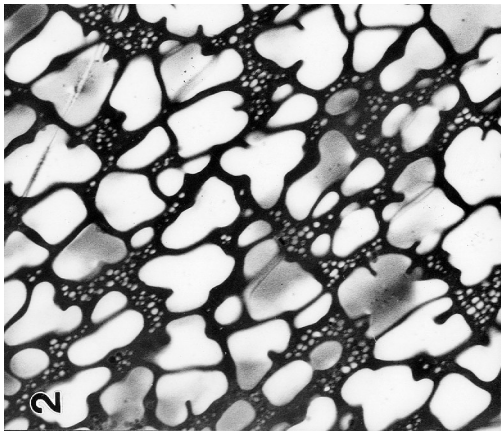
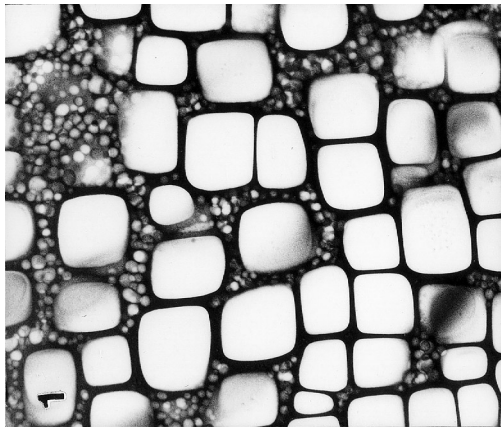


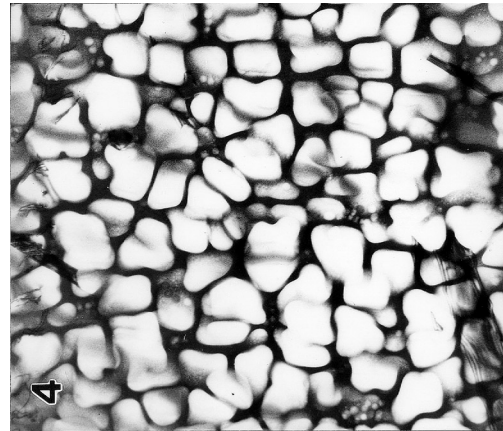
Figure 7c -
SR3 MS Series Fine γ' Size Distributions



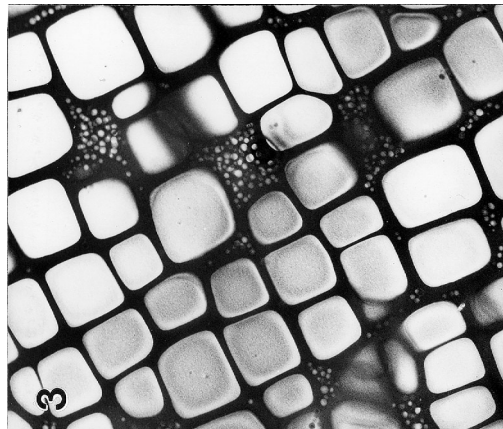
(b) MK2.



(a) MK1.

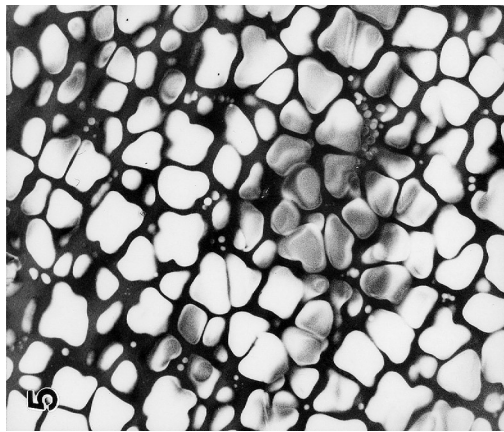


(d) MK4.

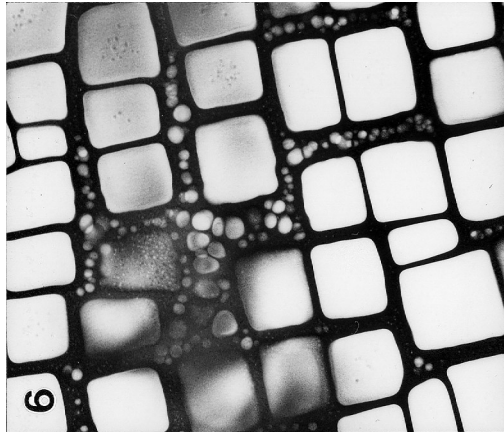


(c) MK3.

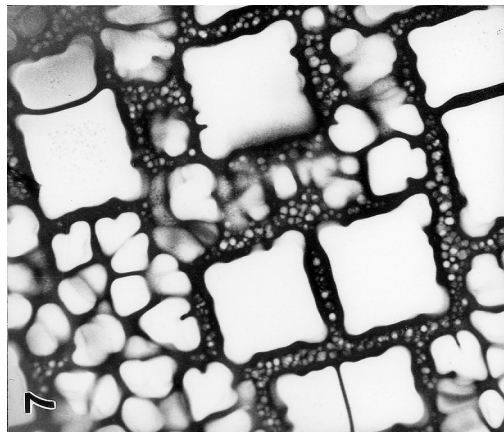
Figure 8.—Comparison of γ' distributions in KM4 MK series samples MK1–MK4.



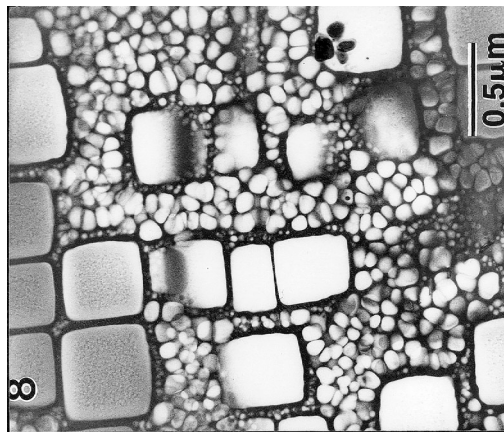
(e) MK5.



(f) MK6.



(g) MK7.



(h) MK8.

Figure 8.—Concluded. Comparison of γ' distributions in KM4 MK series samples MK5–MK8.

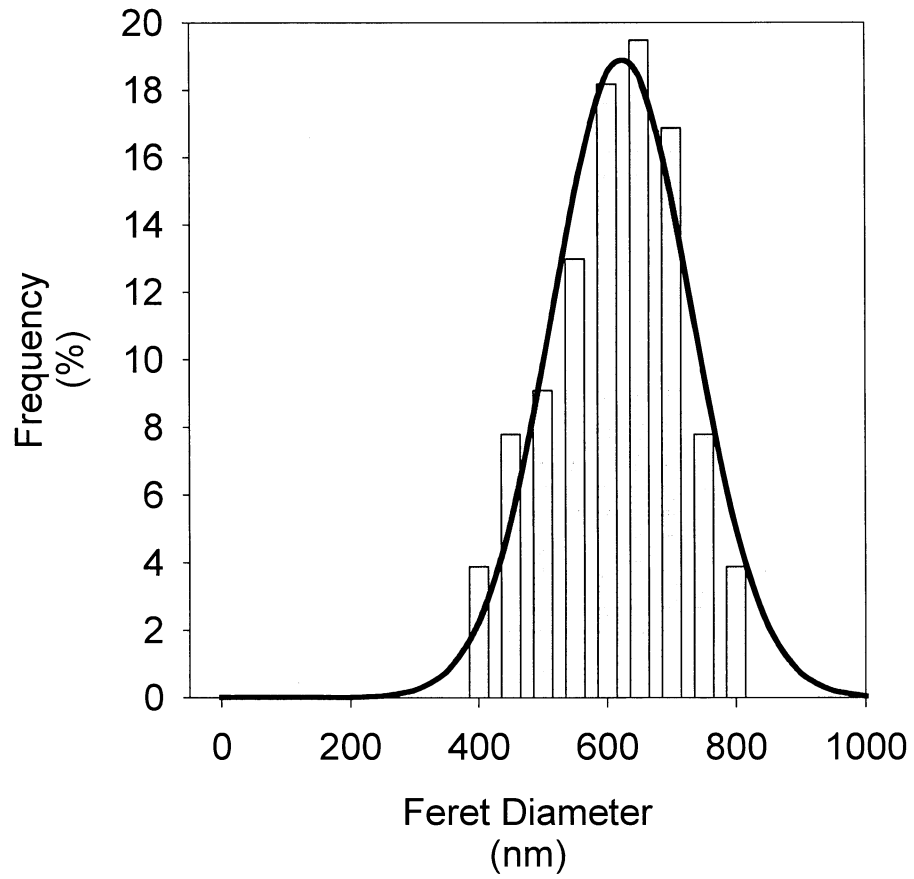
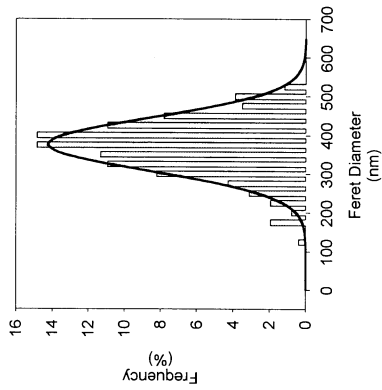
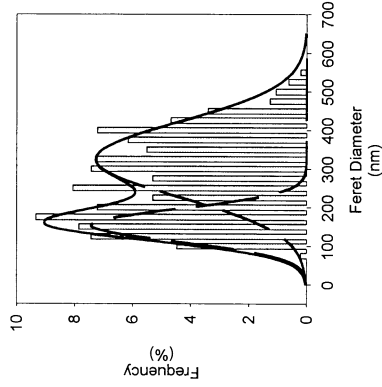


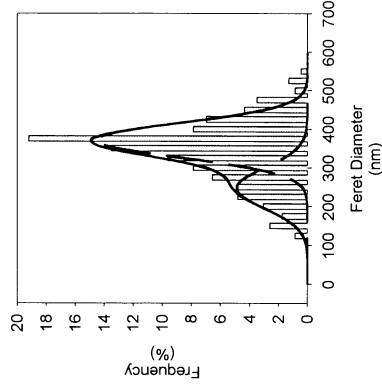
Figure 9a -
KM4 MK7 Large γ' Size Distribution



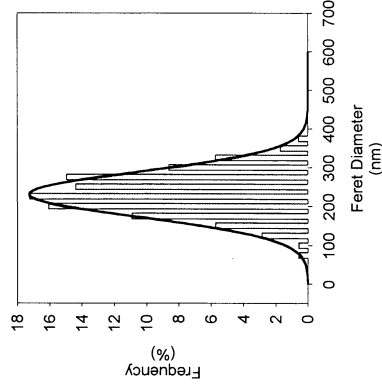
i) MK1



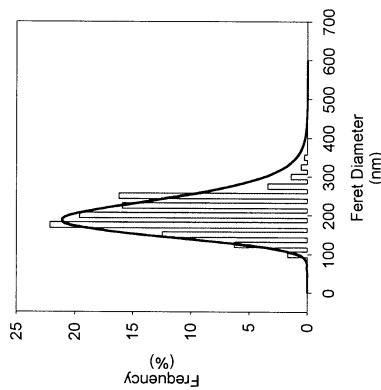
ii) MK2



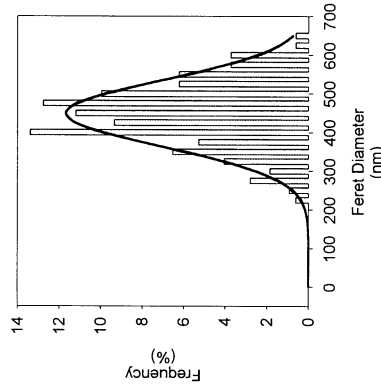
iii) MK3



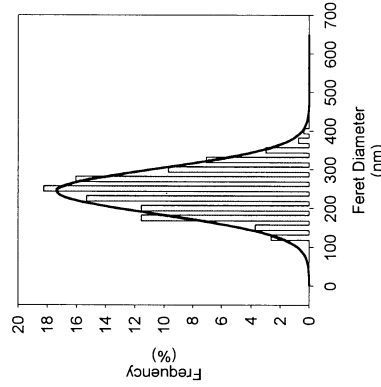
iv) MK4



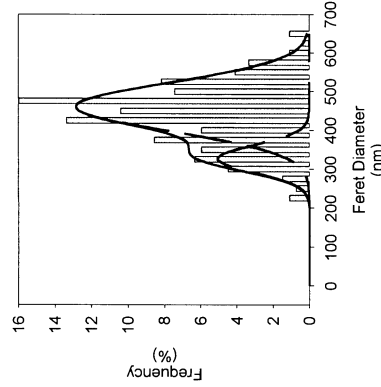
v) MK5



vi) MK6

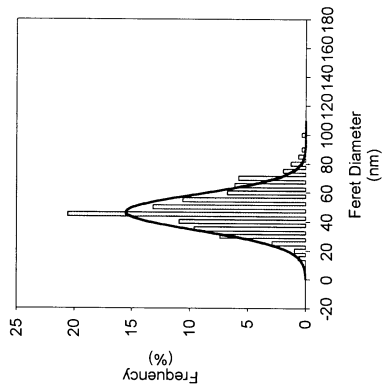


vii) MK7

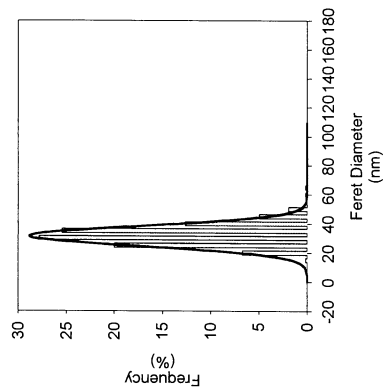


viii) MK8

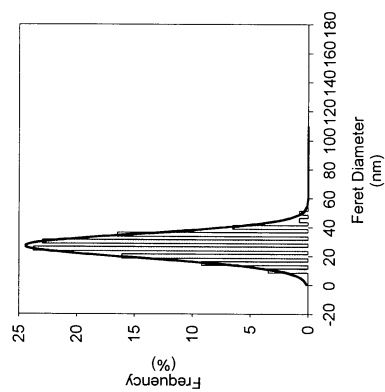
Figure 9b -
KM4 MK Series Medium γ' Size Distributions



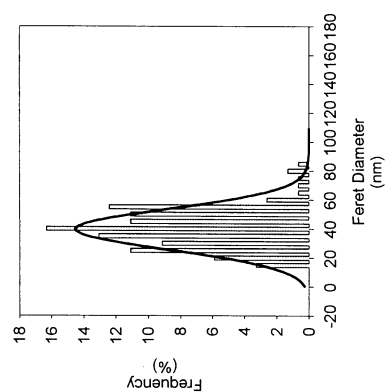
i) MK1



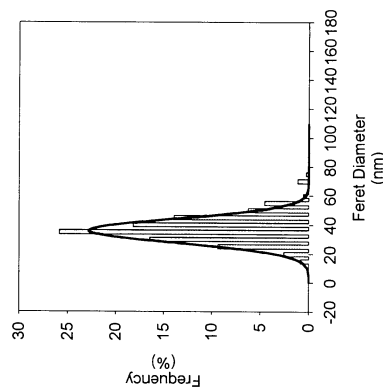
ii) MK2



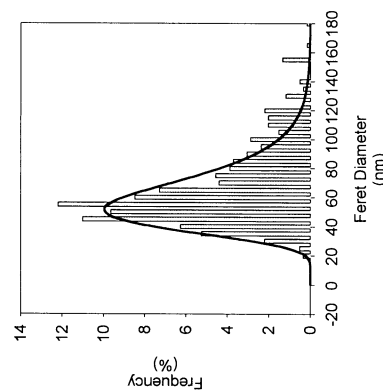
iii) MK3



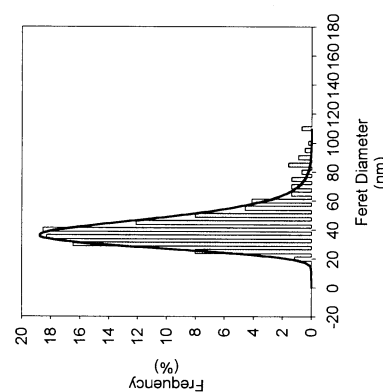
iv) MK4



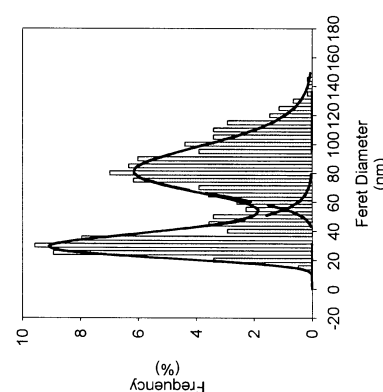
v) MK5



vi) MK6

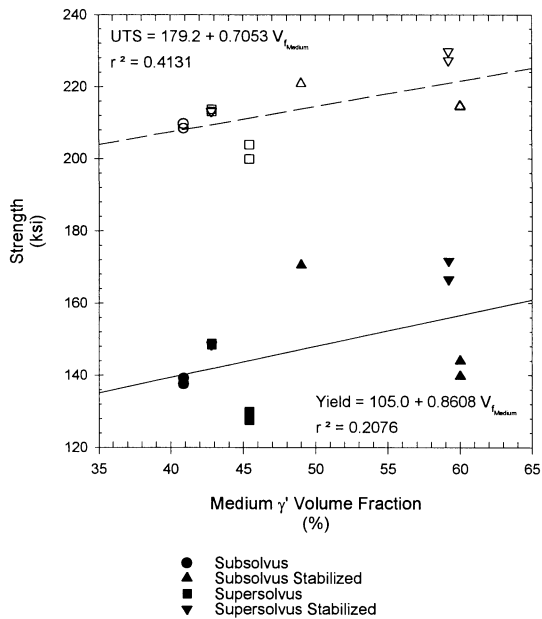


vii) MK7

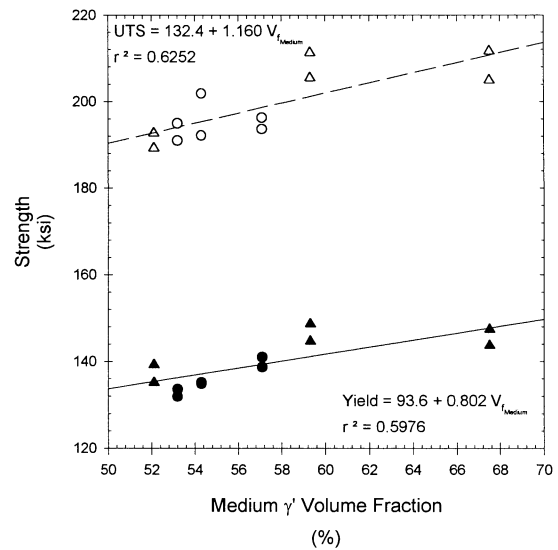


viii) MK8

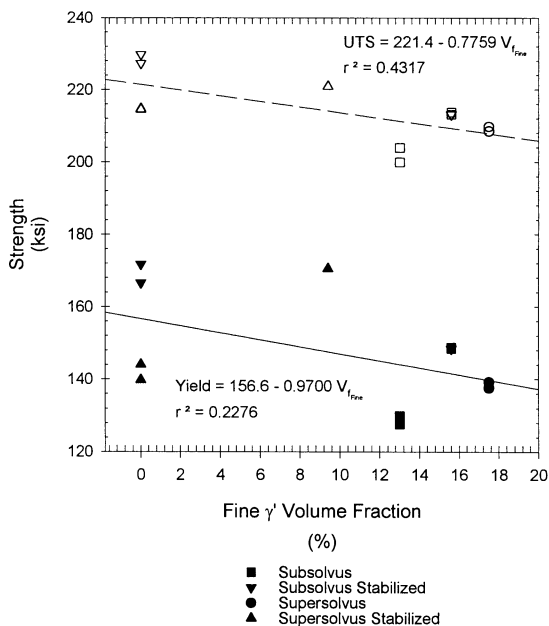
Figure 9c -
KM4 MK Series Fine γ' Size Distributions



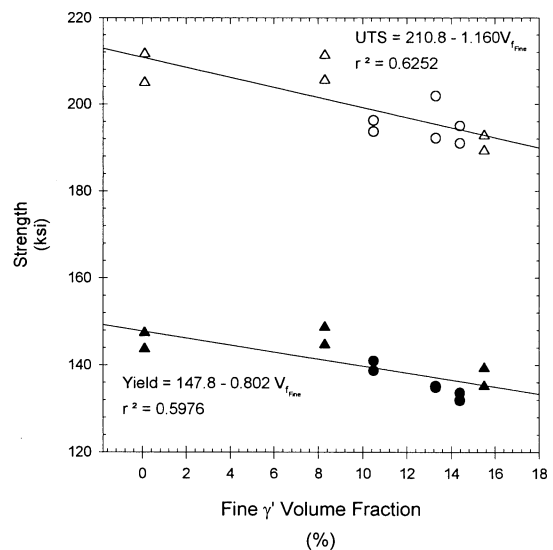
a) SR3 MS Series - Medium γ'



b) KM4 MK Series - Medium γ'

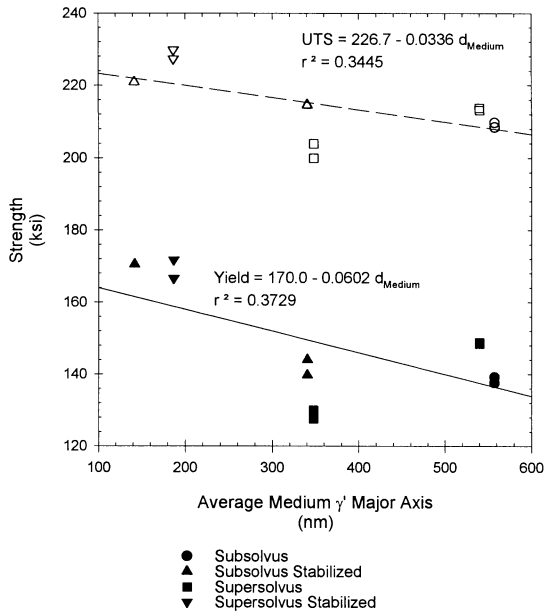


c) SR3 MS Series - Fine γ'

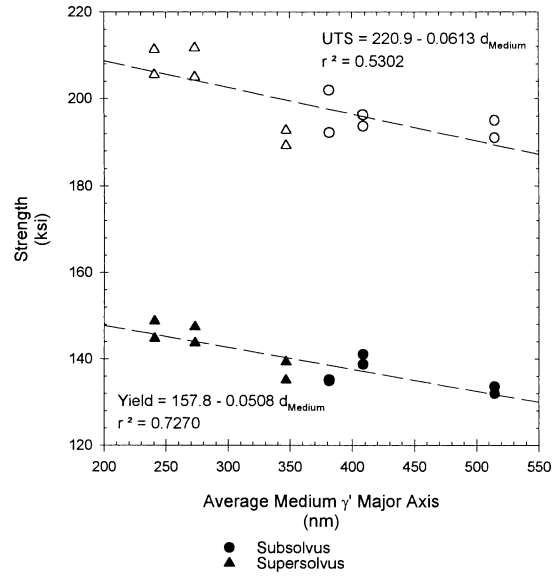


d) KM4 MK Series - Fine γ'

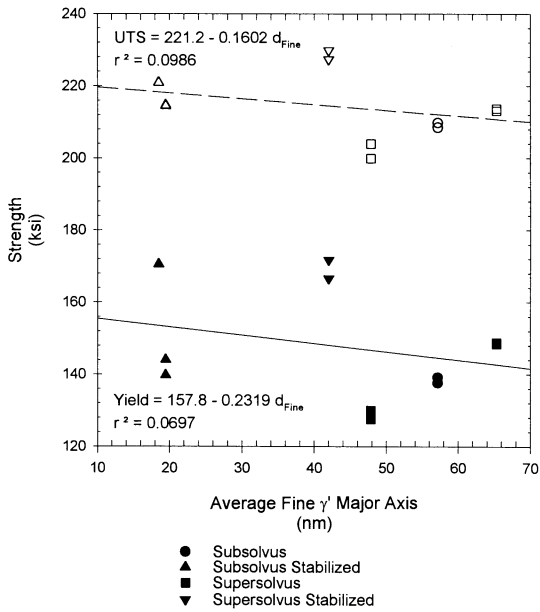
Figure 10 -
1200°F Yield And Ultimate Tensile Strengths Versus γ' Volume Fractions



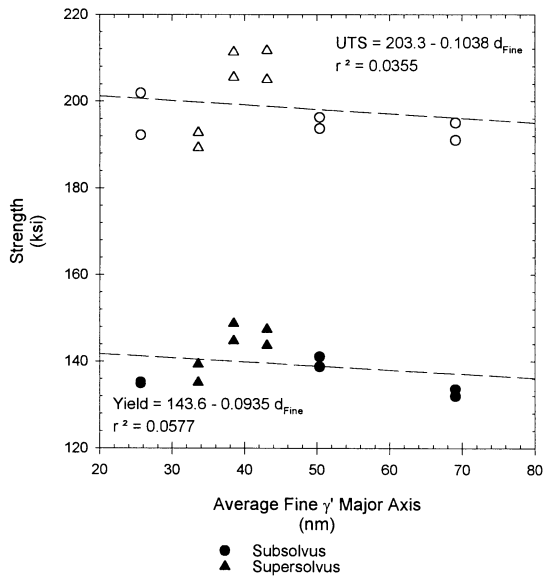
a) SR3 MS Series - Medium γ'



b) KM4 MK Series - Medium γ'

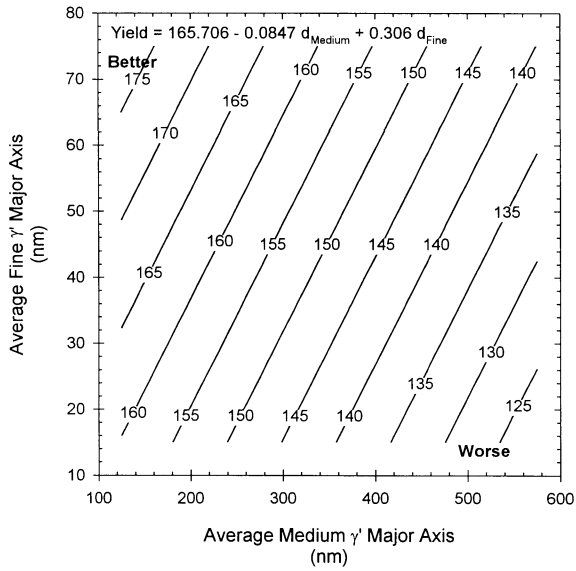


c) SR3 MS Series - Fine γ'

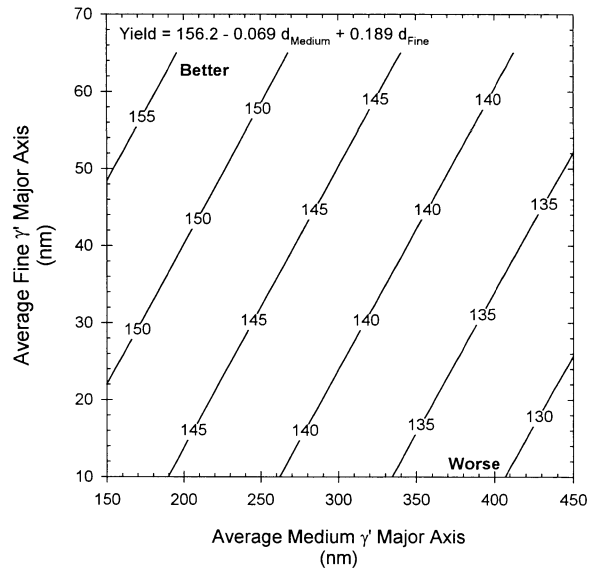


d) KM4 MK Series - Fine γ'

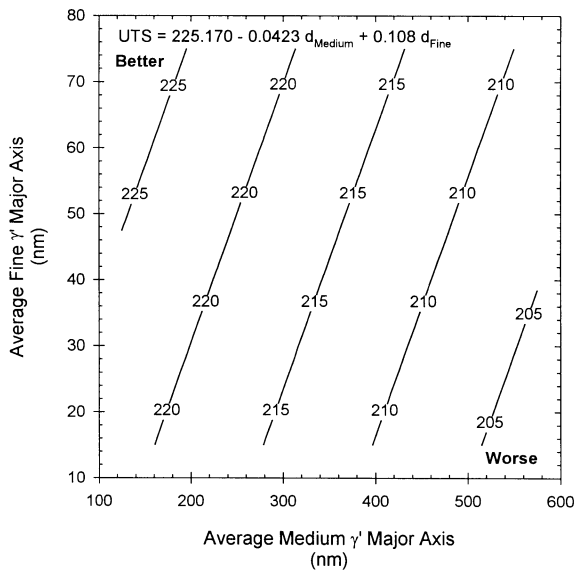
Figure 11 -
1200°F Yield And Ultimate Tensile Strengths Versus Average γ' Major Axes



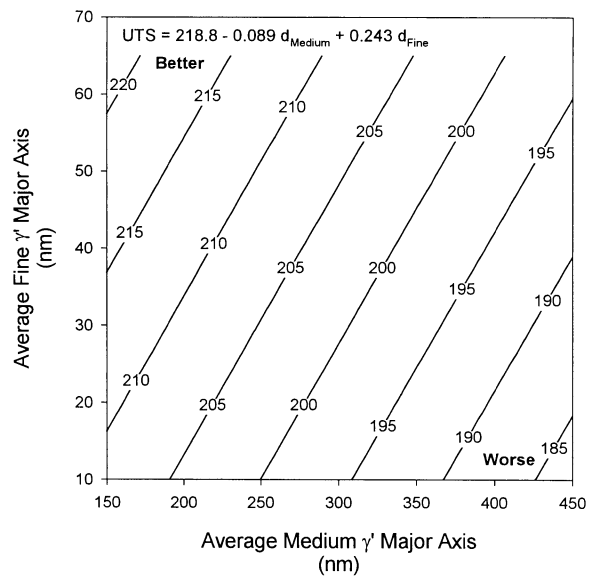
a) SR3 Yield



b) KM4 Yield

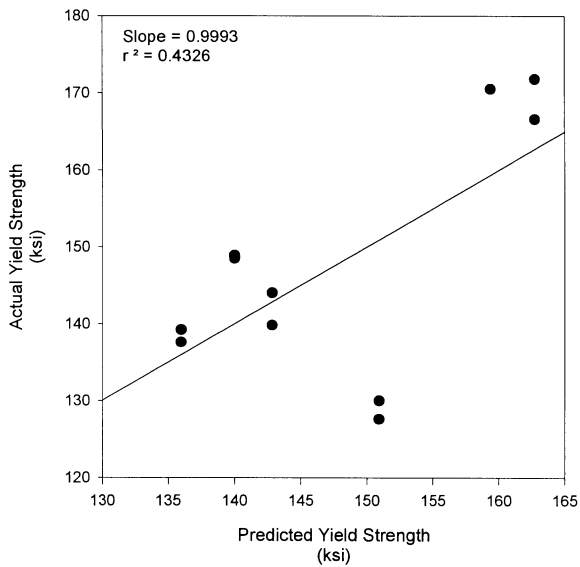


c) SR3 UTS

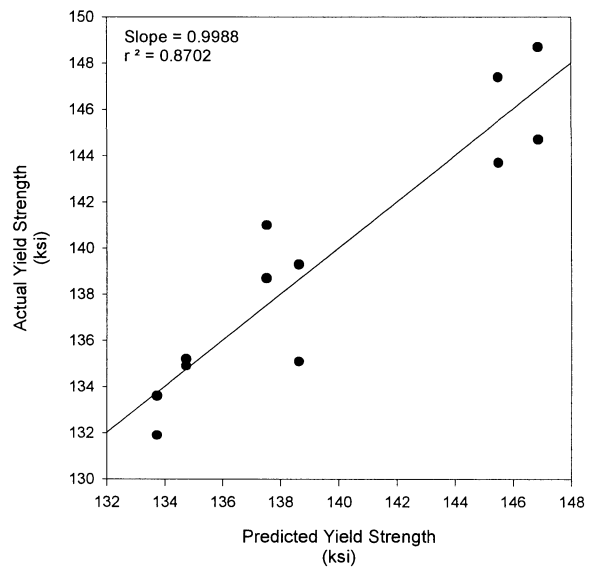


d) KM4 UTS

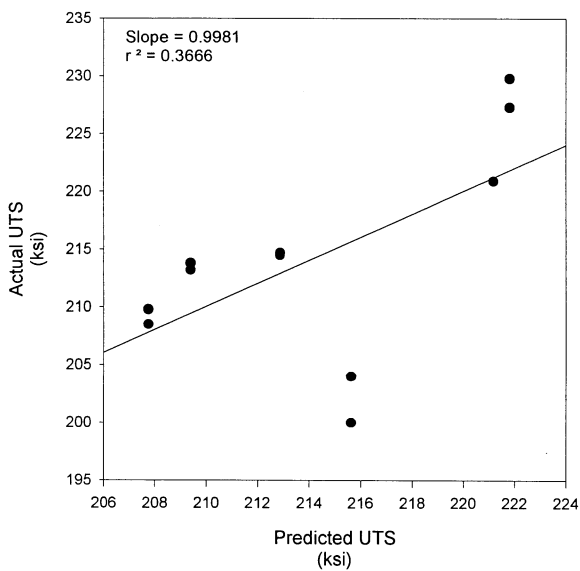
Figure 12 -
Contour Plot Of 1200°F Tensile Strength Two Independent Variable Models



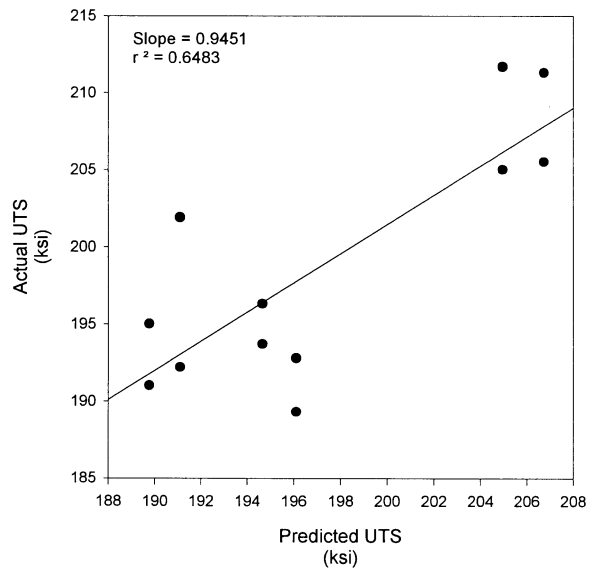
a) SR3 Yield



b) KM4 Yield

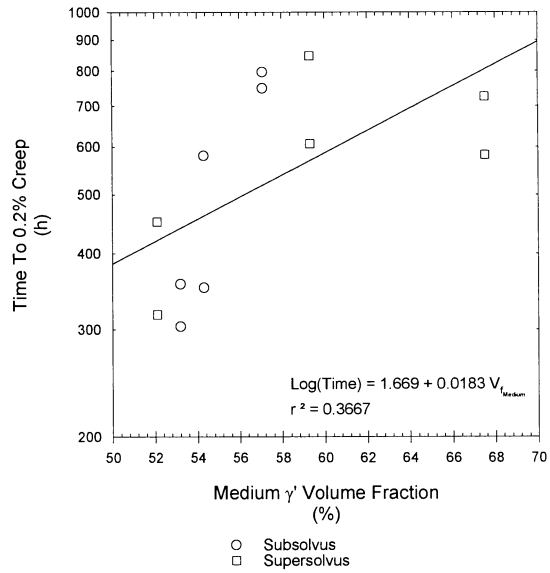
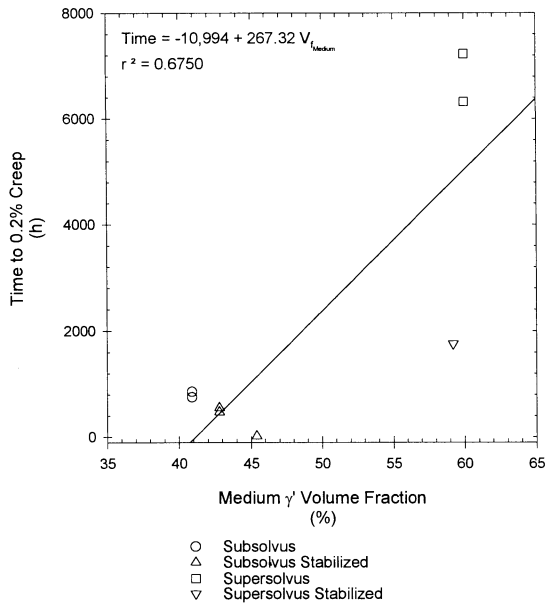


c) SR3 UTS



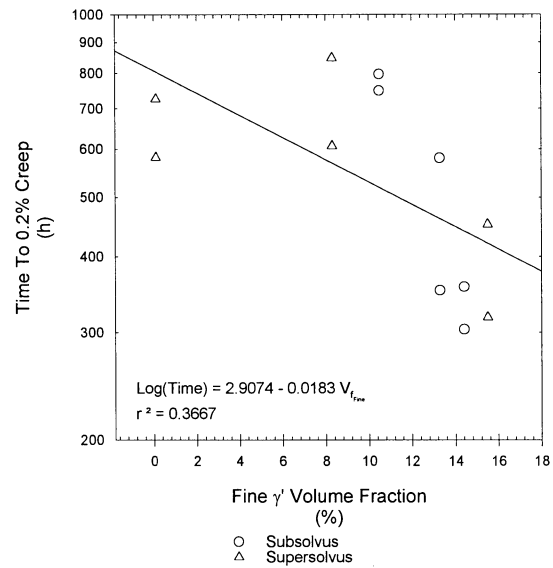
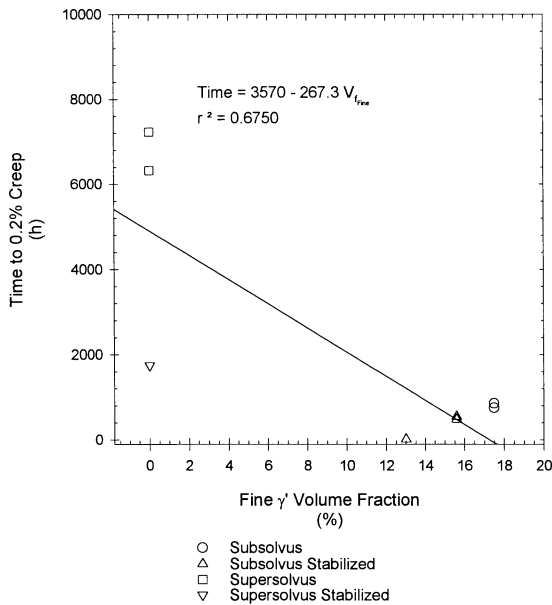
d) KM4 UTS

Figure 13 - Comparison Of Actual And Two Independent Variable Model Predicted 1200°F Tensile Strengths



a) SR3 MS Series - Medium γ'

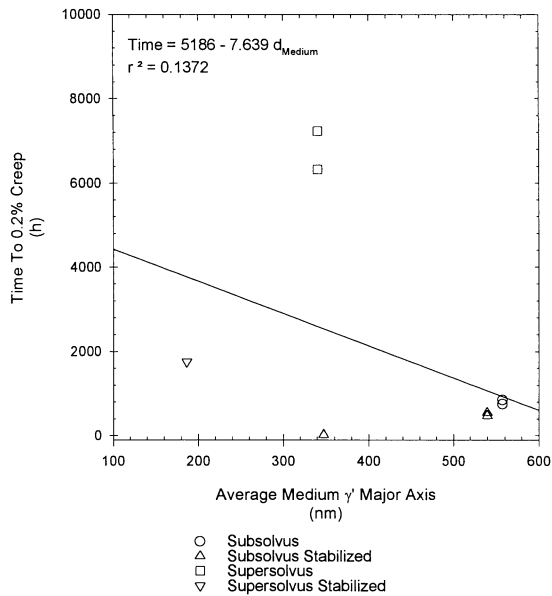
b) KM4 MK Series - Medium γ'



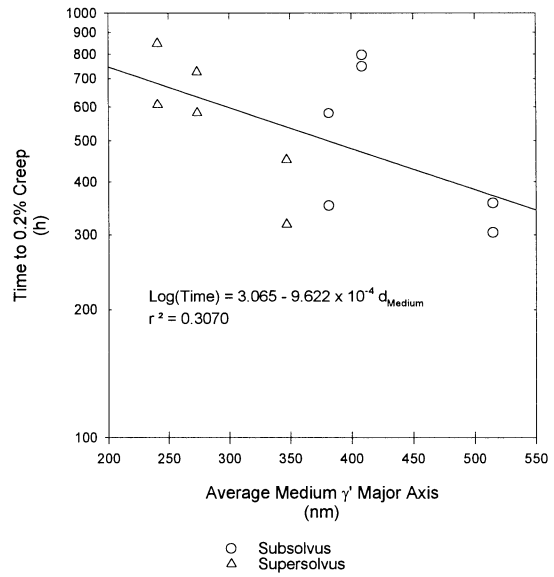
c) SR3 MS Series - Fine γ'

d) KM4 MK Series - Fine γ'

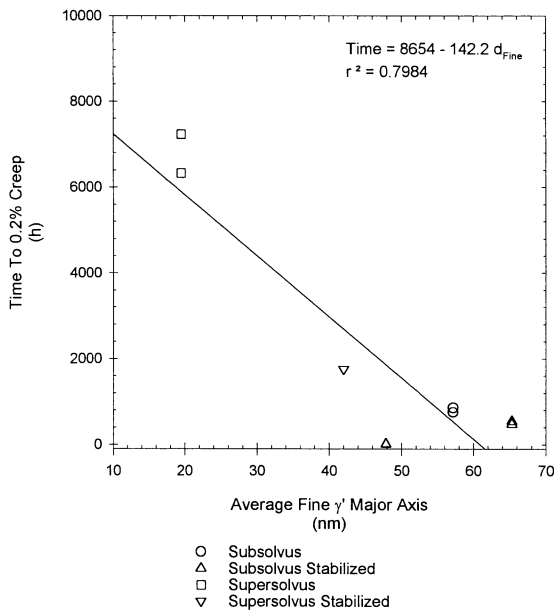
Figure 14 -
 1200°F/115 ksi Time To 0.2% Creep Versus γ' Volume Fractions



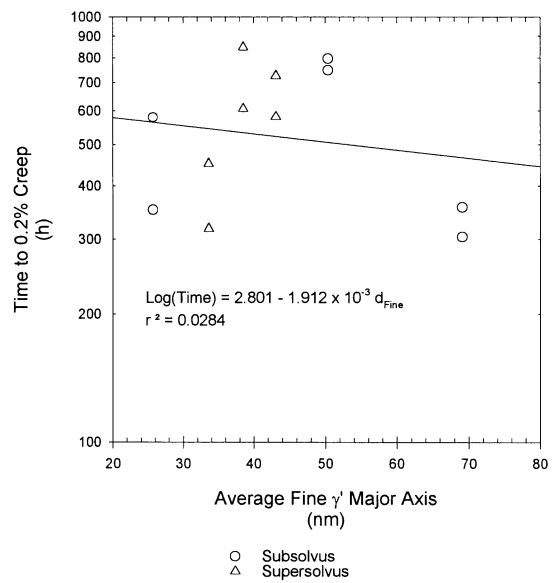
a) SR3 MS Series - Medium γ'



b) KM4 MK Series - Medium γ'



c) SR3 MS Series - Fine γ'



d) KM4 MK Series - Fine γ'

Figure 15 -
 1200°F/115 ksi Time To 0.2% Creep Versus Average γ' Major Axes

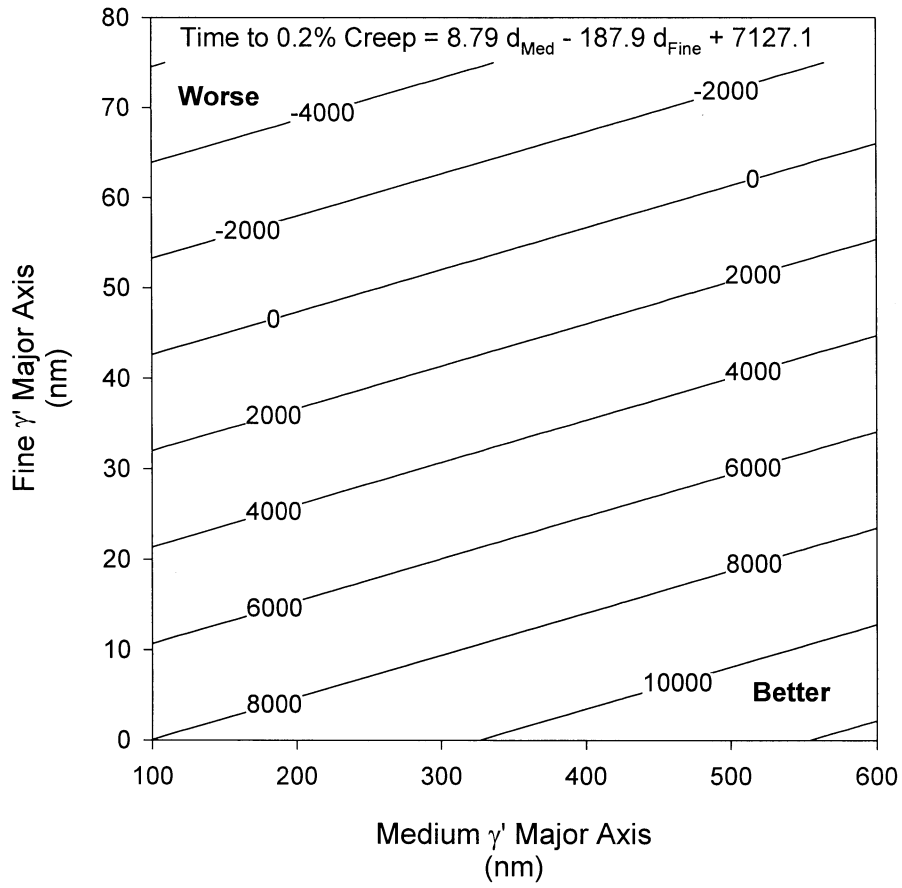


Figure 16 -
SR3 Contour Plot Of Time to 0.2% Creep Two Independent Variable Model

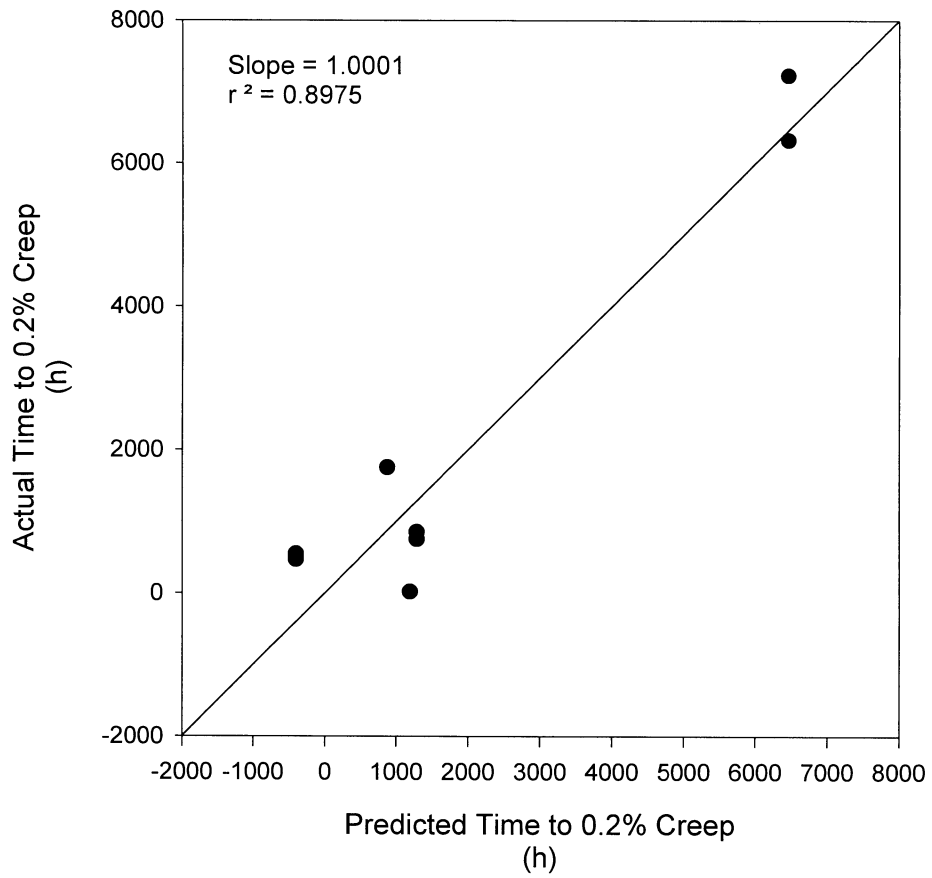
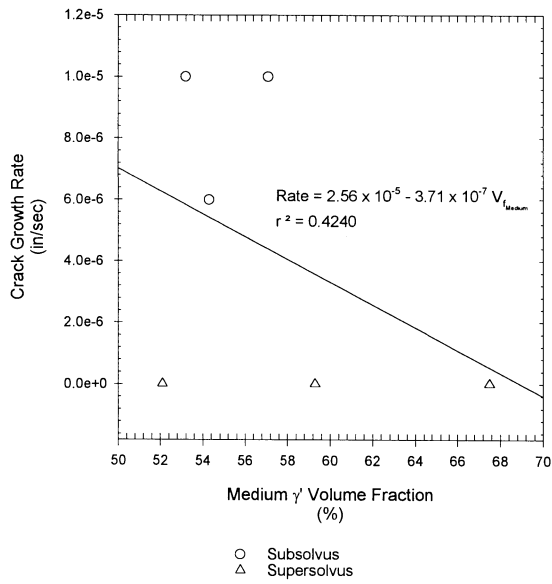
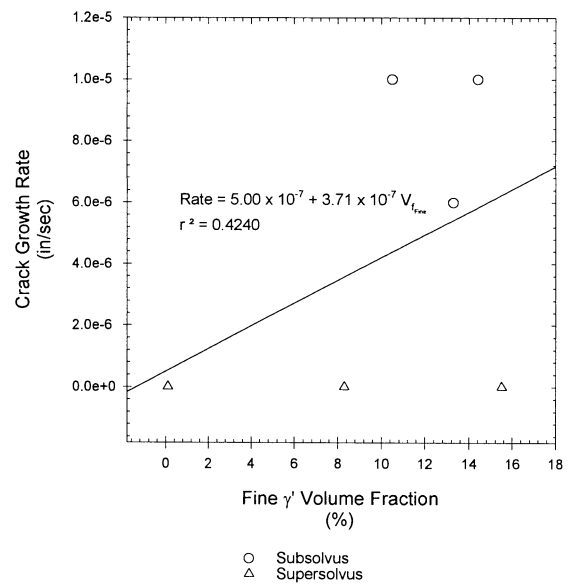


Figure 17 - Comparison Of Actual And Two Independent Variable Model Predicted Times to 0.2% Creep

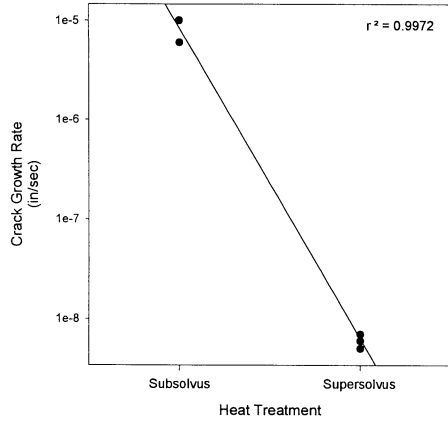


a) KM4 MK Series - Medium γ'

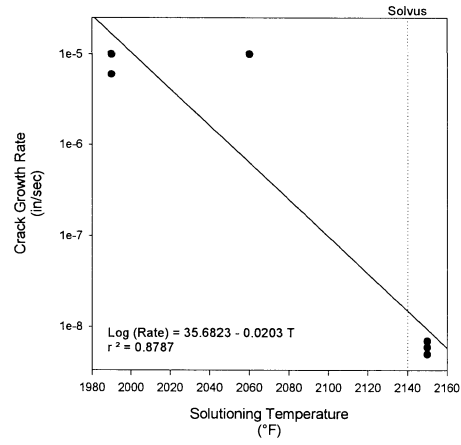


b) KM4 MK Series - Fine γ'

Figure 18 -
KM4 MK Series 1200°F Crack Growth Rate Versus γ' Volume Fractions

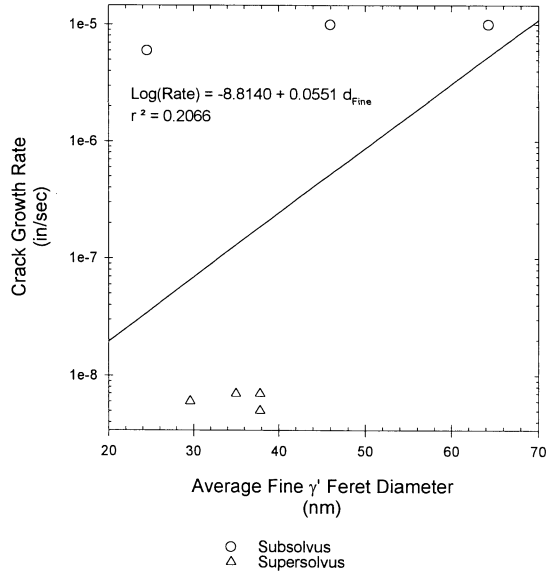
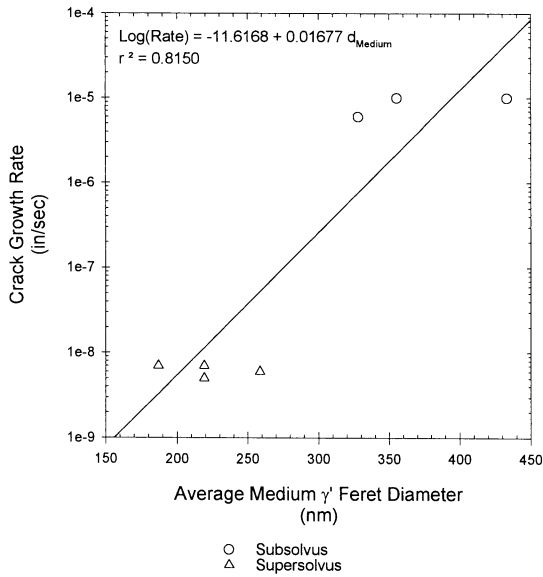


Type Of Solutioning Heat Treatment



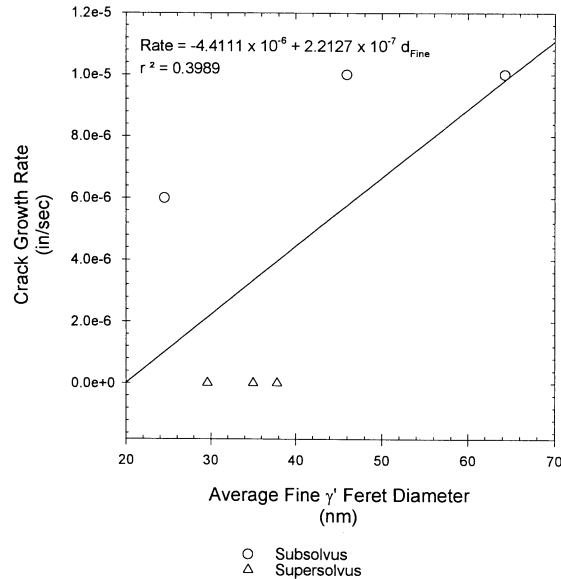
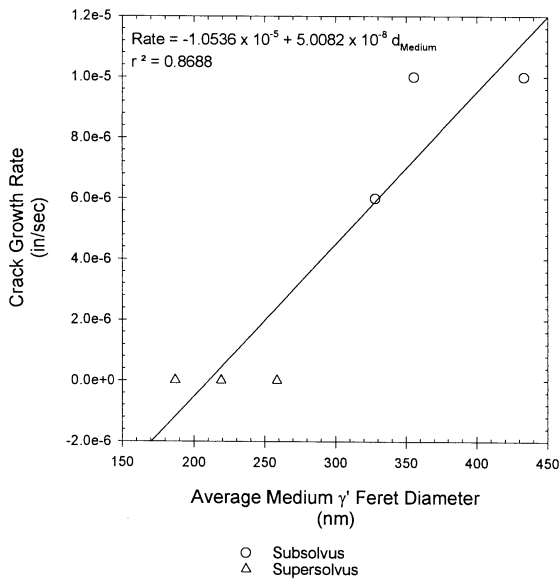
Solution Heat Treatment Temperature

Figure 19 -
KM4 MK Series Dependency Of 1200°F Crack Growth Rate On Solutioning Heat Treatment



a) KM4 MK Series Logarithmic Model - Medium γ'

b) KM4 MK Series Logarithmic Model - Fine γ'



c) KM4 MK Series Linear Model - Medium γ'

d) KM4 MK Series Linear Model - Fine γ'

Figure 20 -
 KM4 MK Series 1200°F Crack Growth Rate Versus Average γ' Feret Diameters

REPORT DOCUMENTATION PAGE

Form Approved
OMB No. 0704-0188

Public reporting burden for this collection of information is estimated to average 1 hour per response, including the time for reviewing instructions, searching existing data sources, gathering and maintaining the data needed, and completing and reviewing the collection of information. Send comments regarding this burden estimate or any other aspect of this collection of information, including suggestions for reducing this burden, to Washington Headquarters Services, Directorate for Information Operations and Reports, 1215 Jefferson Davis Highway, Suite 1204, Arlington, VA 22202-4302, and to the Office of Management and Budget, Paperwork Reduction Project (0704-0188), Washington, DC 20503.

1. AGENCY USE ONLY <i>(Leave blank)</i>	2. REPORT DATE August 2004	3. REPORT TYPE AND DATES COVERED Technical Memorandum	
4. TITLE AND SUBTITLE Microstructural Evaluation of KM4 and SR3 Samples Subjected to Various Heat Treatments		5. FUNDING NUMBERS WBS-22-714-09-46	
6. AUTHOR(S) David Ellis, Timothy Gabb, and Anita Garg			
7. PERFORMING ORGANIZATION NAME(S) AND ADDRESS(ES) National Aeronautics and Space Administration John H. Glenn Research Center at Lewis Field Cleveland, Ohio 44135-3191		8. PERFORMING ORGANIZATION REPORT NUMBER E-14654	
9. SPONSORING/MONITORING AGENCY NAME(S) AND ADDRESS(ES) National Aeronautics and Space Administration Washington, DC 20546-0001		10. SPONSORING/MONITORING AGENCY REPORT NUMBER NASA TM-2004-213140	
11. SUPPLEMENTARY NOTES This research was originally published internally as HSR052 in May 1997. David Ellis and Timothy Gabb, NASA Glenn Research Center; and Anita Garg, University of Toledo, Toledo, Ohio 43606. Responsible person, Timothy Gabb, organization code 5120, 216-433-3272.			
12a. DISTRIBUTION/AVAILABILITY STATEMENT Unclassified - Unlimited Subject Category: 07 Available electronically at http://gltrs.grc.nasa.gov This publication is available from the NASA Center for AeroSpace Information, 301-621-0390.		12b. DISTRIBUTION CODE	
13. ABSTRACT <i>(Maximum 200 words)</i> The γ - γ' microstructures of two advanced powder metallurgy disk alloys, KM4 and SR3, were quantified after a series of heat treatments using transmission electron microscopy and image analysis. Relationships between the heat treatments and the resulting γ distributions were evaluated. Statistical correlations between the γ distributions and the reported tensile strengths, creep resistances, and dwell crack growth resistances were separately assessed for each alloy. To avoid the effects of grain size related mechanisms, the grain size of the samples used in the correlations for each alloy were limited to narrow ranges of about 1.5 in ASTM grain size number. In both alloys, yield and tensile strength increased with increasing fraction of medium sized γ . The strength increased as the size of the medium γ decreased and the size of the fine γ increased. Time to 0.2 percent creep in SR3 increased with increasing medium γ volume fraction, and decreasing fine γ sizes. However, 0.2 percent creep time was not clearly correlated with the γ microstructures of KM4 specimens, apparently due to effects of stabilization heat treatments which greatly suppress creep resistance. Dwell fatigue crack growth rate decreased with increasing medium γ volume fraction, indicating more medium γ is beneficial. The crack growth rate also decreased with decreasing γ size, indicating finer γ is better.			
14. SUBJECT TERMS Disk; Superalloy		15. NUMBER OF PAGES 89	
		16. PRICE CODE	
17. SECURITY CLASSIFICATION OF REPORT Unclassified	18. SECURITY CLASSIFICATION OF THIS PAGE Unclassified	19. SECURITY CLASSIFICATION OF ABSTRACT Unclassified	20. LIMITATION OF ABSTRACT

